EVALUATION OF CO_2 STORAGE POTENTIAL IN OFFSHORE STRATA, MID-SOUTH ATLANTIC: SOUTHEAST OFFSHORE STORAGE RESOURCE ASSESSMENT (SOSRA)

By

DAWOD SALMAN BANAY ALMAYAHI

Bachelor of Science in Geology
University of Basrah
Basrah, Iraq
2001

Master of Science in Geology
University of Basrah
Basrah, Iraq
2005

Submitted to the Faculty of the
Graduate College of the
Oklahoma State University
in partial fulfillment of
the requirements for
the Degree of
DOCTOR OF PHILOSOPHY
July, 2022

EVALUATION OF CO_2 STORAGE POTENTIAL IN OFFSHORE STRATA, MID-SOUTH ATLANTIC: SOUTHEAST OFFSHORE STORAGE RESOURCE ASSESSMENT (SOSRA)

Dissertation Approved:

Dr. James Knapp

Dissertation Adviser

Dr. Camelia Knapp

Dr. Jack Charles Pashin

Dr. Prem Bikkina

ACKNOWLEDGEMENTS

I would thank the Iraqi Ministry of Higher Education and Scientific Research (MOHESR), Maine Science Center (MSC) – Basrah University, and the Iraqi Cultural office in Washington DC for funding and support. I am grateful to Mr. Fadhil Ali Alsahlanee in Computer Sciences- Oklahoma State University for his assistance in machine learning coding and the practical online course he offered me. Gratefully, I would like to thank the US Department of Energy National Energy Technology Laboratory and Angela Goodman for providing further information about the DOE approach and CO_2-SCREEN techniques. Also, I would like to thank Schlumberger for providing access to Petrel software, and I am grateful to the Schlumberger Company for providing access to Petrel software and the technical team for their support.

Name: DAWOD ALMAYAHI

Date of Degree: JULY, 2022

Title of Study: EVALUATION OF CO_2 STORAGE POTENTIAL IN OFFSHORE STRATA, MID-SOUTH ATLANTIC: SOUTHEAST OFFSHORE RESOURCE ASSESSMENT (SOSRA)

Major Field: GEOLOGY

Abstract: Subsurface geological storage of CO_2 has the potential to significantly offset greenhouse gas emissions for safe, economic, and acceptable public use of fossil fuels. Due to legal advantages and vast resource capacity, offshore CO_2 storage provides an attractive alternative to onshore options. Although offshore Lower Cretaceous and Upper Jurassic reservoirs have a vast expected storage capacity, quantitative assessment of the offshore storage resource in the southeastern United States is limited. This work is a part of the Southeast Offshore Storage Resource Assessment (SOSRA) project, which presents quantitative evaluation of a high-quality potential geological repository for CO_2 in the Mid- and South Atlantic Planning Areas. This is the first comprehensive investigation and quantitative assessment of CO_2 storage potential for the outer continental shelf within the Lower Cretaceous and Upper Jurassic rocks, including the Southeast Georgia Embayment and most of the Blake Plateau. An interpretation of 200,000 km of legacy industrial 2D seismic reflection profiles and geophysical well logs (TRANSCO 1005-1, COST GE-1, and EXXON 564-1) are utilized to create structure and thickness maps for the potential reservoirs and seals. Three target reservoirs isolated by seals based on their effective porosity values are identified and assessed. A quantitative evaluation of CO_2 Storage Potential in the Offshore Atlantic Lower Cretaceous and Upper Jurassic Strata is calculated using the DOE-NETL equation for saline formations. The prospective storage resources evaluation ranges between 450 and 4700 Mt of CO_2 within the Lower Cretaceous and between 500 and 5710 Mt within the Upper Jurassic sandstone rocks at P10 to P90. The efficiency factor of the dolomite ranges from 0.64 to 5.36 percent at P10 to P90 for the formation scale. Facies classification of five offshore wells in the Southeast Georgia Embayment was applied to the Machine Learning approach using Support Vector Classifier (SVC) and Random Forest Classifier (RFC). As a result, the SVC and RFC algorithms were compared to evaluate facies classification accuracy; the RFC had the most accurate and effectively used outcomes to classify lithofacies. The Machine Learning approach resulted in reliable and accurate values of predicted facies classification to improve CO_2 storage estimation.

TABLE OF CONTENTS

Chapter Page

LIST OF TABLES

Table Page

Table Page

LIST OF FIGURES

Figure Page

Figure Page

Figure Page

CHAPTER I

INTRODUCTION

The Southeast Offshore Storage Resource Assessment (SOSRA) provided a high-quality prospective storage resource assessment of the eastern Gulf of Mexico and the mid-and south Atlantic Ocean. A variety of data analysis approaches are applied to ensure that a high-quality assessment can estimate storage capacity to within 30%. The Department of Energy (DOE) has announced a Funding Opportunity Announcement (FOA), DE-FOA-0001246, soliciting proposals to address this need and establish a plan for forwarding to commercial implementation, which involves establishing Best Practices Manuals (BPMs).

Offshore geologic storage of carbon dioxide (CO_2) is an efficient tool to reduce CO_2 emissions in the atmosphere and of climate change (Metz et al., 2005). Offshore CO_2 storage refers to the injection of CO_2 into the strata beneath the seabed for permanent storage.

Due to legal advantages and the postulated vast resource capacity, offshore storage offers a

an attractive alternative to onshore storage (Esposito et al., 2016). The Sleipner project in the North Sea was an early opportunity for commercial deployment. Sleipner was the first successful CO_2 storage project that demonstrated the technical feasibility of offshore storage.

Although offshore reservoirs are projected to have a large storage capacity, there has been no complete study of the southeastern United States' offshore storage resource potential. Few studies have been conducted in the southeastern United States (Hendriks et al., 2004). According to Esposito et al. (2010), approximately 170 Gt of CO_2 could be stored in Miocene sandstone, and at least 30 Gt could be stored in deeper Cretaceous layers in a 10,000 square mile area offshore Alabama and the western Florida Panhandle. According to a task group convened by the Southern States Energy Board (SSEB) and the Interstate Oil and Gas Compact Commission, there was no quantitative assessment of the offshore storage resource potential along the Atlantic seaboard and the eastern Gulf of Mexico in the southeastern United States (IOGCC). According to NETL CO_2 Storage Atlases, the U.S. Environmental Protection Agency estimates that the southeast produces about 40% of anthropogenic CO_2 emissions. The lack of an offshore CO_2 assessment is a big hole in our knowledge about how much CO_2 I can store in the region.

1.1 Objectives of Study

This study is a part the large SOSRA project, which conducted research to address the DOE project objectives. This project includes significant advances in knowledge and technology, which can facilitate assessing and quantifying offshore CO_2 storage resources in the study region (Figure 1-1). The central objective of the SOSRA project is to develop an offshore storage resource assessment of saline formations in offshore regions. This research project extends from the Virginia-North Carolina border, where it overlaps with Virginia Tech, to the south of Florida (Figure 1-1), linking up with Oklahoma State University’s study area. This study will be carried out by answering the following questions:

- What are the geological and geophysical characteristics of the Mesozoic strata?
- Do the Mesozoic formations have quantifiable porosity and permeability?
- Do the Mesozoic formations have significant CO_2 storage capacity?
- What are the quality and spatial extent of prospective reservoirs and seals?

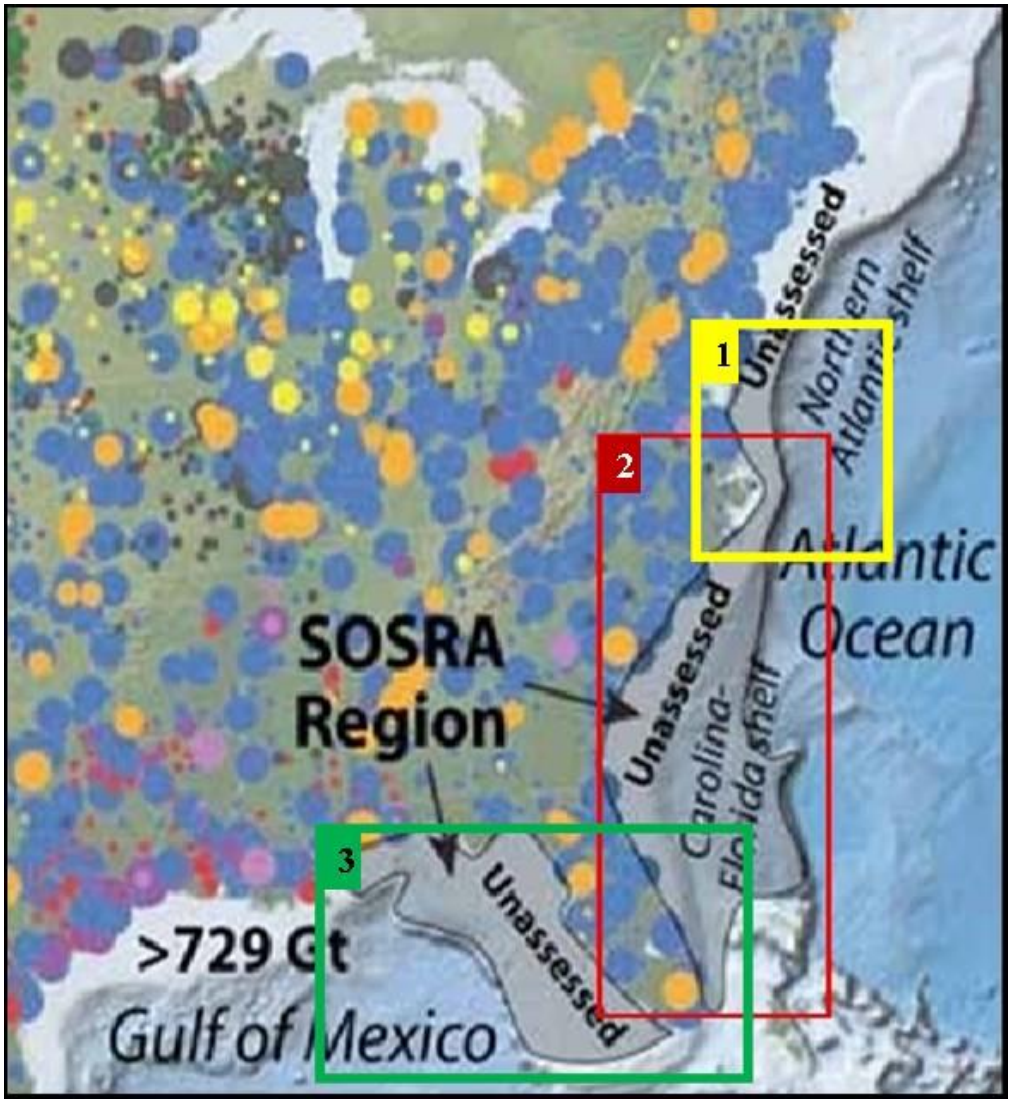

Figure 1-1: Regional map showing proposed SOSRA study area (Tew et al., 2013). The figure also showing three areas which are bounded by colored triangles: area 1 is was analyzed by The Virginia Polytechnic Institute and State University, both areas 2 (i.e. this study), and 3 were analyzed by Oklahoma State University.

1.2 Hypothesis

- The offshore reservoirs could provide vast permanent storage.
- Various estimates of the global CO_2 storage capacity of prospective geological storage have been made. These estimates demonstrated a broad range of values.
- Various porosity and permeability regimes are widely distributed in the Mesozoic strata.
- The Mesozoic strata consist of categorized stratigraphic systems.

1.3 Geological perspective

The evolution of the Atlantic continental margin, including the study area, is broadly characterized by continental rifting beginning in Triassic time (Poag, 1978; Dillon et al., 1979; Scholle, 1979; Dalziel et al., 1994; Poppe et al., 1995). Mesozoic rifting involved tectonic subsidence in extensional basins, following by regional thermal subsidence along the entire eastern North American margin. (Dillon et al., 1983; Pinet and Popenoe, 1985; Badley et al., 1988; Dillon and Popenoe, 1988; Dalziel et al., 1994). Stratigraphic sequences on this type of passive margin are characterized by extensive lateral continuity and offshore dip with relatively minor structural disturbance (Dillon and Popenoe, 1988; Dalziel et al., 1994; Poppe et al., 1995). In the mid-Atlantic and South Atlantic planning areas, there is a thick succession of post-rift strata ranging in age from Jurassic to Pleistocene. The significant depositional centers in these planning areas from north to south include the Baltimore Canyon Trough, the Carolina Trough, the Southeast Georgia Embayment, and the Blake Plateau Basin. The range of sediment column thicknesses is 3,048-7,620m (Maher and Applin, 1971; Scholle, 1979; Lizarralde et al., 1994). The post-rift sediments overlie a regional breakup unconformity that cuts across the entire region and marks the rift-drift transition from165-190Ma (Poag, 1978; Poppe et al., 1995). The oldest post-rift sediments are of Jurassic age including mid Jurassic (Bathonian-Callovian) salt and siliciclastic sediment, transgressive Upper Jurassic (Oxfordian) carbonate

sediment, and a progradational wedge of Upper Jurassic (Kimmeridgian-Tithonian) siliciclastic and carbonate sediment. (Dillon et al., 1982; Dillon and Popenoe, 1988). The Jurassic section thickens seaward, and estimates from geophysical and stratigraphic studies suggest thicknesses of at least 7-8km in basins depocenters (Dillon et al., 1979; Dillon et al., 1983). Typically, the Cretaceous section is characterized by more clastic sedimentation in the north and more carbonate deposition in the south, including a large carbonate platform over the Blake Plateau and offshore Florida. From the Late Cretaceous to the Cenozoic strong direction and evidence for paleocurrents controlled deposition in the clastic offshore. In the Late Cretaceous, the Suwannee Strait deposition to the Blake Plateau created distinct facies change to the neighboring offshore Florida and Bahamas carbonate deposition (Poag, 1978; Pinet and Popenoe, 1985; Poppe et al., 1995). The Suwannee Strait eventually evolved into today's Gulf Stream providing strong erosive power that eroded most of the Paleogene sediments on the Blake Plateau and prevented deposition off the Florida-Hatteras slope where it continues to the north along the shelf edge (Dillon and Popenoe, 1988; Poppe et al., 1995).

1.4 Stratigraphic column

The Continental Offshore Stratigraphic Test (COST) well and Six commercial exploratory wells were drilled in the southeast Georgia embayment from 1979 to 1980 (Poppe et al., 1995) (Figure 1-2). Offshore, two wells, the TRANSCO 1005-1 and COST GE-1 wells penetrate the pre-rift sediments in the Paleozoic, and the EXXON 564-1 penetrate post-rift unconformity (PRU) in the Mesozoic sedimentary section (Figure 1-2). The COST GE-1 well penetrated the PRU at ~10,500ft, and recorded approximately 2,250ft of Paleozoic sedimentary sequence, and total depth (TD) at 13,254ft (Scholle, 19790). The Paleozoic section consists of non-fossiliferous quartzite, shale, and slate, underlain by metamorphic and meta-volcanic rocks (Scholle, 1979). The TRANSCO 1005-1 well recorded the breakup unconformity at a depth of ~9,000ft, penetrated Paleozoic sedimentary rocks at ~2,500ft, and bottomed at TD of 11,635ft (Poppe et al., 1995). The Paleozoic section in the

TRANSCO well is weakly metamorphosed shale and sandstones with the meta-igneous intrusion. Using muds logs, electric logs, drill cuttings, and bio-stratigraphic data, the TRANSCO well has been correlated with Devonian rocks encountered in the COST GE-1 well (Poppe et al., 1995). These wells have also been seismostratigraphically interpreted and correlated with similar Paleozoic sedimentary sequences (Poppe et al., 1995; Lizarralde et al., 1994).

The COST GE-1 well is the deepest stratigraphic test drilled in the offshore southern Atlantic shelf. The total depth of the COST well is over 13,254 ft. (4,040 meters) (Scholle, 1979). This well record a thick section spanning the Paleozoic to Cenozoic (Figure 1-2). The thick fossiliferous chalky limestone below the drill platform reaches 3,300 ft./depth, corresponding to Tertiary. The units to a depth of (3,300 - 5,900) ft are upper cretaceous. Upper cretaceous is composed of calcareous shale, dolomite, and limestone, and the section from 5,900 to 7,200 ft. is Lower Cretaceous which is lying on the upper cretaceous units at and below 11,000 ft. depth consists of highly indurated to weakly metamorphosed pointed to the Paleozoic (Scholle, 1979).

The Exxon 564-1 well encountered the pre-rift unconformity at a depth of ~12,260ft, met up with and recorded 600ft thickness of unknown sedimentary rocks with Triassic intrusive at ~2,500ft bottomed at TD of 12,863ft (Lizarralde et al., 1994). The last 600ft, under the post-rift unconformity in the Exxon well is weakly metamorphosed shale and sandstones with meta-igneous intrusion with the intrusion of Triassic rocks. The Exxon well has been correlated to be approximately equivalent to Devonian rocks encountered in the COST GE-1 well. These wells have also been stratigraphically interpreted and correlated with having similar Mesozoic sedimentary sequences (Poppe et al., 1995).

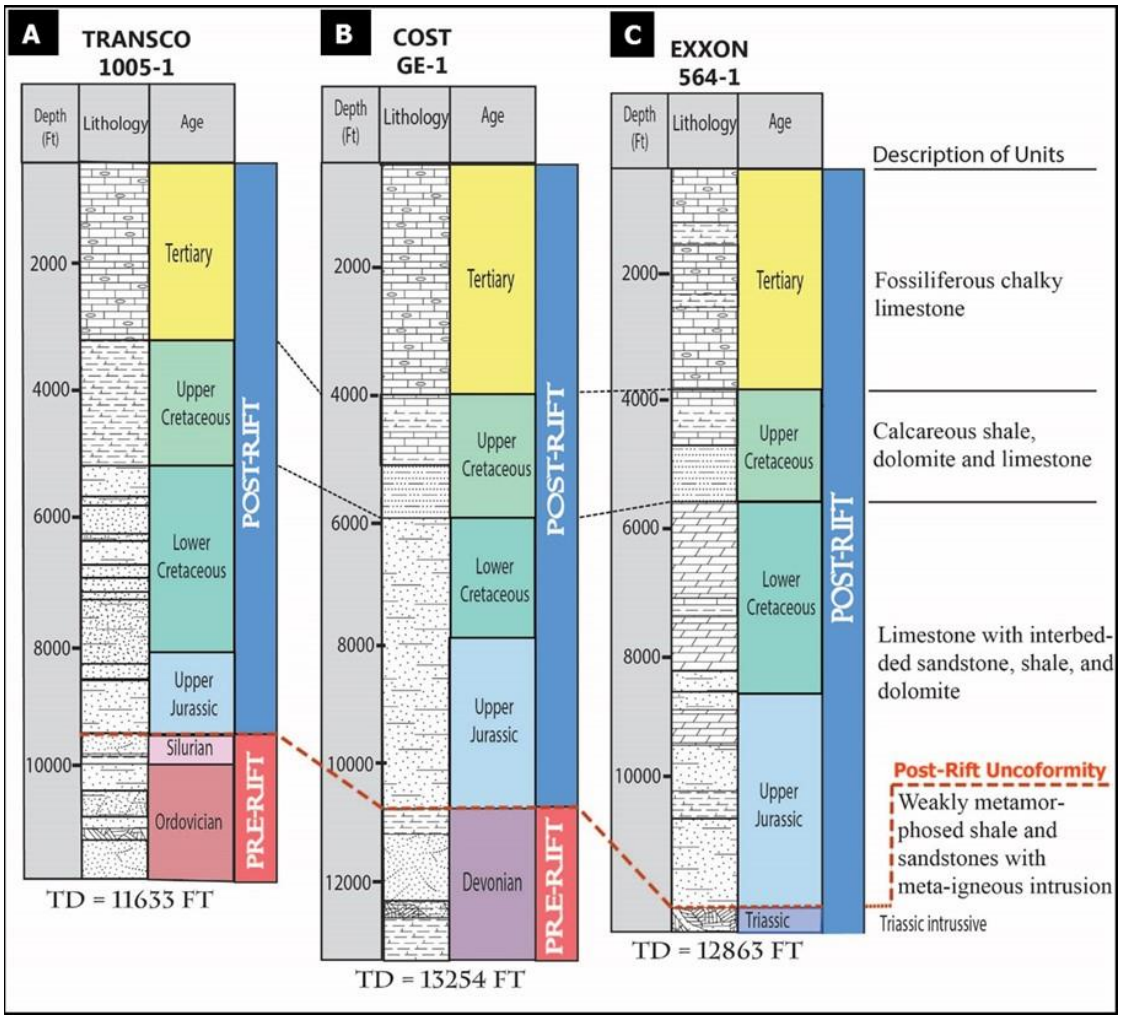

Figure 1-2: Three stratigraphic columns for Exxon 564-1, COST GE-1, and TRANSCO 1005-1 offshore wells conducted, combining and modified after (Scholle, 1979; Poppe et al., 1995; Boote and Knapp, 2016) .

1.5 CO_2 geological storage

The main geological storage options are oil and gas reservoirs, deep saline aquifers, deep-seated coal beds (enhanced coal-bed methane recovery), organic-rich shale, basaltic rocks , caverns, and mines (Lokhorst and Wildenborg, 2005). Between 2004 and 2005, there were high-level evaluations of Carbone Dioxide storage capacity. Due to the lack of geological and geophysical information, the estimations of the CO_2 storage capacity were globally very broad range values for saline aquifers ranging (Table 1-1).

Table 1-1: Global estimation CO_2 storage capacity (Hendriks et al., 2004; Dooley et al., 2005; Manancourt and Gale, 2005; Metz et al., 2005).

Reservoir			Metz et al., 2005	Manancourt and Gale, 2005	Dooley et al., 2005	Hendrick et al., 2004		
						Best estimate		Rang
Coal Beds			3.15-200	150-250	176	267		0-1,480
Saline Aquifers			1,000-10,000	200-200,000	240	240		30-1,081
Oil and Gas field	Depleted	Gas	675-900	500-1,000	1,153	700	239	24-423
		Oil				232	93	42-151
	Remaining	Gas	900-1,200	Not reported	Not reported	1,153	672	388-1,700
		Oil				821	140	12-1,043

Geological key selection criteria respect reservoir depth, thickness, porosity, permeability, seal integrity, and salinity. With storage in dipping strata, the lateral sealing features are also important (Table 1-2). Lateral sealing in reservoirs (compartmentalization) can help retain CO_2 in the desired storage location. Defining the extent, the thickness of stratigraphic units, and resources supports the evaluation of CO_2 storage potential capacity in the study area.

The COST GE-1 well data identifies the storage elements, such as reservoir and confining beds. The porosity and permeability values are compared to the geological indicators for a suitable storage site in table 1-2.

Table 1-2: Key geological selection criteria includes reservoir depth, thickness, porosity, permeability, seal integrity and salinity (Chadwick et al., 2008).

	Properties	Safe Indicator	Cautionary Indicator
Reservoir	Depth (m)	800-2500	Less than 800
	Thickness (m)	Larger than 50	Less than 20
	Porosity (%)	Larger than 10	Less than 10
	Permeability (md)	Larger than 100	Less than 100
	Salinity (ppm)	Larger than 30,000	Less than 30,000
	Stratigraphy	Uniform	Complex lateral variation
	Capacity	Estimated CO_2 storage capacity $\geq 3\times$ injected	Estimated CO_2 storage capacity = injected
Caprock	Lateral continuity	Small or No fault, and lateral uniform stratigraphy	Medium or large fault, Lateral variation stratigraphy
	Thickness (m)	Larger than 20	Less than 20

Based on the reservoir and caprocks properties, the preliminary conclusions are as follows: (1) The porosity of Cenozoic units ranged between 25 to 40 percent, whereas the permeability is very low, which is less than 3 md. Therefore, Cenozoic strata are candidates to be the upper seal. (2) The Mesozoic strata have acceptable porosity and permeability values, good thickness, and depth. Therefore, the Mesozoic strata are qualified to be a good reservoir. (3) The lack of porosity and permeability in the Paleozoic strata made these strata the lower seal.

CHAPTER II

EVALUATION OF CO_2 STORAGE POTENTIAL IN ATLANTIC OFFSHORE LOWER CRETACEOUS STRATA, SOUTHEASTERN UNITED STATES

2.1 Introduction

Offshore geologic storage of carbon dioxide (CO_2) as a part of Carbon Capture and Storage (CCS) technology has recently attracted considerable scientific attention. The CCS technology is a potentially important tool to reduce the level of CO_2 emissions in the atmosphere and to prevent the most dangerous consequences of climate change (Metz et al., 2005; Thomas and Benson, 2005; HART, 2007; Solomon et al., 2008; Hertel et al., 2010; Hortle et al., 2014; Okwen et al., 2014; Cumming et al., 2017). The term offshore CO_2 storage refers to the injection of CO_2 in the geological strata beneath the seabed for safe and permanent storage (Smyth, 2007; Zhou et al., 2008; Schrag, 2009). However, due to legal considerations and the vast resource storage capacity, offshore storage provides an attractive alternative option to onshore storage. The Sleipner project in the North Sea was an early successful opportunity for commercial deployment. Although offshore Lower Cretaceous reservoirs have an expected vast storage capacity, there has been no

comprehensive assessment of the offshore storage resource capacity in the southeastern United States.

Although the storage capacity of offshore reservoirs is expected to be vast, only limited quantitative studies of the offshore CO_2 storage resource have been conducted in the southeast United States. An analysis of a 25,900Km^2 area of offshore Alabama and the western Florida Panhandle suggests that about 170 Gt of CO_2 could be stored in Miocene sandstone, whereas at least 30 Gt could be stored in deeper Cretaceous formations (Esposito et al., 2010). There is around 32 Gt of CO_2 that could be stored within 190,000 Km^2 of the Upper Cretaceous strata in the offshore southeastern United States (Almutairi, 2018). A study offshore of northeastern the United States has recently concluded that the Cretaceous and the Jurassic sandstone is valid to store approximately (37-403) Gt of CO_2 with geologic storage efficiency (1-13) percent (Fukai et al., 2020). Realizing that the U.S. Environmental Protection Agency estimates that about 40 percent of anthropogenic CO_2 emissions in the U.S. are generated in the southeast, the lack of an offshore CO_2 assessment constitutes a major gap in understanding of the prospective regional storage resource (Goodman et al., 2011; Global, 2012; Warwick et al., 2013; Levine et al., 2016).

The research area is located offshore of the Southeastern United States, covering the southern part of the Mid Atlantic Planning Area (including the Carolina Trough), and the South Atlantic Planning Area (including the Southeast Georgia Embayment and Blake Plateau) as defined by the Bureau of Ocean Energy Management (BOEM) (Figure 2-1). Within the Mid Atlantic Planning Area and South Atlantic Planning Area, there is a thick sequence of post-rift stratigraphy, which is considered as a semi-closed saline aquifer, with sediments ranging in age from Jurassic to Pleistocene (Dillon et al., 1979; Dillon et al., 1983). In these areas, the significant sedimentary deposits from north to south include the Carolina Trough, the Southeast Georgia Embayment, and the Blake Plateau Basin, with a range in sediment column thicknesses from 3,048to 7,010m (Maher and Applin, 1971; Poag, 1978; Pinet and Popenoe, 1985; Poppe et al., 1995). A regional

unconformity under the post-rift sediments known as the Post-Rift Unconformity (PRU) that cuts the entire region after rifting between Africa and North America ceased. This mark is the transition to widespread sediment depositional zone during the drifting stage.

This chapter aims to evaluate the CO_2 storage potential offshore within the Lower Cretaceous strata in the Mid and South Atlantic Planning areas.

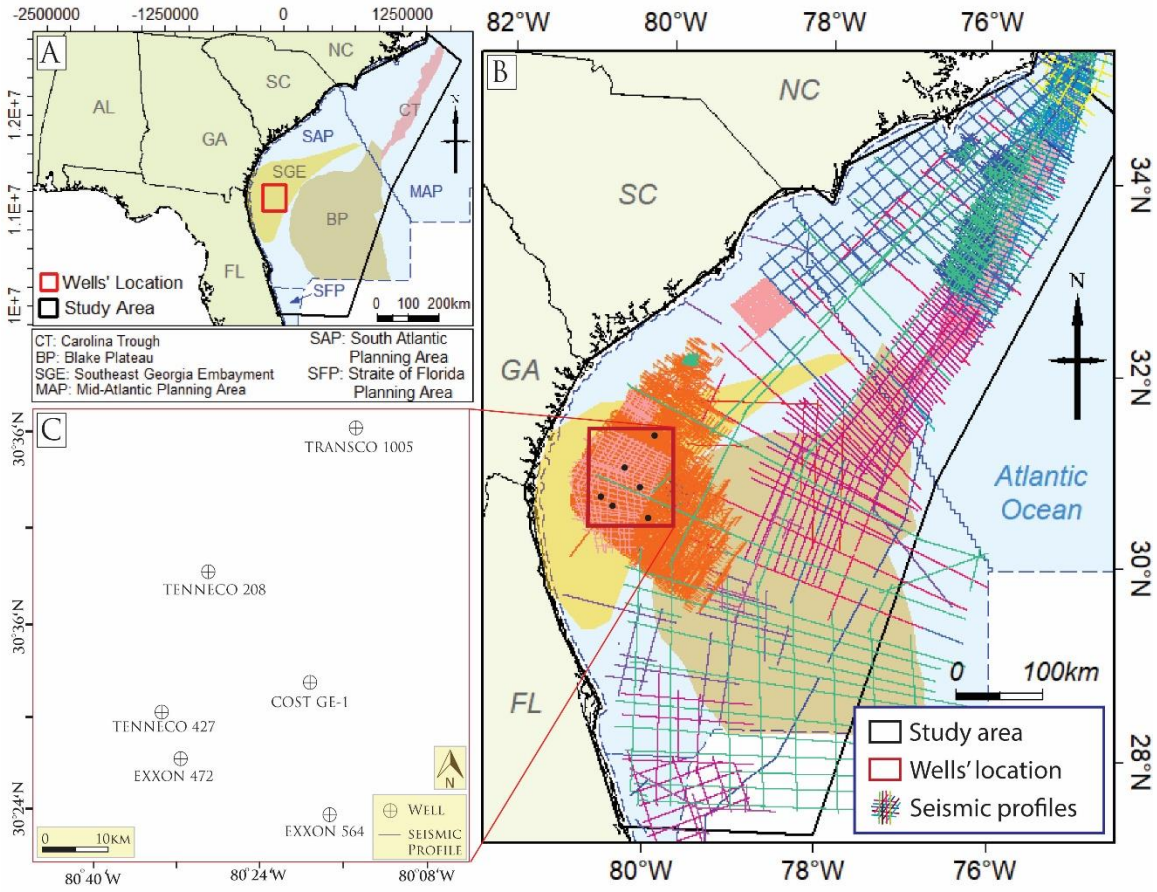

Figure 2-1: Location map of the study area. Panel A is the location of the study area in the regional map, panel B is the study area map, and panel C is the well locations.

2.2 Geologic framework

The Atlantic shelf have a complex tectonic and geologic history, including the study area. The evolution of the Atlantic continental margin has been broadly characterized by the initiation of continental rifting in the earliest Mesozoic time following the terminal collision of the Laurentian and Gondwanan continents in the Late Paleozoic. Early rifting associated tectonic subsidence formed restricted extensional basins followed by regional thermal subsidence along the entire eastern North American margin throughout the past. Stratigraphic sequences on this passive margin are generally characterized by extensive lateral continuity and relatively minor structural disturbance. A thick sequence of post-rift stratigraphy ranging from Jurassic to Pleistocene aged sediments in the mid-Atlantic and South Atlantic planning areas. The major depocenters in these planning areas from North to south include the Baltimore Canyon Trough, the Carolina Trough, the Southeast Georgia Embayment, and the Blake Plateau Basin. The sediment column thickness range is 10,000-25,000ft (Maher and Applin, 1971). The post-rift sediments overlie a regional unconformity known as the "post-rift unconformity" that cuts across the entire region after rifting between Africa and North America ceased and marked the transition to wide-spread sediment deposition during the "drift" phase around 165-190Ma (Poag, 1991).

The oldest post-rift sediments are of the Jurassic age and are the product of rapid clastic sedimentation from erosion followed by a period of evaporite deposition and then initiation of widespread, shallow water, carbonate deposition with some terrigenous input (Dillon et al., 1983; Dillon et al., 1982). The Jurassic section thickens seaward, and estimates from geophysical and stratigraphic studies suggest thicknesses of at least 7-8km in the basins (Dillon et al., 1979). Typically, the Cretaceous section is characterized by more clastic sedimentation in the north and more carbonate deposition in the south, forming a large carbonate platform over the Blake Plateau and offshore Florida.

The Late Cretaceous to the Cenozoic strong paleo-currents controlled deposition in the clastic offshore. In the Upper Cretaceous, the Suwanne Strait deposition to the Blake Plateau created distinct facies change to the neighboring offshore Florida and Bahamas carbonate deposition (Pinet and Popenoe, 1985b). The Suwannee Strait eventually evolved into today's Gulf Stream, providing strong erosive power that eroded most of the Paleogene sediments on the Blake Plateau and prevented deposition off the Florida-Hatteras slope, where it continues to the north along the shelf edge (Pinet and Popenoe, 1985a).

2.3 Main Geologic Provinces

A thick sequence of post-rift stratigraphy was found in the mid-Atlantic and South-Atlantic planning areas, with sediments ranging in age from Jurassic to Pleistocene. In these planning areas, the major sedimentary deposits from north to south include the Carolina Trough, the Southeast Georgia Embayment, and the Blake Plateau Basin (Figure 2-2), with a range in sediment column thicknesses from 10,000 to 23,000 ft. (Maher and Applin, 1971). A regional unconformity under the post-rift sediments known as the post-rift unconformity cuts the entire region after rifting between Africa and North America ceased. The post-rift unconformity marks the transition to wide-spread sediment deposition during the drift stage.

2.3.1 Carolina Trough

The Carolina Trough has located offshore the North Carolina-South Carolina coast within the Atlantic continental margin. The Carolina Trough is considered one of the deepest and largest salt basins, whose width is 97 km (Dillon and Popenoe, 1988). The margin consisted of a wedge of the Mesozoic and the Cenozoic sediments. Tectonically, the basin formed by thinning composed of the continental crust developed during the initiation of continental rifting during the Triassic to Early Jurassic.

A thick salt section was deposited during the Jurassic, followed by a thick accumulation of sediments. The salt deposits are caused to squeeze the salt and then form the Diapiric structures deeper than three kilometers from the water surface (Figure 2-3). In this basin, the sediments are over 40,000 ft. thick in the deep within the basin and are separated by the breakup unconformity.

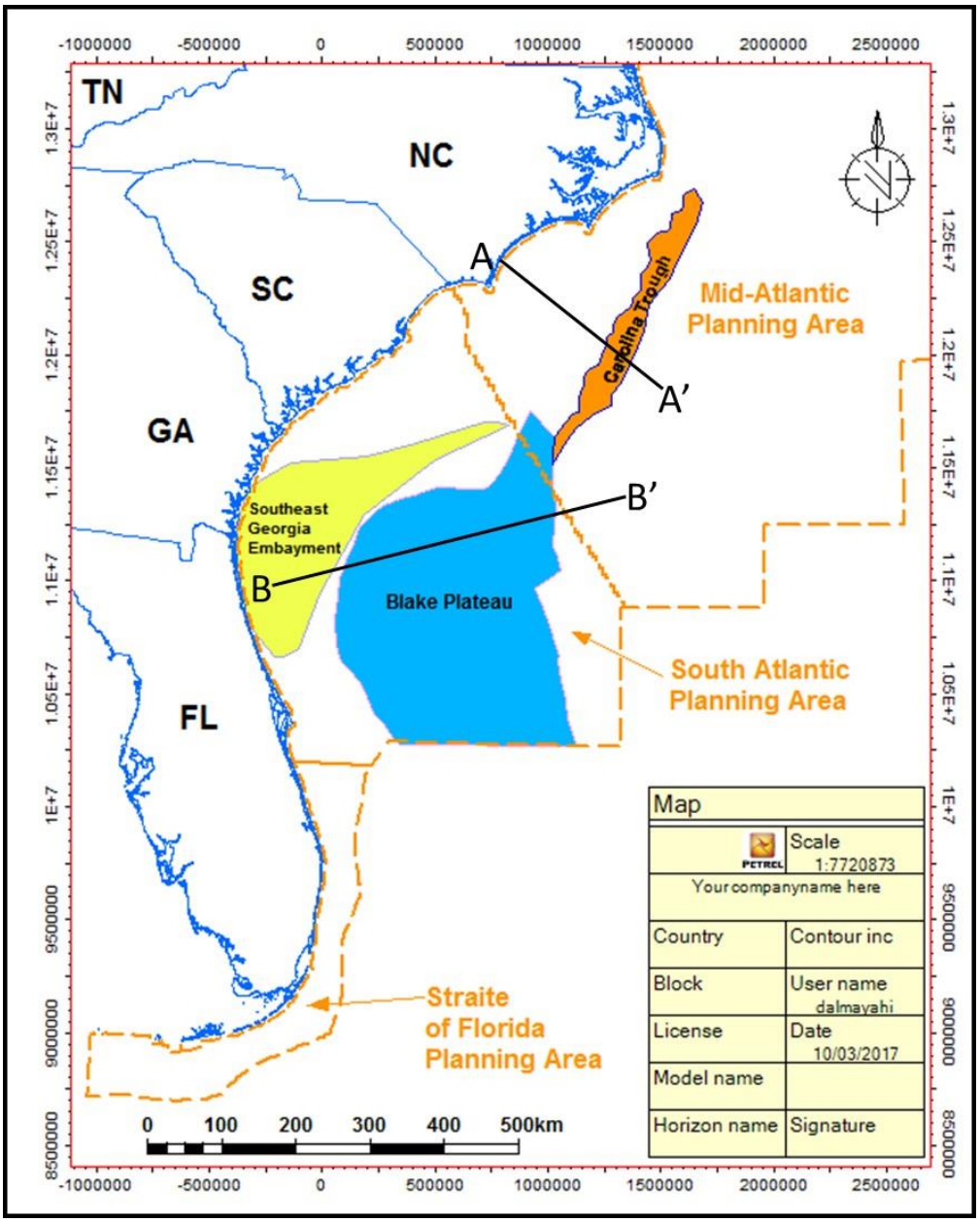

Figure 2-2: Main geological features map; Carolina trough, Blake bateau, and Southeast Georgia embayment in mid and South Atlantic planning area, south east offshore United State.

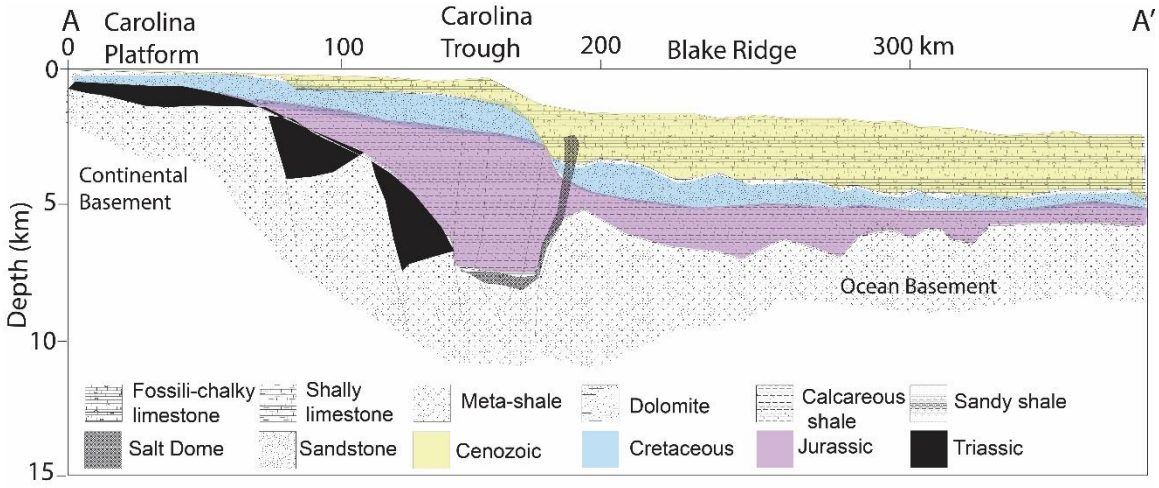

Figure 2-3: Cross section (A-A"), as showing in figure (2-2), through Carolina trough basin offshore North Carolina within study area, modified from (Carpenter and Amato, 1992).

2.3.1 Blake Plateau Basin

The Blake Plateau Basin is a major sedimentary basin within the South Atlantic area. This area is wide and flat and lies at approximately 600 and 1000 m. However, the Blake plateau basin formed at a similar time and processes that formed Carolina Trough. However, the basin subsidence was much greater. Blake Plateau has a complex geologic and tectonic history as the northern portion formed quite differently from the southern part (Poag, 1978). The Blake Spur represents the fracture point and the dividing line between the two regions. The southern part was controlled by the formation of a new oceanic crust during rifting, resulting in increased subsidence of the northern part (Figure 2-4). The seaward edge structure of the southern portion was dominated by Cretaceous reef development rather than depositional, erosional balance shown north of Blake Spur. The western margin of Blake Plateau is also characterized by deep-water coral mounds and elongate depressions that lie along the base of the Florida-Hatteras Slope.

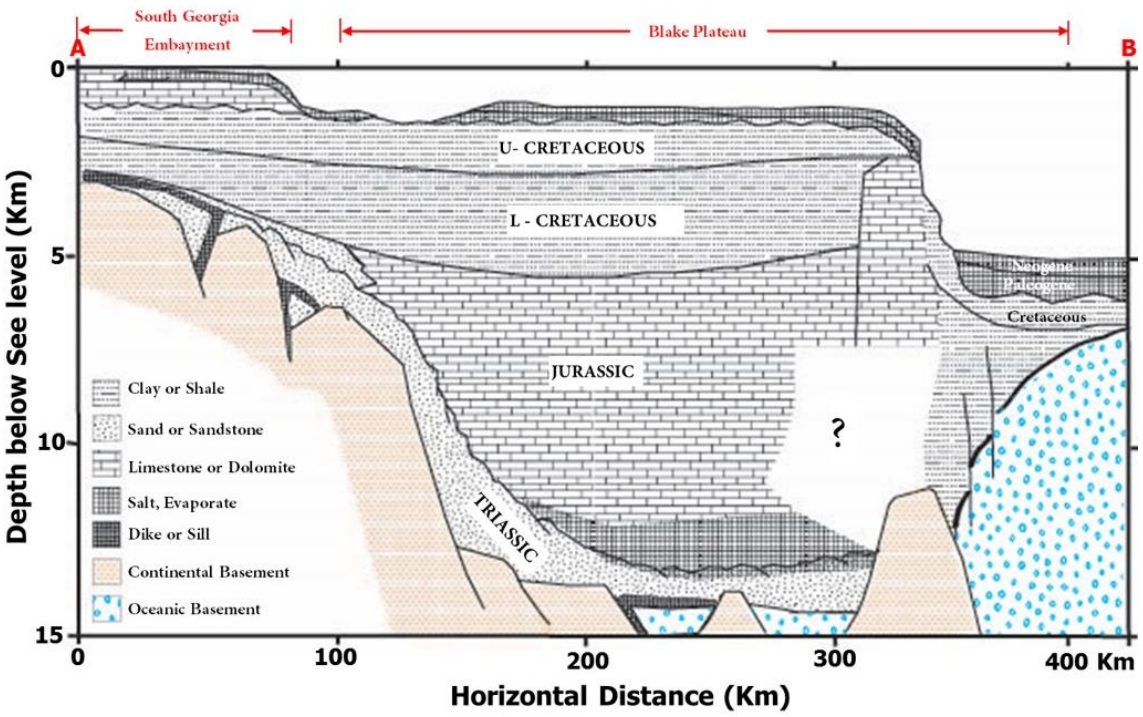

Figure 2-4: Cross section (B-B'), as showing in figure (2-2), through Blake bateau, and Southeast Georgia embayment basins, offshore North Carolina within study area, (composited from Poag, 1978. and Dillon et al 1978).

2.3.1 Southeast Georgia Embayment

The continental Shelf's width between Cape Hatteras and Cape Canaveral ranges from approximately 33 km to a maximum of 135 km. The shelf surface is not flat but is characterized by different topographic features, most remarkably the numerous sand ridges which trend gently toward the coast (Figure 2-4). Other topographic features include low algal banks along the Carolina Coast, scattered outcrops of hard or live bottoms, and at least seven terraces or submerged shores that are roughly subparallel to the present shoreline and are thought to be considered be old strandlines. The Southeast Georgia Embayment, an east-plunging depression recessed into the Atlantic Coastal Plain, is a major structural feature in the Florida-Hatteras Shelf. However, compared to other sedimentary basins in the South Atlantic, the Southeast Georgia Embayment is a minor sedimentary geologic formation.

2.4 Database and methods

This chapter involves the integration of geological and geophysical data, combining regional 2-D seismic reflection surveys, published sidewall core analyses, and well logs from commercial exploration wells. Seismic reflection data provide fundamental structural control over the subsurface geology confined by accessible exploration wells. A total of 36 separate 2-D seismic surveys were integrated and analyzed (Figure 2-1 B), and a seismic mis-tie analysis was conducted to merge the individual surveys for this study. The well logs were then calibrated with the seismic reflection profiles. The seismic surveys were interpreted regionally for key stratigraphic horizons, and then porosities and permeabilities were derived from the log data and core reports. Subsequently, the porosity and permeability estimates were compared between the published sidewall core data and the derived values.

2.4.1 Well sections

Seven commercial exploratory offshore wells (GETTY 913, TRANSCO 1005-1-1, TENNECO 208, COST GE-1, TENNECO 427, EXXON 472, and EXXON 564-1), (Figure 2-1 C), were drilled in southeast Georgia embayment from 1979 to 1980. These wells were stratigraphically correlated by Poppe et al. (1995) and have also been seismic stratigraphically interpreted and correlated with having a similar Mesozoic sedimentary sequence (Lizarralde et al., 1994). TRANSCO 1005-1, COST GE-1, and EXXON 564-1 are the deepest three wells in the Southeast Georgia Embayment that were used in the current study. TRANSCO 1005-1 well and COST GE-1 well are the only two wells that penetrate the pre-rift sedimentary sequences in the Paleozoic era, and the EXXON 564-1 well penetrates only the post-rift sedimentary sequence in the Mesozoic era.

The TRANSCO 1005-1 well encounters the pre-rift unconformity at a depth of ~2,743 m and bottomed in Paleozoic sedimentary rocks at a Total Depth (TD) of 3,546 m (Poppe et al., 1995).

The Paleozoic section in the TRANSCO 1005-1 well is a weakly metamorphosed shale and sandstone with meta-igneous intrusions (Figure 2-5). The log suite for this well included mud logs, electric logs, drill cuttings, and biostratigraphic data. The Paleozoic rocks in the TRANSCO 1005-1 well have been correlated with Devonian strata in the COST GE-1 well (Poppe et al., 1995).

The COST GE-1 well penetrated the pre-rift unconformity at 3,200 m which drilled approximately 686 m of the Paleozoic sedimentary sequences and TD-ed at a depth of 4,040 m (Scholle, 1979). The COST GE-1 well showed a thick sequence from Paleozoic to Cenozoic (Figure 2-5). The Paleozoic section generally consists of non-fossiliferous quartzite, shale, and salt, underlain by metamorphic and meta-volcanic rocks (Scholle, 1979).

Scholle (1979) provided an analysis of the COST GE-1 well data and described the stratigraphic units, porosity, and permeability measurements by both a conventional core and sidewall core with respect to depth. The thickness of fossiliferous chalky limestone below the drill platform reaches 1,006 m corresponding to strata of Tertiary age. The Upper Cretaceous section is marked at a depth ranging from 1,006 m to 1,798 m. The Upper Cretaceous is composed of calcareous shale, dolomite, and limestone. The section from 1,798 to 2,195 m is the Lower Cretaceous. Rocks encountered below 3,353 m depth consist of highly indurated to weakly metamorphosed Paleozoic strata (Scholle, 1979).

The EXXON 564-1 well encountered the pre-rift unconformity at a depth of 3,737 m (Lizarralde et al., 1994). The last 183 m, under the post-rift unconformity in the EXXON 564-1 well, is a weakly metamorphosed shale and sandstone with meta-igneous intrusion of Triassic rocks. The EXXON 564-1 well has been correlated to approximately the equivalent to the Devonian rocks corresponding to the COST GE-1 well (Figure 2-5).

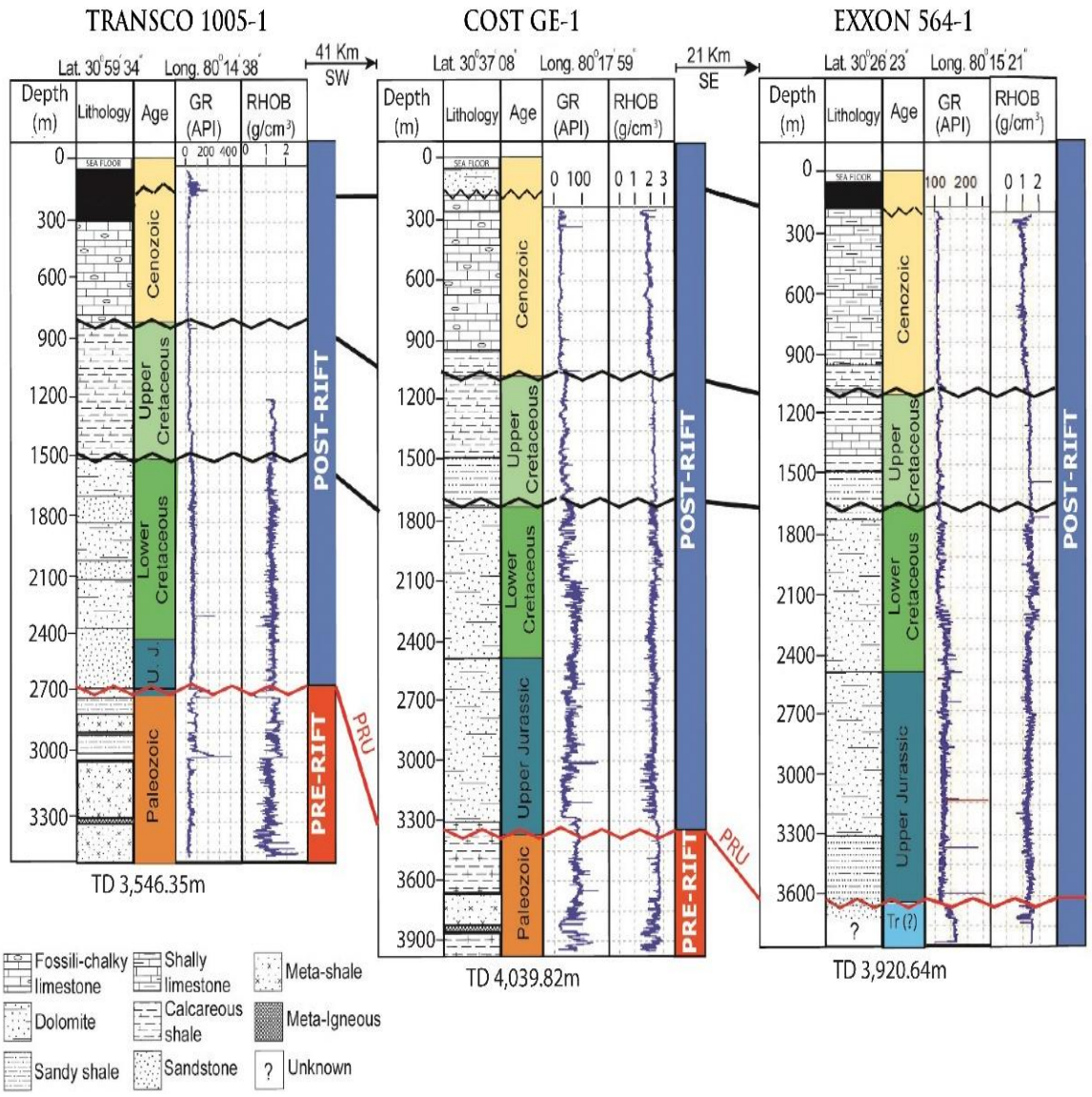

Figure 2-5: TRANSCO 1005-1, COST GE-1, and EXXON 564-1 are three wells that have stratigraphically and geophysically correlated by logs and lithology, modified and combined after (Poppe et al., 1995;Boote and Knapp, 2016).

2.4.1 Seismic interpretation

The primary dataset consists of legacy 2D seismic reflection profiles offshore the southeastern United States in the Atlantic Ocean. The dataset has been released by the Bureau of Ocean and Energy Management (Figure 2-1 B). I interpreted and correlated a continuous surface stratigraphy of the storage elements (sinks and reservoir seals) along 200,000 km of the seismic profiles,

covering approximately 200,000 Km^2. Seismic interpretation started with picking high-frequency stratigraphy sequences targeted at creating three-dimensional maps of the reservoirs and seals. The TRANSCO 1005-1 well, COST GE-1 well, and EXXON 564-1 well were tied with the seismic profiles (Figure 2-6). The Schlumberger Petrel software can generate advanced velocity models using check shot data. The velocity model uses input parameters such as tops and surfaces and the time-depth link (Roth, 1993). The velocity model is created based on the time-depth relationship from the well data. The time-depth conversion uses linear velocity related to depth functions ($V=V0+K\times Z$) and ($V=V0+K\times(Z-Z0)$) for evaluating a velocity model (Schlumberger, 2016). Both K and the linear velocity slope indicate that the velocity increases with depth and reflects layer compaction. The compaction factor K is estimated with the fewest mistakes feasible and used to generate a V0 surface, any modifications incorporated into the velocity model are reflected on the V0 surface. The check shot data of the three wells (COST GE-1, Exxon 564-1, and Transco 1005-1) were used to identify the depth of the upper and bottom surfaces of the Lower Cretaceous section.

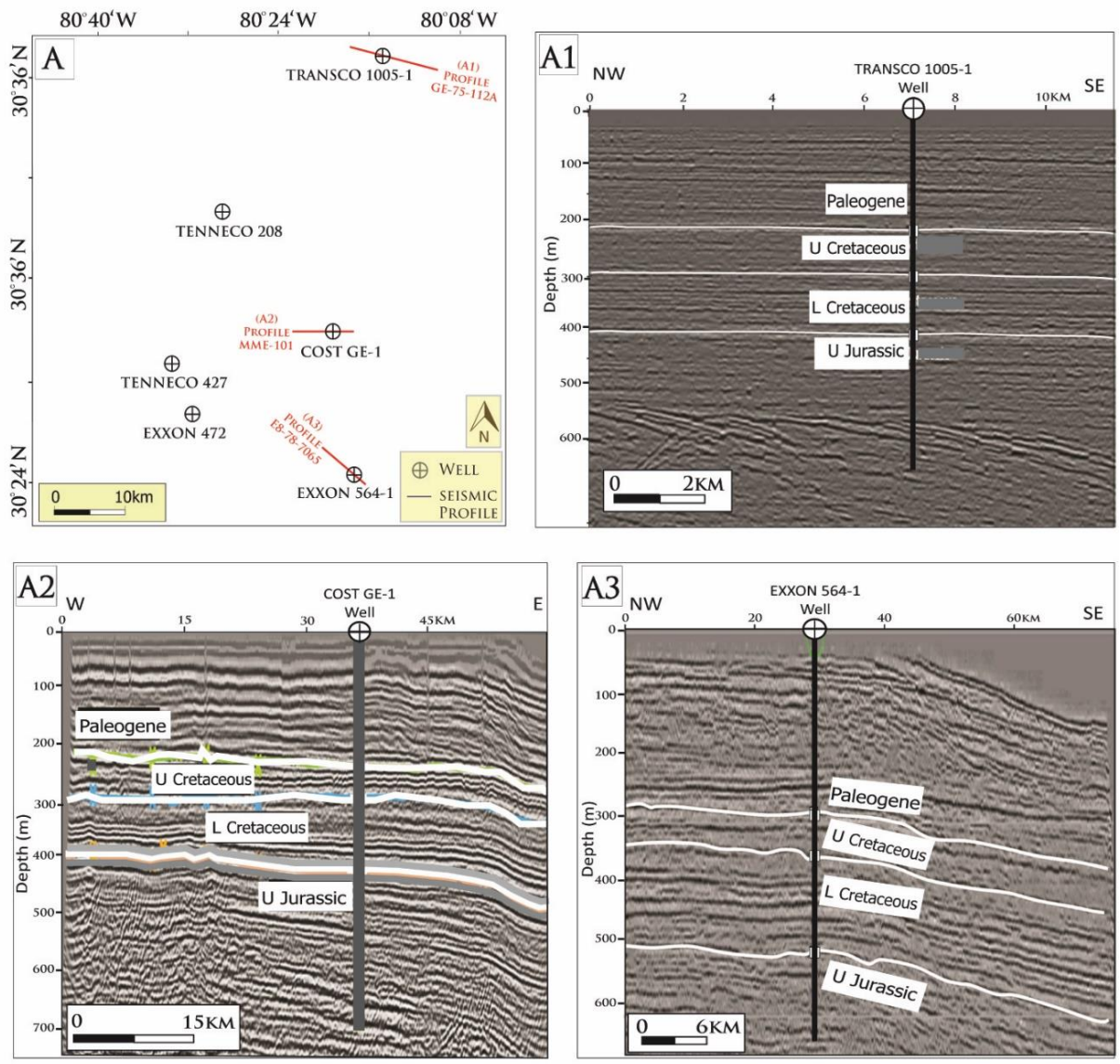

Figure 2-6: Seismic-well tie analysis for tree wells: Panel A is the location map of the commercial wells in 6-2 Figure Southeast Georgia Embayment. Panel A1 is the seismic profile Number GE-75-112A intersected TRANSCO 1005-1-1 well. Panel A2 is the seismic profile Number MME-101 intersected COST GE-1 well. Panel A3 is the seismic profile Number E8-78-7065 intersected EXXON 564-1 well.

2.4.1 Calculation of CO_2 Storage Capacity

I developed an estimate of the regional CO_2 storage capacity offshore of the Lower Cretaceous section in the mid-south Atlantic Ocean by using the U.S. Department of Energy (DOE) National Energy Technology Laboratory (NETL) method (Gorecki et al., 2009; Goodman, 2011).

The US-DOE approach estimates CO_2 storage volume based on geologic parameters such as formation area, thickness, and porosity (Brennan et al., 2010; Goodman et al., 2011; Global, 2012). Goodman et al. (2011) used the static volumetric methodology, and the CO_2 storage prospective resource estimation excel analysis (CO_2-SCREEN) tool developed by the U.S. Department of Energy National Energy Technology Laboratory (DOE-NETL) (equation 2.1). The equation 2-1 is mathematically expressed:

$$GCO_2 = A \times hg \times \varphi \times \rho \times E \qquad 2\text{-}1$$

Where, GCO_2 is the total mass of CO_2 in a giga ton (Gt), A is target area (in square meter), hg is gross strata thickness (in meter), φ is the effective porosity, ρ is CO_2 density in-unit kilogram per cubic meter (kg/m3), ρCO_2 is the average CO_2 density evaluated at pressure and temperature that represents storage conditions anticipated for a specific deep saline aquifer. The CO_2 density transforms the volume of CO_2 in the reservoir into mass. As a result of heat transfer from the inside to the exterior of the earth, (Holloway, 2007) found that the average temperature in many sedimentary basins rises by 25–308 ºC/km below the ground surface or sea bed. However, geothermal gradients vary widely, both within and between basins (Tissot and Welte, 1978). The subsurface units suitable for geologic carbon sequestration, however, are 800 meters or deeper below ground and seem to have higher pressure and temperature at depths greater than the CO_2 critical point. This indicates that CO_2 injected at these temperatures and pressures will be supercritical.

CO_2 and certain other supercritical gases possess gas viscosity, which reduces resistance to flow compared to a liquid, and semi-liquid density, which significantly reduces the volume required to store a given mass of fluid. Carbon dioxide behaves as a supercritical fluid at temperatures and pressures above the critical points of 30.85 °C and 7.38 MPa. The 800m depth condition is a reasonable guess that varies based on the geothermal gradient and formation pressure at a given location (Bachu, 2003). The pressure in the pore spaces of sedimentary rocks is identical to hydrostatic pressure, which is the pressure generated by a column of water at a corresponding elevation to the depth of the pore space. This is because the pore space is frequently filled with water and, though in a convoluted manner, is connected to the ground surface. When the pore space is not connected to equilibrium with the surface, the pressure exceeds hydrostatic, and overpressure occurs. CO_2 density rises dramatically when it is stored underground, resulting in a volume reduction at depths of 600–1000 m, depending on geothermal conditions and pressure (Ennis-King and Paterson, 2001).

Scholle (1979) pointed out that pressure and temperature data for the COST GE-1 were identified based on three temperature logs. The temperature of the lower Cretaceous is ranged between 72.3 °C at the top and 81.4 °C at the bottom, with a geothermal gradient of 16 °C/km. Based on the geothermal gradient at the COST GE-1 well, I estimate the temperature at the target depth in the study area. The parameters (A, h, and φ) are the yield of the total pore volume of the interesting section. The (ρ) parameter is the volume conversion to the mass of CO_2 and the efficiency factor (E) is reducing the total CO_2 mass for storage to an accurate realistic value. Related to the specific aquifer (Table 2-1), the efficiency factor has been determined by several factors (Zhou et al., 2008; Gorecki et al., 2009b; van der Meer and Yavuz, 2009; Goodman et al., 2011). According to the USDOE approach, storage efficiency is a function of aquifer characteristics such as area, thickness, and porosity, the product of which represents the aquifer pore volume, as well as

displacement efficiency components such as areal, vertical, and microscopic, and is expressed as the product of these individual efficiencies (Gorecki et al., 2009c; Gray, 2010; Goodman et al., 2011).

Table 2-1: Numerical method and Monte Carlo method for saline formation efficiency factor (percent) at the formation scale that has determined by several factors (Preston et al., 2009; Goodman et al., 2011).

Lithology	Monte Carlo Method (E%)			Numerical Method (E%)		
	P_{10}	P_{50}	P_{90}	P_{10}	P_{50}	P_{90}
Clastic	1.86	2.7	6	1.2	2.4	4.1
Dolomite	2.58	3.26	5.54	2	2.7	3.6
Limestone	1.41	2.04	3.27	1.3	2	2.8

Goodman et al. (2011) used Monte Carlo sampling to calculate both local and regional-scale storage efficiency values based on statistical properties (such as mean values, standard deviation, ranges, and distributions) that describe geologic and displacement parameters for the three lithologies: clastics, dolomite, and limestone. They obtained slightly lower values for storage efficiency (E) than Gorecki et al. (2009). Calculating efficiency in saline formations is stated in equation (2-2):

$$E_{saline} = E_{AN/AT} \times E_{HN/Hg} \times E_{\phi e/\phi t} \times E_a \times E_v \times E_d \qquad 2\text{-}2$$

Where, $E_{An/At}$ is the percentage to total area ratio that is ideal for CO_2 storage. $E_{Hn/Hg}$ is the fraction-to-gross-thickness ratio that meets the porosity and permeability standards for CO_2 storage. The ratio of linked porosity to total porosity is represented by $E_{Øe/Øt}$. E_A is the effective aquifer area. E_v is volumetric displacement. E_d is microscopic displacement. The net to total area ratio $E_{An/At}$ is the proportion of the aquifer area suitable for CO_2 storage expressed as a net-to-

gross thickness ratio. $E_{Hn/Hg}$ is the fraction of the geological formation in the vertical dimension that meets the porosity and permeability requirements for CO_2 injection and storage, and $E_{Øe/Øt}$ is the effective (interconnected) porosity to total porosity ratio. These coefficients have a value of unity in local-scale assessments or, more broadly, when the effective aquifer area, thickness, and porosity are known. In this method, I used the value of the efficiency factor suggested by Goodman (2011) (Table 2-1).

Goodman et al. (2016) demonstrated that geology data uncertainty has a greater impact on storage estimation than the approach that has been used. Thus, it is critical to determine the geologic qualities and ranges of storage efficiency factors for certain geologic parameters to improve or refine storage estimates.

However, due to the legacy of seismic data and the relatively limited well data available over 200,000 Km^2 study area, uncertainty associated with subsurface data gab is conceded into the storage resource assessment. The potential capacity of the several reservoirs of the whole Lower Cretaceous section has been calculated using all parameters in equation (2-1).

2.5 Results and discussions

2.5.1 Well data analysis

The well log interpretation is the most fundamental geophysical approach for geological and geophysical reservoir characterizations. The density log (RHOB) provides data for lithology interpretation, porosity calculation, and petrophysical properties. The Gamma Ray (GR) log is used for lithology interpretation, porosity, and permeability calculations. The spontaneous potential log (SP) is useful for lithology identification and permeability calculation. Both GR and SP have a similar response to porous layers and can be used to determine lithology and correlate stratigraphy. Density logs (RHOB) provide a continuous record of the bulk density, which is

determined by the porosity of the formation and the fluid content of the pore spaces. GR and ROHB logs for TRANSCO 1005-1 well, COST GE-1 well, and EXXON 564-1 well have stratigraphically interpreted and correlated in this study to have similar equivalents of the sedimentary sequences (Figure 2-5). Related to the sidewall core analysis on the COST GE-1 well, the porosity has been valued between 0.12 and 0.35 and the permeability has been estimated between 9.87×10^{-18} and 5.4×10^{-13}m 2 within the Lower Cretaceous strata (Scholle, 1979).

The Lower Cretaceous strata, between depth 1,798m and 2,195m, has fourteen lithological intervals which are mainly composed of varying proportions of calcite, clay, shale, sandstone, limestone, and dolomite with carbonite materials (Scholle, 1979) (Table 2-2).

For the COST GE-1 well, the net porosity was geophysically derived by the ratio between the density log (RHOB) and the gamma-ray log (GR). The values calculated from the log data were then compared to the measured values from the conventional and sidewall cores for Lower Cretaceous lithological units to identify potential reservoirs and seals (Figure 2-7). That indicates a significant potential for CO_2 storage, where high primary and secondary porosity values ranged from 0.20 to 0.33. Accounting for most of the greatest permeability range of 1.97×10^{-13} to 5.43×10^{-132} recorded in the Lower Cretaceous section at the well COST GE-1. Porosity versus Permeability (Figure 2-8) shows the comparison correlation between porosity and permeability. A linear relationship (correlation coefficient) basically exists between the porosity and permeability of the Cenozoic (R=0.58, and slope=10.35), Upper Cretaceous (R=0.45, and slope=0.35), Lower Cretaceous (R=0.63, and slope=0.87), and Upper Jurassic (R=0.83, and slope=1.96) rocks.

Table 2-2: The fourteen lithological intervals of the Lower Cretaceous strata, between depth 1,798 and 2,195 m in COST GE-1 well, after (Scholle, 1979).

Unit	Depth		Lithology	Porosity
	ft	m		
1	5900	1798	Shale, gray, silty, calcareous, micaceous, and sandstone	low
2	5990	1826	Shale, silty, calcareous, micaceous, non-calcareous sandstone.	very low
3	6080	1853	More shale, slightly calcareous, carbonaceous, fossiliferous,	low to moderate
4	6320	1926	Coarse to medium crystals, dense, and fossil fragments.	low to high
5	6500	1981	Partly sandy, dense silty, hard, calcareous to non-calcareous	low
6	6800	2073	Sandstone, shell, sandstone, anhydrite, and gypsum.	low to high
7	6890	2100	Limestone, shale, very fine-grained calcareously cemented sandstone, and anhydrite with denes dolomite.	moderate
8	7020	2140	Dolomite, finely crystalline to dolomite, limestone increasing with depth, shale, and sandstone,	low to high
9	7070	2155	Limestone, fossifillerous, dolomite, and non-calcareous.	low to high
10	7160	2182	Shale and sandstone, much calcareous cement.	moderate to low
11	7200	2195	Shale, sandstone, and silty shale with calcareous cement. Limestone, some dolomite, and fossifillerous to non-fossifillerous	high
12	7400	2256	Shale, some gravel trace, dolomite, and fossifillerous to non-fossifillerous.	high
13	7490	2283	Lithology like unit 12 with decreasing shale, increasing dolomite,	high
14	7910	2411	Shale to fine sandstone, gravel, faintly calcareous, and shale non-calcareous, dolomite with some clayey coatings, non-fossifillerous, much coal, anhydrite, and sandy dolomite.	moderate

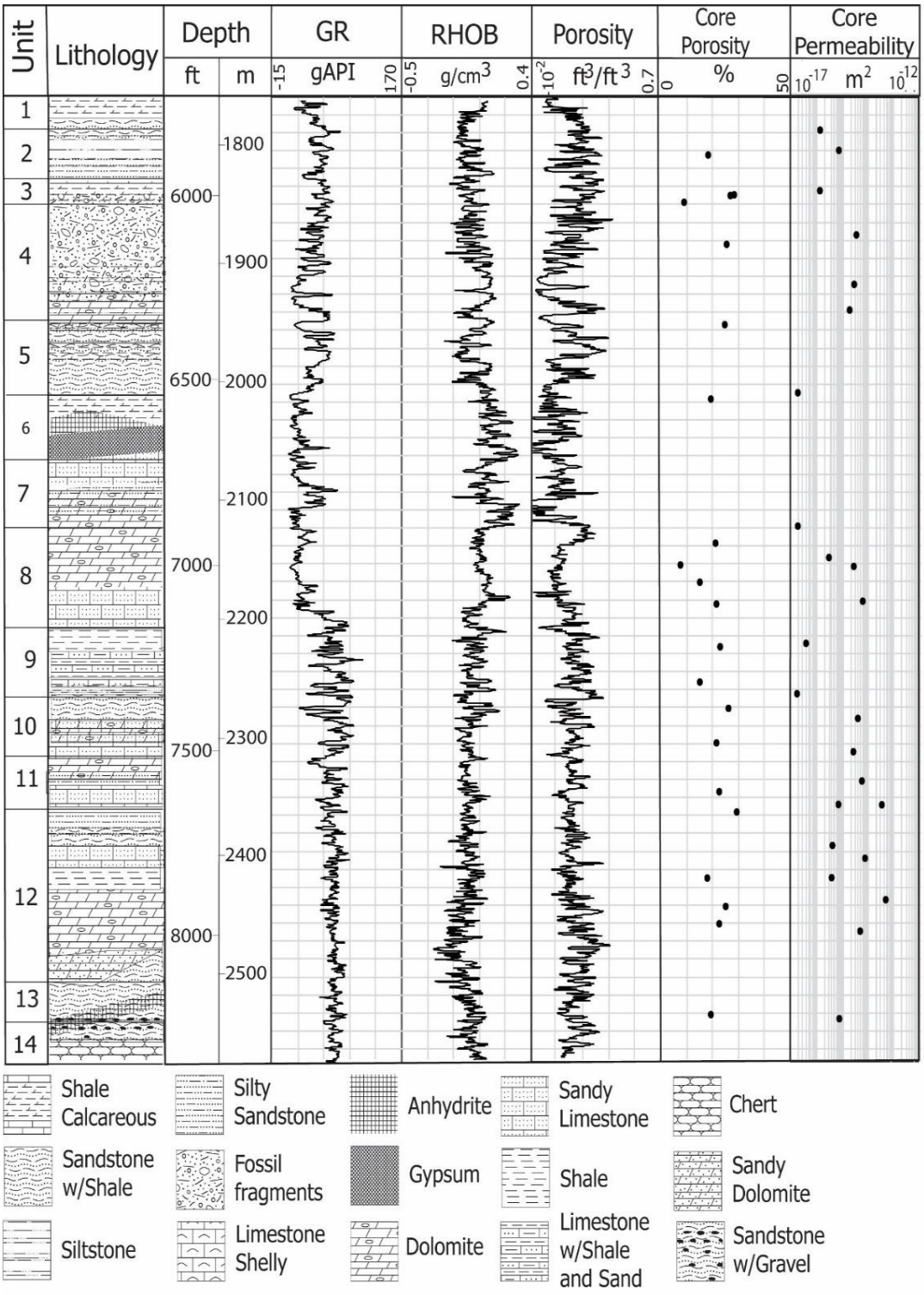

Figure 2-7: Analysis of density log and gamma-ray log to generate porosity log that is compared with estimated porosity from core samples analysis from COST GE-1 well.

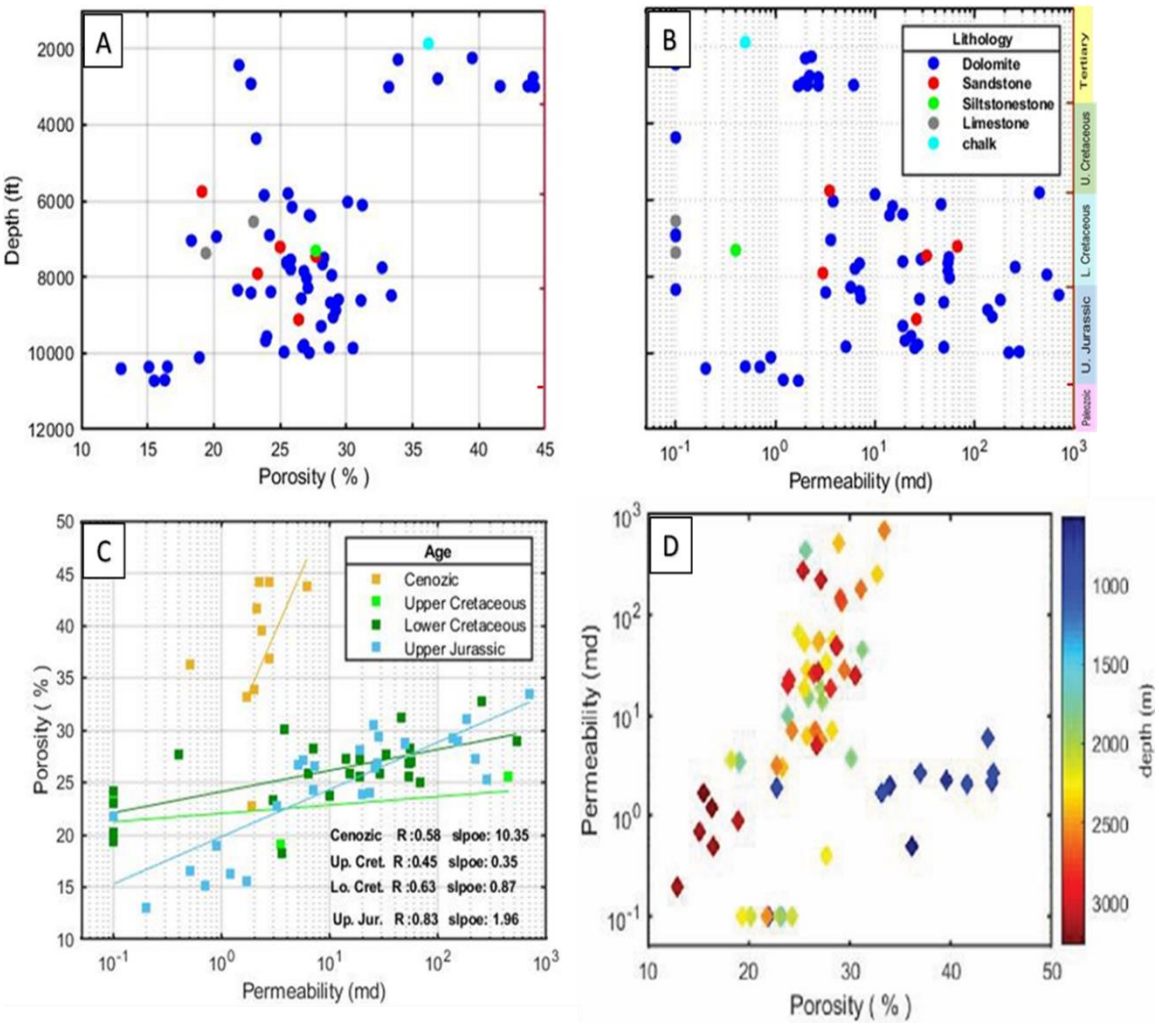

Figure 2-8: Porosity and permeability measured on conventional and sidewall cores from the COST GE-1 well as a function of depth. For the Cenozoic, Mesozoic, and Paleozoic rocks panel A is the porosity with depth, panel B is the permeability with depth, panel C is the porosity and permeability relationship with the correlation coefficient (R), and panel D is the porosity and permeability with the depth function.

2.5.1 Geological CO_2 storage

In a practical CO_2 storage evaluation, Chadwick et al. (2008) identified the ideal geological criteria for a reservoir depth of 1,000–2,500 m with a thickness of 21–50 m, where porosity is greater than 0.20 and permeability is greater than $1.978\times10\text{-}13^2$. The ideal seal thickness is 100m with lateral continuity and no major faults or capillary entry pressure. (Table 2-3).

The Lower Cretaceous section from the COST GE-1 well was described in terms of lithology and rock properties through fourteen core samples (Scholle, 1979). Dolomite rocks are the most dominant rocks in this section. Porosity and permeability of the different stratigraphic intervals were the primary basis for the identification of the main storage units. The reservoirs and seals are classified and evaluated with the observance of the positive indicators of the CO_2 storage criteria based on (Chadwick et al., 2008) (Figure 2-9). Three reservoirs are separated by three seals have been identified within the Lower Cretaceous section. Figure 2-7 illustrates the fourteen intervals that appear to be most prospective for permanent CO_2 offshore storage. Figure 2-10 reveals structure maps for top and bottom topographic surfaces, and thickness of the lower cretaceous. The Lower Cretaceous section ranges in depth between 1,798 m and 2,539 m and consists of dolomite interbedded with sandstones and calcareous silty shales. Based on the rock composition with rock properties, this section, (Table 2-2) records the lithologic description and porosity value with depth for the COST GE-1 well based on core analyses and geophysical logs. Figure 2-9 provides the potential CO_2 storage reservoirs and seals based on the rock properties as compared with the favorable conditions for CO_2 storage (Chadwick et al., 2008). Scholle (1979) pointed out that there is impermeable shale with calcareous shale layers interbedded with the highly permeable dolomite in the COST GE-1 well. However, a few samples of sandstone were marked between 1,768m and 2,530 m, the high primary and secondary porosity with high permeability, which is suitable to be a reservoir rock for CO_2 sequestration. This section is

dominated by dolomite with porosities that vary widely and unsystematically with depth from 0.17 to 0.32, and the permeability is between 2096×10-16 and 5.43×10-13[2]. The porosity log was derived and calculated from well logs to fill hiatus between the core intervals (Figure 2-7).

Table 2-3: Ideal CO_2 geological storage criteria for reservoir properties and Caprocks (Chadwick et al., 2008; Chadwick et al., 2017).

Media	Properties	Positive Indicators	Cautionary Indicators
Reservoir	Static storage capacity	Evaluated effective CO2 storage capacity greater than total injected CO2	Evaluated effective CO2 storage capacity equal to total injected CO2
	Dynamic storage capacity	Predicted injection-induced pressures below the rate of inducing geomechanical damage to the reservoir or caprock.	Geomechanical instability limits reaching the predicted injection-induced pressures.
	Depth (m)	Greater than 800	Less than 800
	Thickness (m)	Greater than 50	Less than 20
	Porosity	Greater than 0.20	Less than 0.10
	Permeability (m2)	Greater than 4.93 × 10−12	Less than 1.97 × 10−13
	Stratigraphy	Capacity much larger than total injected CO2	Capacity ≤ total injected CO2
Caprocks	Lateral stratigraphy	Uniform and small or no fault	Lateral variations and medium-to-large fault
	Thickness (m)	Greater than 20	Less than 20
	Capillary entry pressure	Greater than the maximum predicted injection-induced pressure increase	Equal to the maximum predicted injection-induced pressure increase

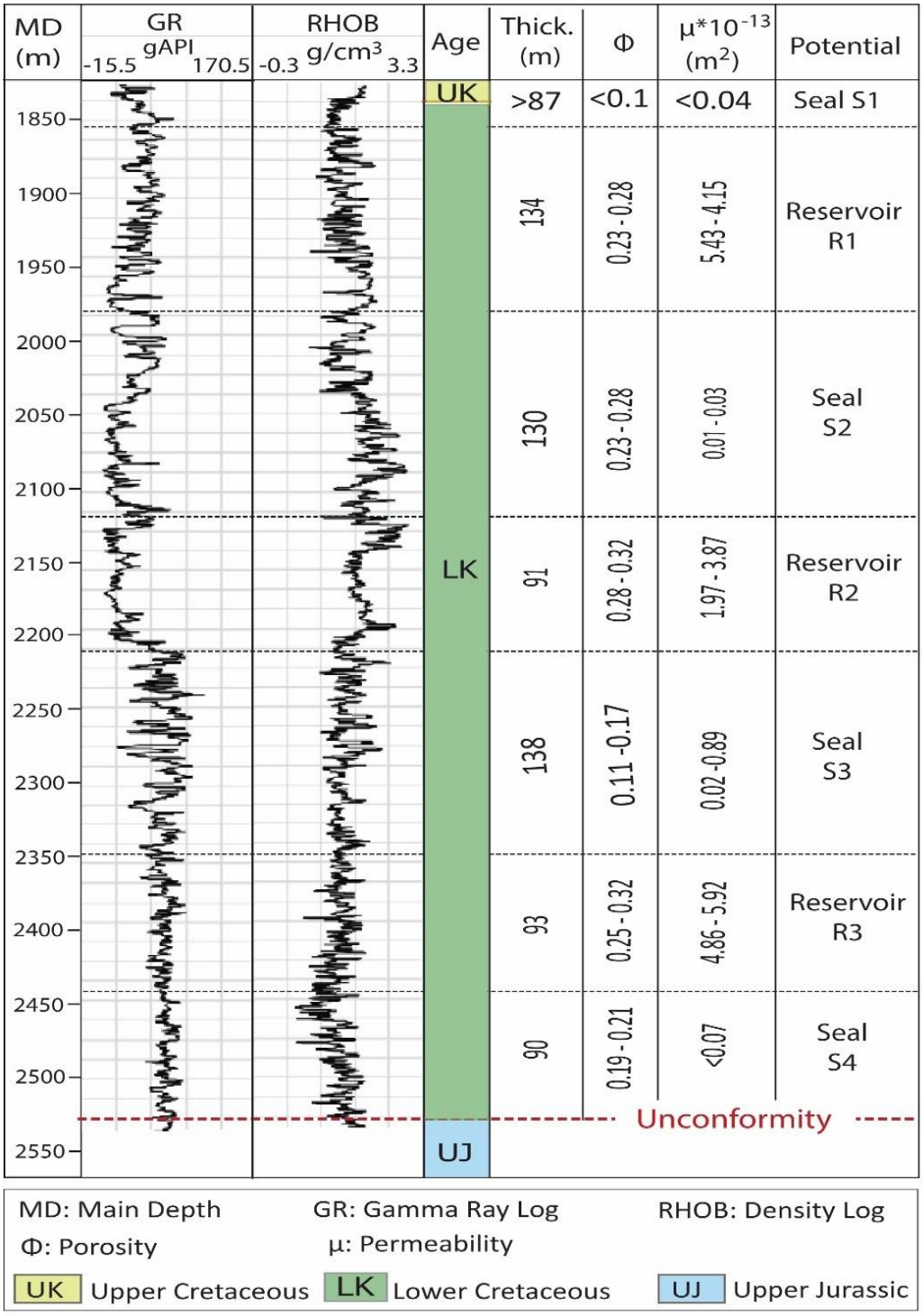

Figure 2-9: Characterizations of the storage elements; seals and reservoirs that are identified based on the geological and geophysical data at the COST GE-1 well.

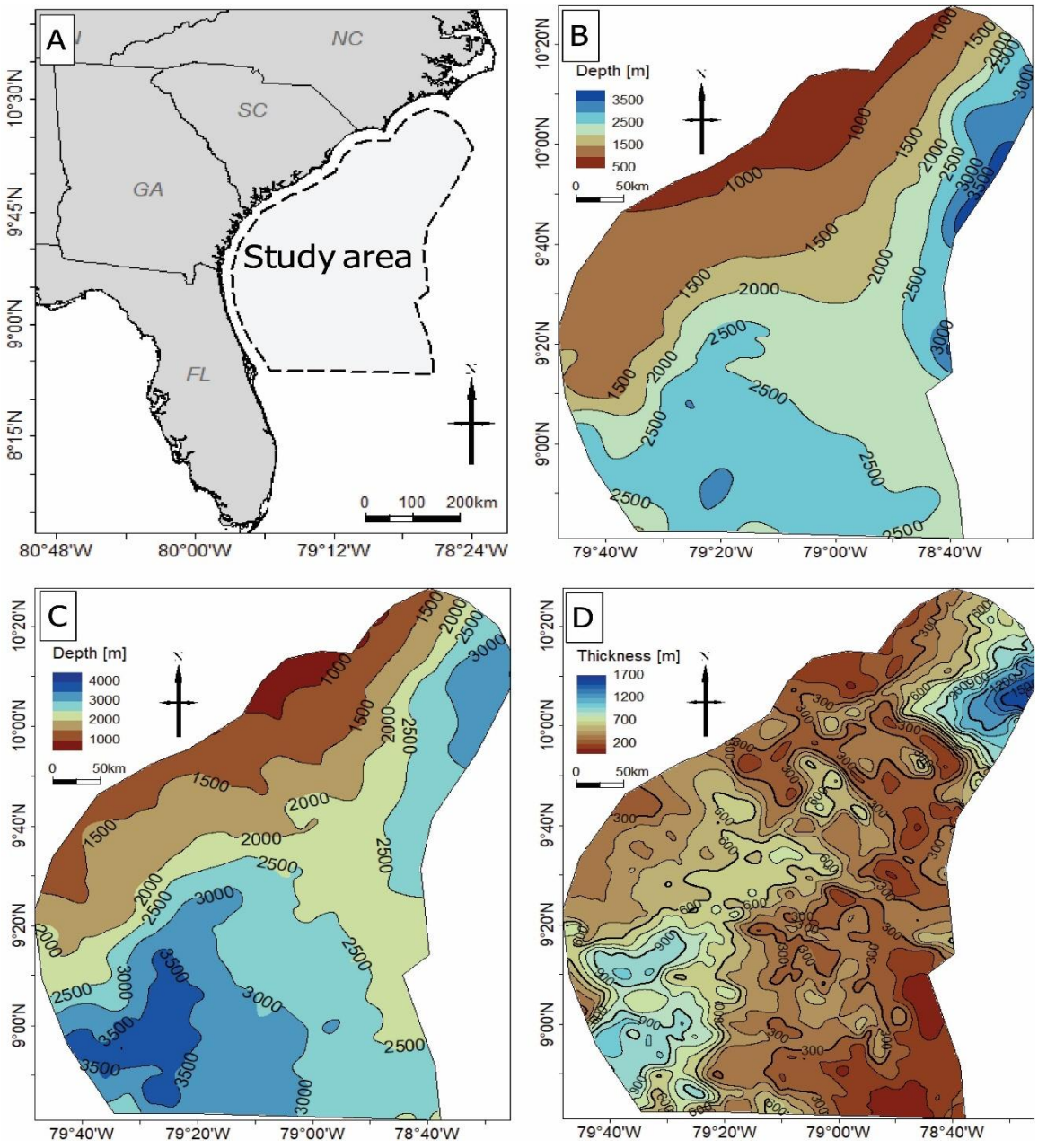

Figure 2-10: Structure maps of the study area; A is the location map for the top topographic surface of the Lower Cretaceous, B is the depth map for the bottom topographic surface of the Lower Cretaceous, and C is the thickness map of the Lower Cretaceous section.

2.5.1 CO_2 storage Capacity Calculations

The capacity for CO_2 storage potential of the Lower Cretaceous section was calculated based on the rock compositions and petrophysical properties at the COST GE-1 well. Three potential reservoirs are associated with four potential seals that were characterized and assessed in the Lower Cretaceous section. The three reservoirs are sealed by thick caprocks that are mainly composed of shale, siltstone, anhydrite, and limestone. These reservoirs are signed as (R1), (R2), and (R3), and their seals are signed (S1, S2, S3, and S4) (Figure 2-9). According to Scholle (1979), the trapping mechanism, characterized as an overlying seal, involves stratigraphic trapping through lateral facies variations. Figure 2-9 shows that reservoir R1 is ranged in the depth of 1,855-1,989m, reservoir R2 is ranged in the depth of 2,119-2,210m, and reservoir R3 is ranged in the depth of 2,349-2,442m. The composition of the three reservoirs; (1) R1 is composed of calcareous shale, anhydrite, and gypsum. (2) R2 is composed of limestone and shale. (3) R3 is composed of calcareous shale, anhydrite, fossil fragments, and gypsum. The average porosities of the reservoirs (R1, R2, and R3) are ranging from 0.23-0.28, 0.28-0.32, and 0.25-0.32, respectively. I used equation (1), which is developed earlier by Goodman et al. (2011), for applying the dolomite efficiency factors (E) at the formation scale are 2.0%, 2.7%, and 3.6% for probability 0.10, 0.50, and 0.90 respectively. The probabilities have been considered in this work for the parameter of Area (A) with wide thickness range values over the area to apply equation 1. To reduce the uncertainty that is incorporated in the variety of depth and thickness of the Lower Cretaceous section (Figure 2-10), CO_2 density was calculated based on the depth of each reservoir. For accuracy of CO_2 density values, the Lower Cretaceous section is divided into three depth zones: (1) shallow depth (SLK) is ranged of 300-1000m, (2) Depth at COST GE-1 well (GLK) is ranged of 1600-2450m, and (3) deep depth (DLK) is ranged of 3000-3500m.To identify the temperature for the reservoirs in the thee depth zones, I assumed that the geothermal gradient at COST GE-1 well (16º C) is constant across the study area (Figure 2-11 A) (Table 2-4). Based

on the Temperature Pressure Density graph suggested by Bachu (2003) (Figure 2-11 B). The density values of supercritical CO_2 were estimated based on the depth. (1) Reservoir R1 is 700, 722, and 760 kg/m3 at depths 1100, 1855, and 2550 m respectively. (2) Reservoir R2 is 708, 732, and 768 kg/m3 at depths 1300, 2120, and 2680 m respectively. (3) Reservoir R3 is 712, 740, and 778 kg/m3 at depths 1550, 2350, and 22860 m (Table 2-4).

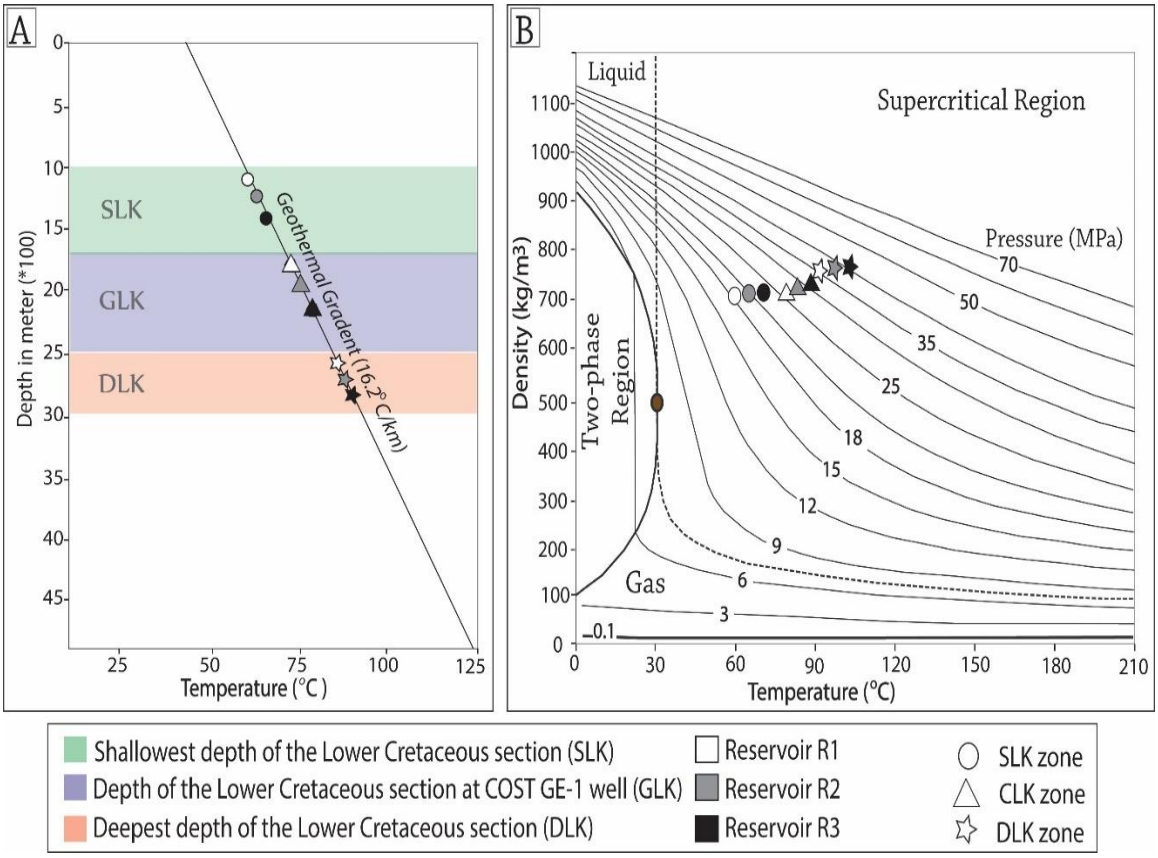

Figure 2-11: Panel A is the three reservoirs in three depth zones that are plotted in the geothermal gradient at the COST GE-1 well. Panel B is Time-Depth- Pressure graph to identify the density of supercritical CO_2 for three reservoirs in the tree depth zones of the Lower Cretaceous section.

Table 2-4:CO_2 density values that are estimated based on depth, temperature, and overburden pressure for the reservoirs at three depth zones.

Zone	Reservoir	Depth (m)	Temp. (ºC)	Pressure (MPa)	Density (kg/m3)
SLK	R1	1100	56.2	18-22	700
	R2	1300	58.6		708
	R3	1550	60.2		712
GLK	R1	1855	72.8	25-32	722
	R2	2120	76.2		732
	R3	2350	75.4		740
DLK	R1	2550	81.1	35-43	760
	R2	2680	85.4		768
	R3	2860	90.9		778

For the purpose of high accuracy and a comparison, I estimated the potential storage resources of the three reservoirs that have been calculated for local and regional areas. The local area has been detected where seismic profiles and wells data are densely concentrated in the Southeast Georgia Embayment, which covered approximately (10,000 Km^2). Region storage resource is approximately covered (200,000 Km^2) that I detected based on abundance and density of the data. I considered three probabilities values (P10, P50, and P90) of the geologic storage efficiency factor for each reservoir in both areas. For the integrity and safety of CO_2 storage, I interpreted and evaluated impermeable rock units that are signed as seals. Although the seismic interpretation indicated no significant fault was detected in the Lower Cretaceous section, the uniform lateral stratigraphy is a significant concern due to the lack of wells data in the study area.

Local and regional potential storage resources were calculated for the Lower Cretaceous potential reservoirs. The total capacity of three storage resources with a geologic storage efficiency (E) of dolomite between 0.65 – 5.40 percentage ranged between 49 and 377 Mt of CO_2 for the local area, and between 451 and 4705 Mt of CO_2 for the regional area (Table 2-5, and 2-6) (Figure 2-12).

At P50, the average storage resource per unit area of the Lower Cretaceous section in the study area is approximately 1.15 Mt CO_2/Km^2. Reservoir R1 has a maximum storage resource value of > 0.42 Mt CO_2/Km^2. In reservoirs, R2 and R3, the middle and lowest values at P50 are equal to or less than 0.37 Mt CO_2/Km^2.

Table 2-5: Probability The physical parameters for the three reservoirs applied in the NETL method (DOE equation) in the local and regional zones.

Zone	Reservoir	Area (km^2)	Gross Thickness (m)		Total Porosity (%)		Pressure (MPa)		Temperature (°C)	
			Mean	Std Dev	Mean	Std Dev	Mean	Std Dev	Mean	Std Dev
Local	1	10,000	134	0.0093	0.28	0.0012	26	0.0004	72.8	0.06
	2	10,000	91	0	0.32	3×10^{-18}	29	0.0193	75.4	0.006
	3	10,000	93	0	0.32	0	32	0.0385	76.2	0.06
Regional	1	200,000	83	0.193	0.245	0.012	26.3	0.1925	70	1.6
	2	200,000	60	0.0001	0.3	3×10^{-17}	29.3	0.1925	73.4	1.6
	3	200,000	63	0.0001	0.285	0	32.6	0.3849	75.5	0.06

Table 2-6: Volumetric CO_2 storage capacity (GCO_2) in Mt with the storage efficiency factor (E%) at P10, P50, and P90 for the three Lower Cretaceous reservoirs within local and regional zones in the Mid–South Atlantic Ocean.

Zone	Reservoir	Storage Resource (Mt)			Storage Efficiency (%)		
		P_{10}	P_{50}	P_{90}	P_{10}	P_{50}	P_{90}
Local	1	19.12	60.45	146.57	0.69	2.19	5.31
	2	14.85	47.77	117.57	0.67	2.17	5.34
	3	15.01	51.08	122.56	0.65	2.2	5.28
Regional	1	182.63	635.83	1628.72	0.65	2.18	5.25
	2	88.54	414.75	1574.37	0.67	2.22	5.4
	3	179.67	597.97	1502.37	0.67	2.17	5.3

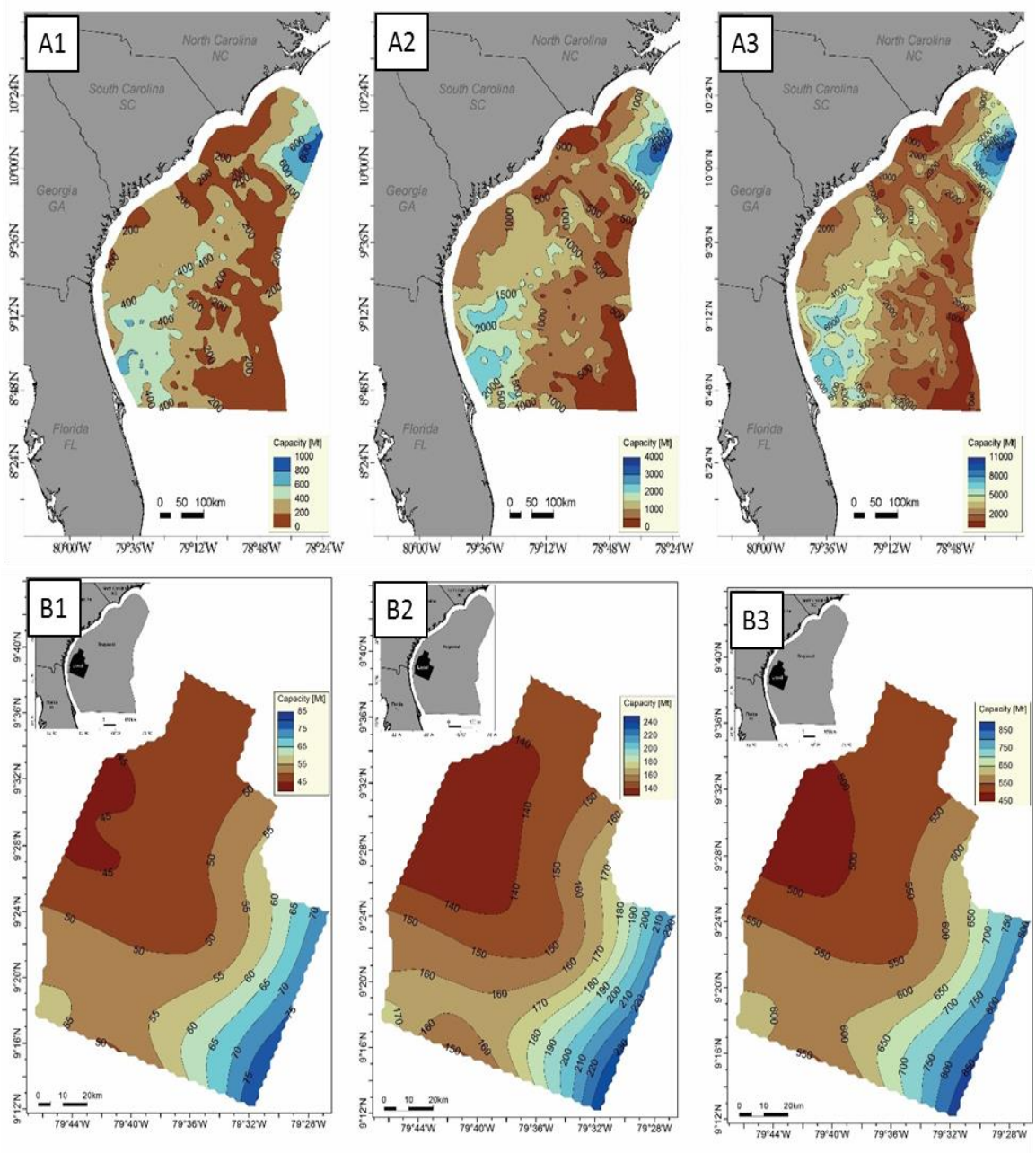

Figure 2-12:The total CO_2 storage capacity in mega tons (Mt) for the Lower Cretaceous section. A1 is the total capacity at P10, A2 is the total capacity at P50, and A3 is the total capacity at P90 in the regional area. Panels B1 is the total capacity at P10, B2 is the total capacity at P50, and B3 is the total capacity at P90 in the local.

2.6 Summary and Conclusions

This chapter presented the first comprehensive study to identify, and evaluate the CO_2 storage potential of mid-south Atlantic offshore in the Lower Cretaceous section, Southeastern United States. Based on the analysis of three wells data in Southeast Georgia Embayment, CO_2 geological storage resource has provided a determination of three significant permeable storage strata that are isolated by impermeable seal strata in the depth of 1,767.84-2,529.84 m. Based on analysis of COST GE-1 well of this section, I identified widely and unsystematically porosity ranged from 0.17 to 0.32, and widely permeability ranged between 2096×10^{-16} and 5.43×10^{-13} m^2 of layers that are composed of low percent of sandstone and high percent of dolomite. These layers are suitable reservoir rock that is qualified to be permanent CO_2 storage.

The US-DOE methodology is used for calculating pore volume spaces to estimate the geologic CO_2 storage potential capacity in billion tons (Gt). The capacity for CO_2 storage potential of the Lower Cretaceous section is calculated based on the rock compositions and petrophysical properties at the COST GE-1 well. Three potential reservoirs are associated with four potential seals that are characterized and assessed. According to Scholle (1979), the trapping mechanism, characterized by an overlying seal, involves stratigraphic variations. The prospective storage resources of the three reservoirs were calculated locally where seismic profiles and wells data were densely concentrated in the Southeast Georgia Embayment (10,000 Km^2), and regionally where I suggested as a regional storage resource (200,000 Km^2). I considered three probabilities values (P10, P50, and P90) of the geologic storage efficiency factor for each reservoir in both areas. The result of this chapter exhibits that there is approximately from 3.9 to 28.3 Gt locally, and from 68.011 to 546.205 Gt regionally of CO_2 could be safely stored in three Lower Cretaceous reservoirs with geologic storage efficiency from 2% to 3.6%.

The average storage resource potential is approximately 1.15 Mt of CO_2 that could be safely stored per 1 Km^2 offshore of the Lower Cretaceous section at a probability of 0.5. The largest storage resource value for Reservoir R1 was > 0.42 Mt CO_2/Km^2. The middle and lowest values at P50 in reservoirs R2 and R3 are less than or equal to 0.37 Mt CO_2/Km^2.

The uncertainty associated with subsurface data gab is incorporated into the storage resource evaluation due to the legacy of seismic data and the relatively limited well data available over the study area.

CHAPTER III

ESTIMATES CO_2 STORAGE RESOURCE PROSPECTIVE IN ATLANTIC OFFSHORE UPPER JURASSIC SEQUENCES, SOUTHEASTERN UNITED STATES

3.1 Introduction

Carbon Capture and Storage (CCS) is a timely technology for reducing greenhouse gas emissions and limiting the global climate. CCS is an advanced tool for providing a variety of renewable energy sources to satisfy future energy demand in the United States and globally. The U.S. Department of Energy-National Energy Technology Laboratory (DOE-NETL) initiative provides the Mid Atlantic Offshore Carbon Storage Resource Assessment, which focuses on improving the efficiency of carbon dioxide (CO_2) storage technology. Gross greenhouse gas emissions from fossil fuels have increased by 2 percent since 1990 (Usepa, 2022). However, emissions fluctuate throughout the year due to economic changes, increased fuel, and other variables. That is, compared to 2020, greenhouse gas emissions dropped an around 1.7 and 9.1 percent in 2019 and 2020 in the United States (Figure 3-1) (Zhongming et al., 2020)

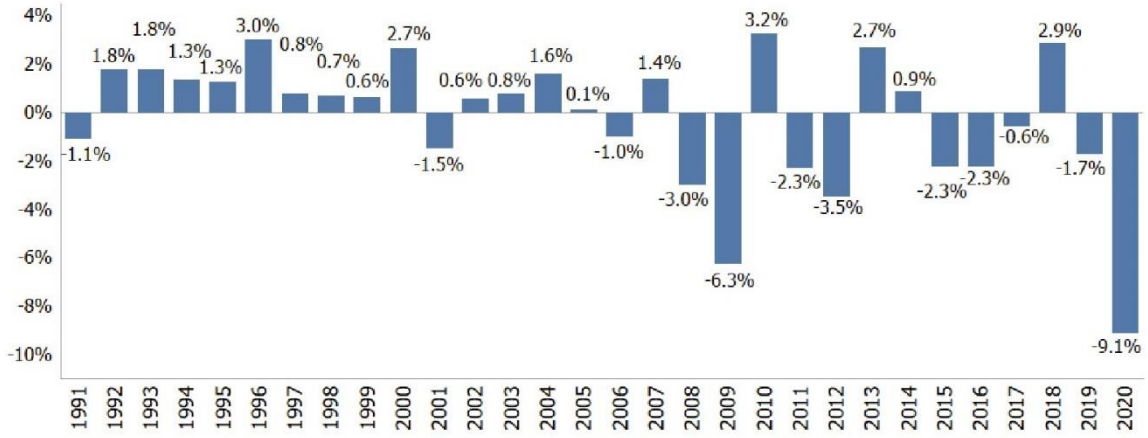

Figure 3-1: Annual greenhouse gas emissions percentage (y-axis) fluctuate due to economic changes (Zhongming et al., 2020).

Since the Norwegian Sleipner project in the North Sea was an early successful commercial deployment possibility, the storage capacity of offshore reservoirs is anticipated to be considerable. Relatively few offshore CO_2 storage resource studies have been performed in the southeast U.S. A variety of academic and government bodies across the world have developed several approaches for assessing carbon dioxide storage capacity in various geological media. The US Department of Energy created a practical methodology for estimating storage capacity of large-scale saline aquifers by assessing the total aquifer storage capacity and utilizing a sequence of Efficiency Factors that trying to appropriate for geologic heterogeneity in the form of a probabilistic cumulative total value of fractions (Laboratory and Energy 2008).

Although subsurface deep saline formation is exceptional, most renewable energy sources are offered to meet long-term energy demand. Within an extensively studied deep saline aquifer, the study site consists of the stratigraphic interval with several penetrated wells. A successful play on reservoir horizons and an overlaying seal interval make up this interval. By integrating available data and evaluating storage capacity, the targeted site can be characterized in terms of potential

CO_2 storage. I emphasize uncertainty, incorporating insufficient data and creating the first screening method extended to the poorly understood geological strata with immense CO_2 storage potential.

The objective of this chapter is to address the analysis of the Upper Jurassic rocks in the offshore region southeastern United States (Figure 3-2), approximately covered by 180,000 Km^2 of two-dimensional legacy seismic reflection profiles. Thus, it applies the most suitability of recently published techniques regarding storage capacity calculations of the conventional reservoirs.

3.2 Study area and Geological perspective

The study area extends between 200 to 500 km offshore, encompassing the inner continental shelf to portions of the continental slope. It is covered approximately 175,000 Km^2 along southern the mid-Atlantic states of North Carolina, South Carolina, Georgia, and Florida. The study area comprises three major sedimentary basins: Carolina Trough, Blake Plateau, and Southeast Georgia Embayment (Figure 3-2).

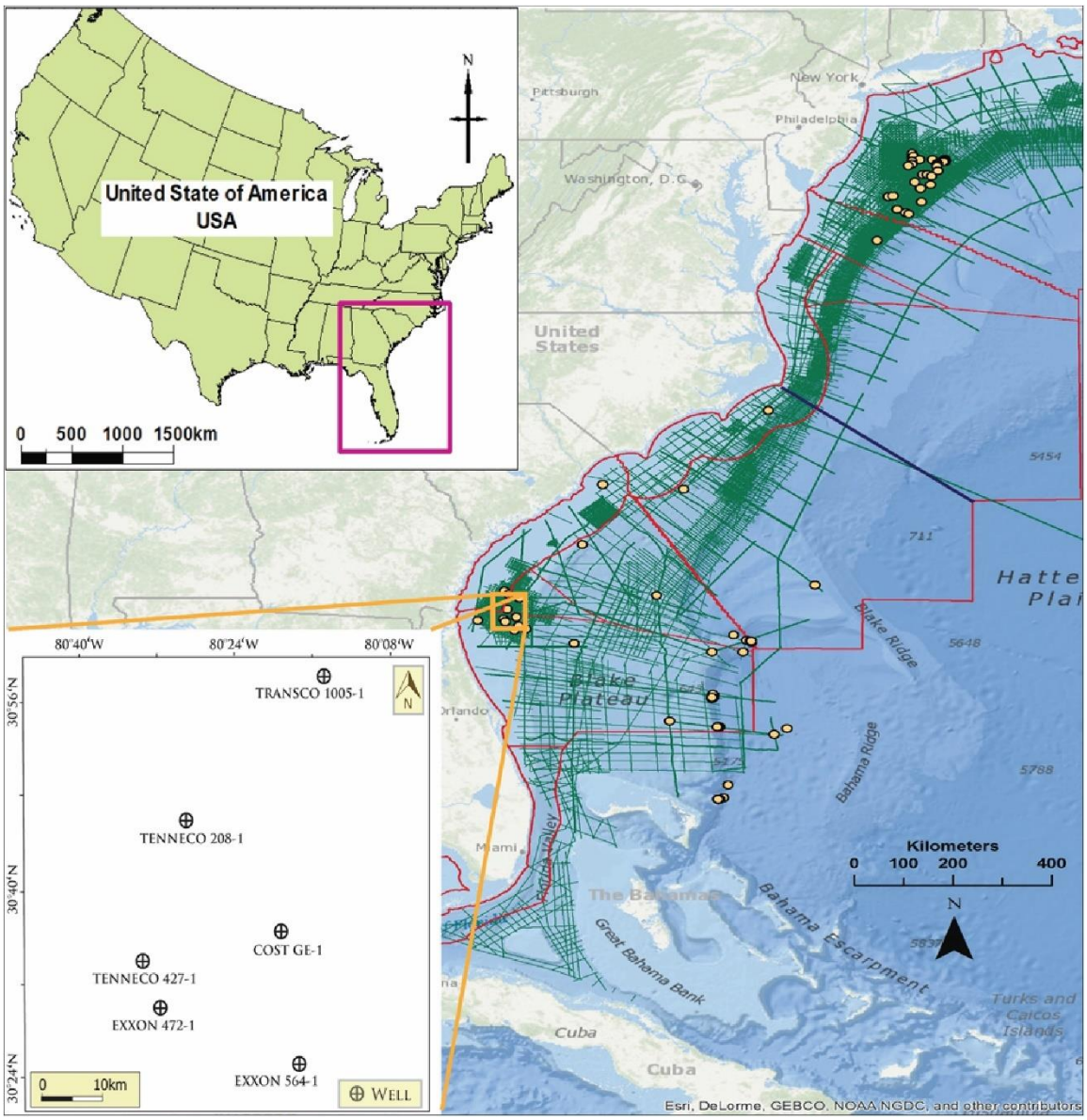

Figure 3-2: Location map of available geophysical and geological data; legacy Atlantic margin seismic reflection surveys and location of the wells in the Southeast Georgia Embayment.

The evolution of the Atlantic continental margin, including the study area, is broadly characterized by the terminal collision of the Laurentian and Gondwanan continents in the Late Paleozoic Era followed by continental rifting beginning in the earliest Triassic time following (Poag, 1978; Dillon et al., 1979; Scholle, 1979; Dalziel et al., 1994; Poppe et al., 1995). Mesozoic rifting involved local tectonic subsidence in early restricted extensional basins, followed by regional thermal subsidence along the eastern North American margin. (Dillon et al., 1983; Pinet and Popenoe, 1985; Badley et al., 1988; Dillon and Popenoe, 1988; Dalziel et al., 1994). The mid-south Atlantic United States passive continental margin contains thick (7-8 km) post-rift Jurassic– Holocene sediments on the Blake Plateau basin (Dillon et al., 1979; Dillon et al., 1983). The offshore saline basins contain a thick section of Jurassic–Paleogene sedimentary rocks above Post-Rift Unconformity that lies at depths of 3,048–7,620m (Maher and Applin, 1971; Scholle, 1979; Lizarralde et al., 1994). The post-rift sediments overlie a regional unconformity known as the post-rift unconformity that cuts across the entire region after rifting between Africa and North America ceased and marked the transition to wide-spread sediment deposition during the drift phase around 165-190Ma (Poag, 1978; Poppe et al., 1995). The oldest post-rift sediments are of the Jurassic age and are the product of rapid clastic sedimentation from erosion followed by a period of evaporating deposition and then initiation of broad, shallow water, carbonate deposition with some terrigenous intrusions (Dillon et al., 1982; Dillon and Popenoe, 1988). The Jurassic section thickens seaward, and estimates from geophysical and stratigraphic studies suggest thicknesses of at least 7-8km in the basins (Dillon et al., 1979; Dillon et al., 1983).

The sedimentary rocks of interest as cap rocks and storage zones consist of Jurassic -age mudstone, shale, and sandstone sequences that generally dip to the east toward the continental slope (Maher and Applin, 1971; Poag, 1978; Pinet and Popenoe, 1985; Poppe et al., 1995). Previous studies have identified porous and permeable sandstone units within Upper Cretaceous

and Lower Cretaceous in mid-south Atlantic planning area (Almutairi, 2018; Almayahi et al., 2022). The Upper Jurassic sequences at depths between approximately 2,225 and 3,500 m (Scholle, 1977; Pinet and Popenoe 1985). Stratigraphic sequences on this passive margin are extensive lateral continuity and relatively minor structural disturbance (Dillon and Popenoe, 1988; Dalziel et al., 1994; Poppe et al., 1995).

This interval is overlain by Cretaceous mudstone and shale that extends regionally across the study area that is considered as a cap rock to ensure CO_2 storage confinement. High-level static storage resource estimates reported in previous work suggest storage potential exists in Cretaceous-age sandstones in the Southeast Georgia Embayment and Blake Plateau saline basins (Almutairi, 2018; Almayahi et al., 2022). This involved extensive efforts in data compilation, preservation, digitization, and integration into map grids and models.

The outcomes are used to define offshore-specific site selection criteria and calculate offshore-specific probability values for storage efficiency parameters that were used, respectively, to help identify regional storage resources and inform volumetric estimates of storable quantities for deep saline reservoirs of interest. Localized estimates of storable quantities derived from simplified dynamic models and site-specific storage efficiencies are reported for a selected area near the Great Stone Dome structure. The results of this work provide a foundation for future CCS development efforts in the mid-Atlantic offshore region when the market conditions are appropriate. As part of this procedure, a systematic work-flow has been employed to quantify and categorize CO_2 storage resources for the mid-Atlantic United States offshore region extending from Maryland to Massachusetts. The workflow includes (1) data integration and physical property mapping, (2) regional-scale storage resource calculations, and (3) local-scale storage resource calculation refinement. Results from each subregion were used to delineate selected areas to refine static prospective resource estimates and conduct dynamic simulations of CO_2

injection and storage performance for zones of interest. Risk factors identified as an essential part of this study, such as basin age and maturity, sediment lithification, and hydrostatic pressures, are integrated with recommended best practices for onshore geologic CO_2 storage. US Department of Energy National Energy Technology Laboratory (U.S., 2015; Levine et al., 2016) to develop the following screening criteria for offshore storage resource assessment as following:

- Formation depth must be adequate (~1000 m [~3000 ft]) to ensure the (1) temperature and pressure conditions are suitable to store CO_2 in a supercritical phase and (2) sediment is sufficiently consolidated such that the risk of soft-sediment deformation is minimized (Gupta, 2019).

- A suitable seal or cap rock overlies the targeted storage zone to inhibit the vertical migration of CO_2 to the surface.

- Hydrogeologic conditions such as structural, stratigraphic, and hydrodynamic traps are present to retain the injected CO_2 within the targeted storage zone.

3.3 CO_2 geological storage estimation

Several institutions and government departments worldwide have developed several approaches for assessing carbon dioxide storage capacity in various geological media. The US Department of Energy developed a simple methodology for calculating the storage capacity of regional-scale saline aquifers, that's calculating the total aquifer volume and applying a series of efficiency factors. However, this attempts to correct for geologic heterogeneity in the form of a probabilistic multiplicative sum of fractions (Laboratory and Energy, 2008). Several authors have worked hard to enhance and improve this approach, focusing notably on efficiency factors (Kopp et al., 2009). Since then, two widely used approaches have been developed, based on the DOE method

(Laboratory and Energy, 2008; Goodman et al., 2011) and the Carbon Sequestration Leadership Forum method (Bachu, 2008a), as summarized by Kopp et al. (2009). In addition, the controversial method stated that the geological formations performed as sealed containers after CO_2 injection, quickly increasing pressure that occurring with considerable challenges related to the CO_2 storage (Ehlig-Economides and Economides, 2010).

3.4 Database

3.4.1 Seismic data

For petroleum exploration, 36 offshore seismic surveys (350,000 km) were surveyed in the Atlantic planning areas via the Bureau of Ocean Energy Management (BOEM) Resource Evaluation Program in geological and geophysical data acquisition between 1968 and 1992 (Dellagiarino, 2001). Approximately 195,000 km of industrial 2-D legacy seismic reflection profiles were analyzed and interpreted to identify prospective storage elements and determine the lateral extending and thickness of the significant stratigraphic units. Since the data are zero-phase migrated, an increase in acoustic impedance is represented by a red-black-red reflection sequence in the seismic data depicted in this study, which indicates an increase in acoustic impedance. I identified the significant stratigraphic and lithological units (stratigraphic boundaries, unconformities, and reservoir and seal geometries). Seismic profiles are interpreted using horizon keys and calibrated against available well control. Due to the considerable horizon being tied to the seismic data and available well data, the base location of the reservoir is regarded with high uncertainty.

3.4.2 Well data

Six commercial exploration offshore wells (TRANSCO 1005-1, TENNECO 208-1, COST GE-1, TENNECO 427-1, EXXON 472-1, and EXXON 564-1) (Figure 3-2, Table 3-1) were drilled in

the southeast Georgia embayment from 1979 to 1980. Only the deepest three wells (TRANSCO 1005-1, COST GE-1, and EXXON 564-1) penetrated the Upper Jurassic section in the mid-south Atlantic area. The deepest three wells allow seismic data and lithological key horizons, rock property, and age calibration. These wells were publicly released in 1990. Stratigraphy is obtained using petrological reporting of recoverable borehole core cuttings integrated using gamma-ray, sonic, and resistivity petrophysical logs in the well logs. Only COST GE-1 well, limited pore pressure measurement is available, including direct pressure measurements and the pressure and density of drilling mud in the wellbore. The production testing data is unavailable due to the lack of oil and gas wells in the mid-south Atlantic. A core was available from the well COST GE-1, but no other cores were accessible or analyzed in the mid-south offshore Atlantic area. The porosity, permeability, and other key parameters are only available from the COST GE-1 well in the study area. The COST GE-1 well penetrated the pre-rift unconformity at 3,200m which drilled approximately 686m of the Paleozoic sedimentary sequences, and the total depth (TD) at 4,040m(Scholle, 1979; Amato and Bebout, 1980). The COST GE-1 well showed a thick sequence from Paleozoic to Cenozoic, where the Paleozoic section generally consists of non-fossiliferous quartzite, shale, and salt, underlain by metamorphic and meta-volcanic rocks (Scholle, 1979).

The COST GE-1 well data was significantly utilized to provide equivalent stratigraphy for the mid-south Atlantic offshore. The fracture pressure was provided from the leak-off test data below the deepest casing shoe(Amato and Bebout, 1978; Amato and Bebout, 1980). This greatest pressure can determine the maximum pressure used while drilling in that formation. The pressure measurements estimate how much CO_2 is pumped into the sealing unit without fracturing.

Table 3-1: Essential information for the offshore wells located in the Southeast Georgia Embayment.

No	Operator	Well No	Block No	Water Depth (m)	Kelly Bushing KB (m)	Total Depth TD (m)	Location (deg/min/sec)	
							Lat. (N)	Long. (W)
1	Transco	1	1005	40.84	30.78	3,546.35	30 59 34	80 14 38
2	Tenneco	1	208	37.8	31.7	2,363.42	30 46 43	80 28 14
3	Ocean Prod	COST GE-1	387	41.45	30.18	4,039.82	30 37 08	80 17 59
4	Tenneco	1	427	29.87	36.27	2,277.47	30 34 34	80 31 59
5	Exxon	1	472	38.1	27.74	2,364.64	30 31 36	80 29 54
6	Exxon	1	564	44.2	24.69	3,920.64	30 26 23	80 15 21

3.5 Geological and storage perspectives

The Upper Jurassic section is overlain by Cretaceous mudstone and shale that extends regionally across the study area, considered a cap rock to ensure CO_2 storage confinement. High-level static storage resource estimates reported in previous work suggest storage potential exists within the Upper and Lower Cretaceous sandstones in the Southeast Georgia Embayment and Blake Plateau saline basins (Almutairi, 2018; Almayahi et al., 2022). In this study, the Mid-south Atlantic offshore involved extensive efforts in data compilation, preservation, digitization, integration, and storage evaluation.

Several institutions and government departments worldwide have developed approaches for assessing carbon dioxide storage capacity in various geological media. The US Department of Energy developed a simple methodology for calculating the storage capacity of regional-scale saline aquifers by calculating the total aquifer volume and applying a series of efficiency factors that attempt to correct for geologic heterogeneity in the form of a probabilistic multiplicative sum of fractions (Laboratory and Energy, 2008; Solomon et al., 2008). Several authors have enhanced and improved this approach, focusing on efficiency factors. Since then, two widely used approaches have been developed, based on the DOE method (Laboratory and Energy, 2008;

Goodman et al., 2011)and the Carbon Sequestration Leadership Forum (CSLF) method (Bachu, 2008a; Kopp et al., 2009), as summarized by Kopp et al. (2009). In addition, the controversial method stated that the geological formations performed as sealed containers after CO_2 injection, quickly increasing pressure occurring with considerable challenges related to the CO_2 storage (Ehlig-Economides and Economides, 2010).

The results of processed database is utilized to characterize offshore specific site selection criteria and calculate offshore-specific probability values for storage efficiency parameters, which are utilized to identify regional storage resources and estimate volumetric of storable quantities for the Upper Jurassic deep saline reservoirs.

3.6 Methods

This research develops an estimation of the future regarding carbon capture and storage in the southern mid-Atlantic offshore region, assuming economic conditions are suitable. A methodical workflow was used to assess and characterize CO_2 storage resources in the mid-Atlantic US offshore region, extending from North Carolina to Florida. This workflow included integrating geological and geophysical data and estimating regional-scale storage resources. The results of each area pointed to specific parts used to improve static capacity estimations. The stratigraphic and rock physical properties analyses characterize resource calculation limitations, estimate offshore storage efficiencies, and calculate CO_2 storage resources for the target deep saline aquifer. Well logs, laboratory core analyses, and seismic data to support the storage resource assessment. The geophysical logs of the COST GE-1 well are interpreted to identify sequence stratigraphy, lithofacies, and physical rock properties. The seismic data and well data are utilized to create a structure map and define the stratigraphic perspective of the caprocks and storage sources. The lithology, porosity, and permeability are identified by integrating the well logs and laboratory core analyses. Integration of geophysical and geological data developed the storage

elements: regional depth, thickness, and porosity. Risk factors such as sediment lithification and hydrostatic pressures are integrated based on the US Department of Energy-National Energy Technology Laboratory (US DOE-NETL) (Cumming et al., 2017; Rodosta et al., 2017; Sanguinito et al., 2018) to develop the following screening criteria for the offshore storage resource assessment as following: (A) The storage depth is deeper than 800 m to ensure the temperature and pressure conditions are suitable for squeezing CO_2 under supercritical conditions. (B) A suitable seal or cap rock overlies the potential reservoirs to inhibit the vertical migration of CO_2 to the surface. (C) The structural and stratigraphical trap conditions control the injected CO_2 in the reservoirs for integrity and safe storage. Screening grids were performed as input for offshore CO_2 storage calculations utilizing the static volumetric methodology by the CO_2 Storage Perspective Resource Estimation Excel Analysis (CO_2-SCREEN) tool developed by the US DOE-NETL. The screening criteria were complemented with stratigraphic and physical characteristics analysis to establish storage resource calculation parameters, evaluate offshore storage efficiencies, and calculate CO_2 storage resources for the Upper Jurassic deep saline aquifer. To support the storage resource assessment, well logs and core and drill cuttings from the COST GE-1 well and legacy seismic data were interpreted and integrated. The challenges of the storage assessment workflow are related to the uncertainties and gaps associated with the legacy seismic data and a lack of well data.

3.6.1 Data analysis

The structural and stratigraphic offshore Jurassic sequences are determined using seismic data interpretation and correlation. Reservoirs and cap rocks characterize reservoirs and seals in the study area. To generate regional structure and thickness maps, interpreted seismic horizons for storage and cap rocks identified in this study were depth converted, tied to the COST GW-1 well, and integrated into a continuous, interpolated two-dimensional grid surface. The Upper Jurassic depth interval is interpolated and interpreted for the study area based on the COST GE-1 well

data, structure Upper Jurassic maps for top and bottom surfaces are illustrated in figure 3-3 to figure 3-5 and figure 3-6 and figure 3-7 that illustrate thickness maps of the Upper Jurassic section and net-to-gross sandstone Upper Jurassic reservoir. A quality validation and quality control approach is used to confirm seismic horizons, and well log sequence stratigraphic and lithostratigraphic picks were equivalent to within 100 m. The storage and caprock structure and depth limitations were analyzed to detect storage calculation boundaries according to screening criteria.

The lithological description used the standard USGS rock-type designations such as shale, siltstone, sandstone, limestone, dolomite, and quartzite. The results of the core and sidewall analyses are effective tools used in this study to evaluate the lithology and porosity of the Upper Jurassic section. The rocks between 1,500 and 2,200 m in depth are potentially related to Lower Cretaceous (Scholle, 1979); however, the section below 2,200 m is signed as Upper Jurassic (Amato and Bebout, 1980). Rocks from a depth of 3,350 m to the base of the well are composed of green and gray-green, very fine-grained, highly indurated to weakly metamorphosed, sedimentary rocks, with intrusive and extrusive meta-igneous rocks especially abundant in the lower part of this interval.

The Upper Jurassic section at 2,200 and 3,350 m is composed of interbedded sandstones, and shales predominate, although individual beds of limestone, dolomite, and anhydrite, and, in the lower part of the section, coal are common (Table 3-2 and Figure 3-8). This section, deposited in inner-shelf terrestrial environments, is largely barren of fossils. The depositional environments of the beds across the COST GE-1 well range from the middle shelf to the upper slope (Maher and Applin, 1971; Poag, 1978; Amato and Bebout, 1980; Dillon et al., 1982). Regarding the porosity and permeability of conventional and sidewall core samples from the GE-1 well, the porosity of the Upper Jurassic rocks decreased through compacting, pressure solution, and cementation of silica, calcite, and anhydrite. The porosity ranges from 0.15 to 0.31, and corresponding

permeabilities are mostly 9.87×10^{-16} to 9.87×10^{-14} m^2 as shown in figure 3-8. This range is common at a depth range of 2,200-3,050 m. However, the average permeability of a few coarser sandstones is approximately 4.05×10^{-12} m^2 (Figure 3-8). At a depth of 3,050–3,350 m, porosity and permeability are significantly decreased by diagenetic processes (Amato and Bebout, 1978; Scholle, 1979).

Due to the diagenetic alteration obliterating all significant porosity in the slightly metamorphosed, no reservoir rocks are expected in the section below 3,350 m. The impermeable beds are qualified to seal the prospective reservoirs throughout the Upper Jurassic section. The thick shale and calcareous shale, thinner shale, and anhydrite beds in the deeper parts of the Upper Jurassic section are the best potential seals. This study examines and evaluates a reservoir within a regional stratigraphic trap hosted by the Upper Jurassic sandstone layers. Whereas a quantifiable caprock or seal represents the impermeable rocks, I can identify the base seal of a potential reservoir. The sandstone layers underlay the target reservoir, and the shale beds are regionally extended across the study area. At a depth 2,525 – 3,106 m, the COST GE-1 well includes seven Upper Jurassic sandstone potential reservoirs (Figure 3-8). The sandstone layers underlay the target reservoir, and the shale beds are regionally extended across the study area.

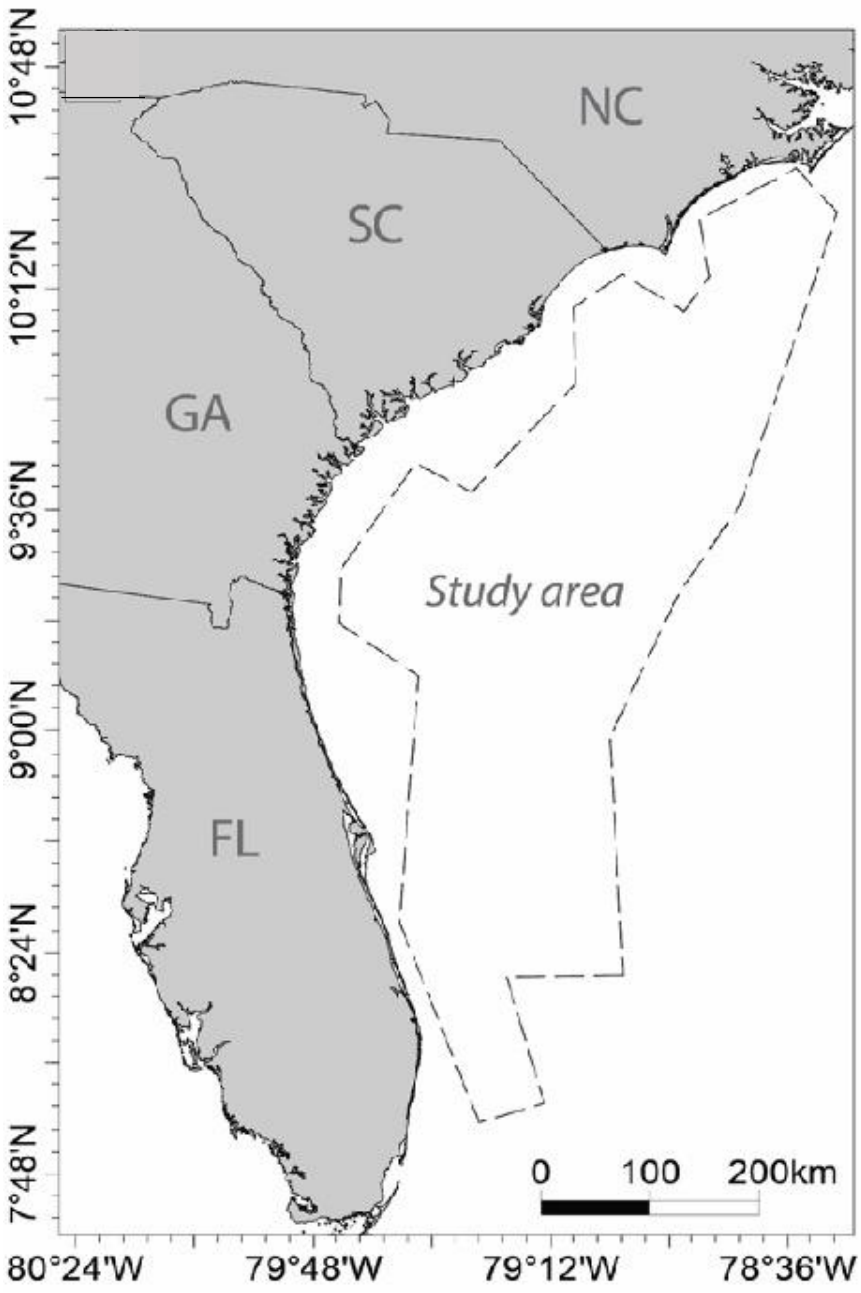

Figure 3-3: Location map for the study area.

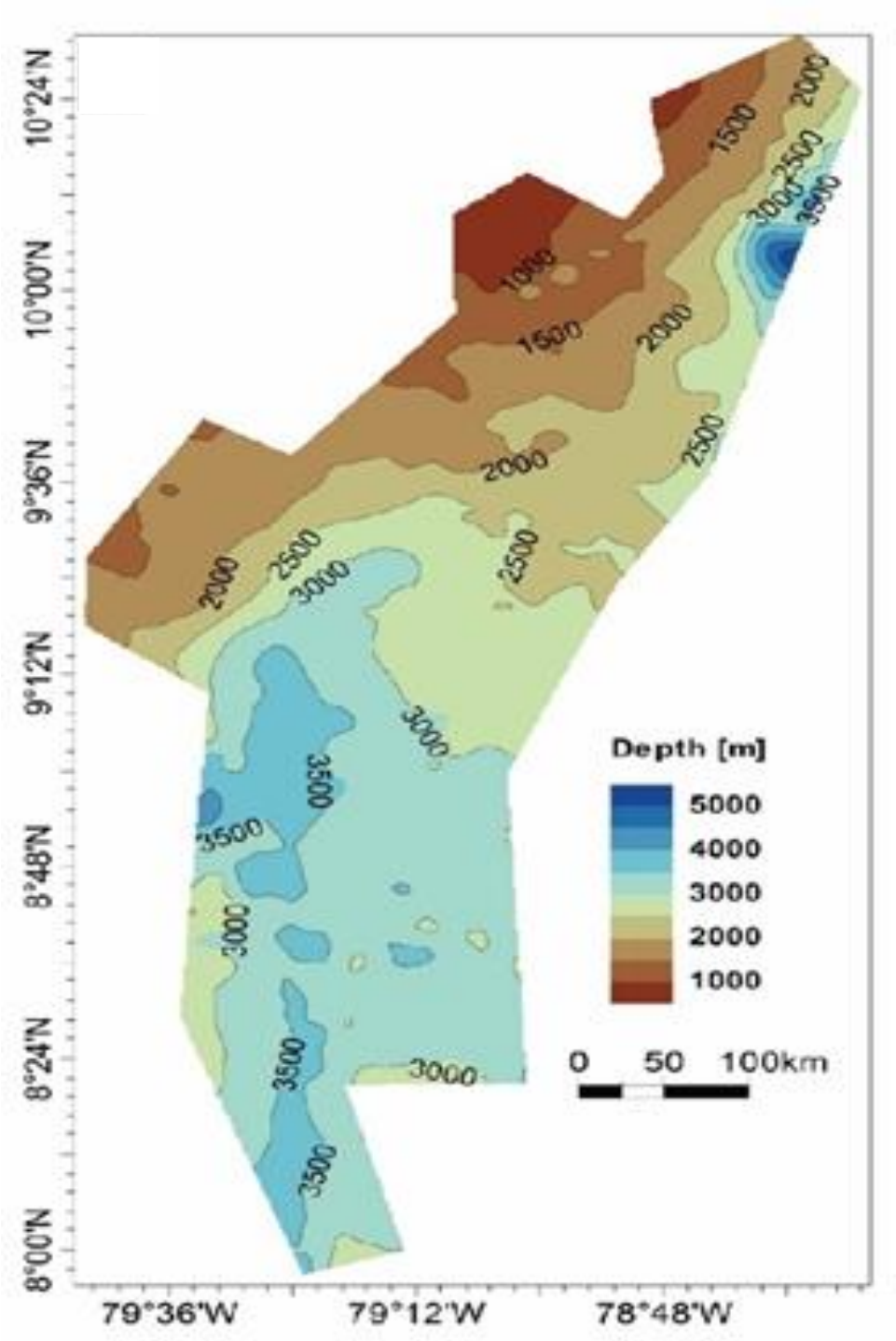

Figure 3-4: Structural map for the top surface (in meters) of the Upper Jurassic sequences.

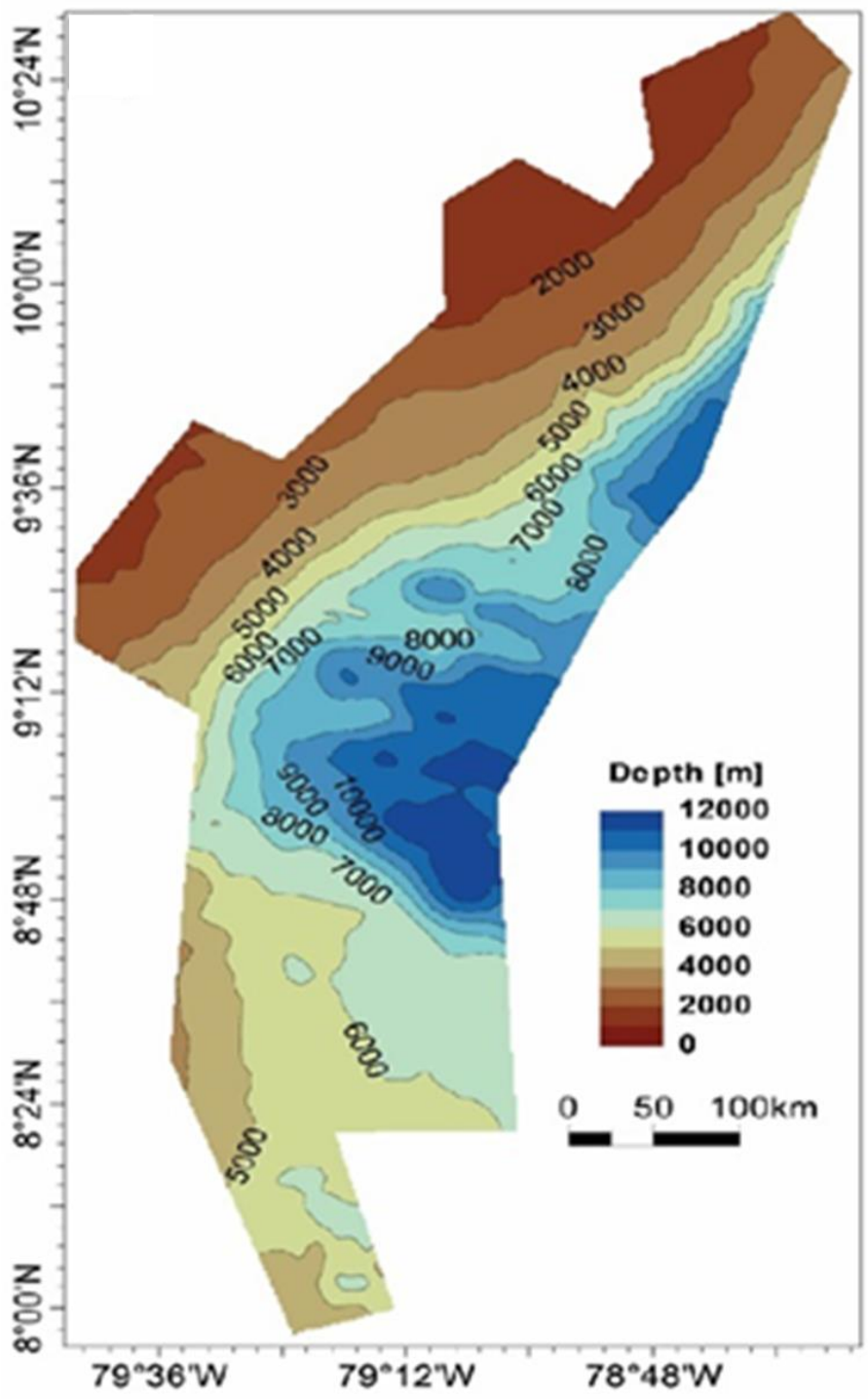

Figure 3-5: Structural map for the base surface (in meters) of the Upper Jurassic sequences.

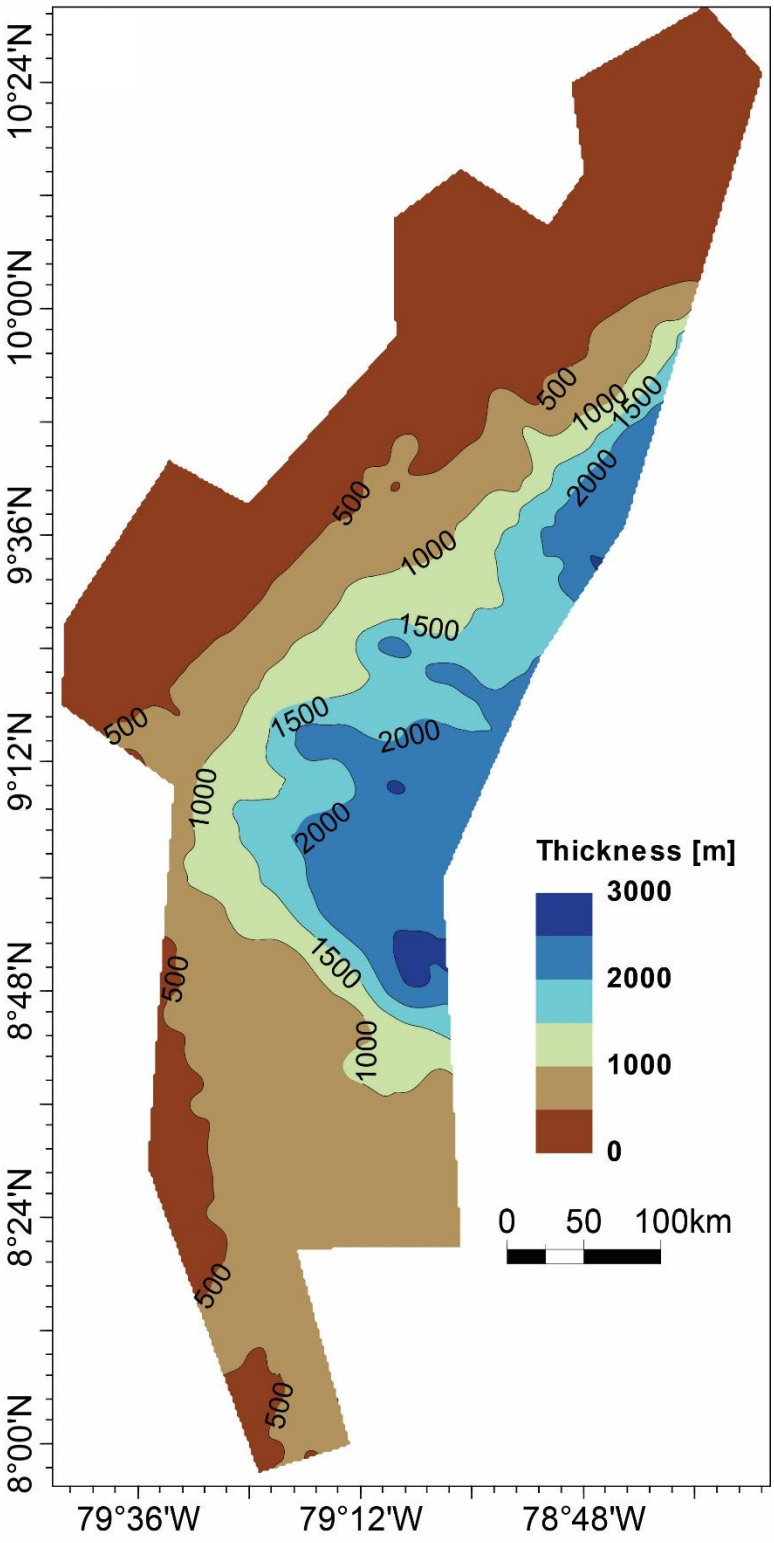

Figure 3-6: Thickness map (in meters) for the Upper Jurassic section (in meters.

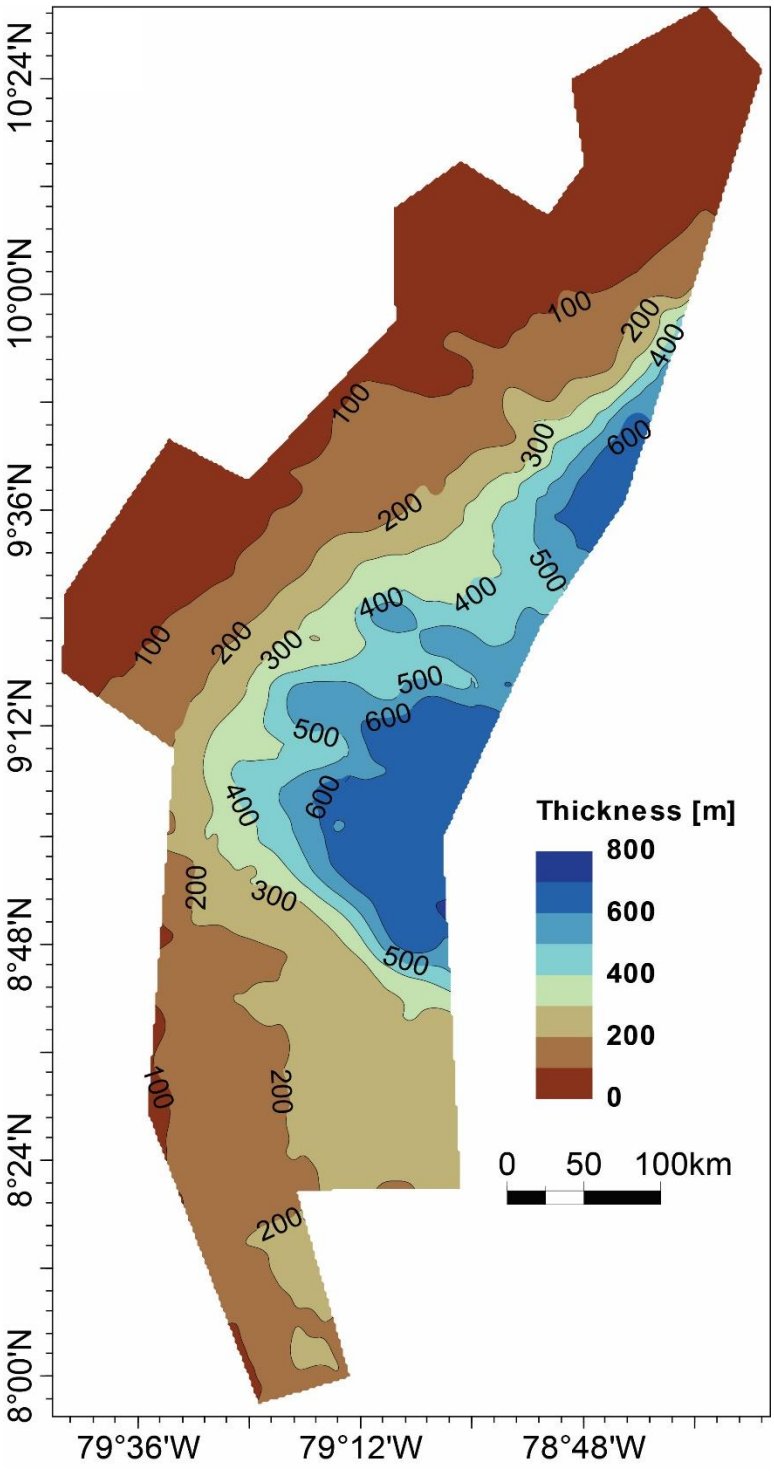

Figure 3-7: Thickness map (in meters) for the Upper Jurassic sandstone reservoir.

Table 3-2: Lithologic description of the Upper Jurassic sequences using core and cutting samples with the depth intervals (in meters) from the COST GE-1 well.

Depth interval (m)	Porosity	Lithology
2,525-2,825	0.23-0.31	Coarse sand unconsolidated with thick interbedded red-brown-gray shale, some coal, and pyrite.
2,825-2,995	0.21-0.27	Consolidated medium-grain sandstone interbedded red-brown-green shale and limestone.
2,995-3,030	0.12-0.24	Fine-medium crystalline limestone and fossiliferous micrite at the base.
3,030-3,190	0.19-0.25	Thin interbeds shale with abundant carbonaceous limestone, a few thin sandstone beds and thin limestone bed in the base.
3,190-3,395	0.20-0.25	Thinly sandstone interbeds crystalline dolomite, and shale.
3,395-3,425	0.23-0.25	Molted gray Limestone.
3,425-3,560	0.12-0.24	Thin fine to medium-grain sandstone interbedded, shale, a few limestone beds with seams coal at the base.
3,560-3,600	0.23-0.24	Dense dolomite and fine limestone trace coal.
3,600-3,695	0.18-0.23	Shale, dolomitic shale interbedded sandstone with trace coal.
3,695-3,975	0.22-0.28	Dolomite and sandy silt interbed of anhydrite, gypsum nodules with a trace of coal.

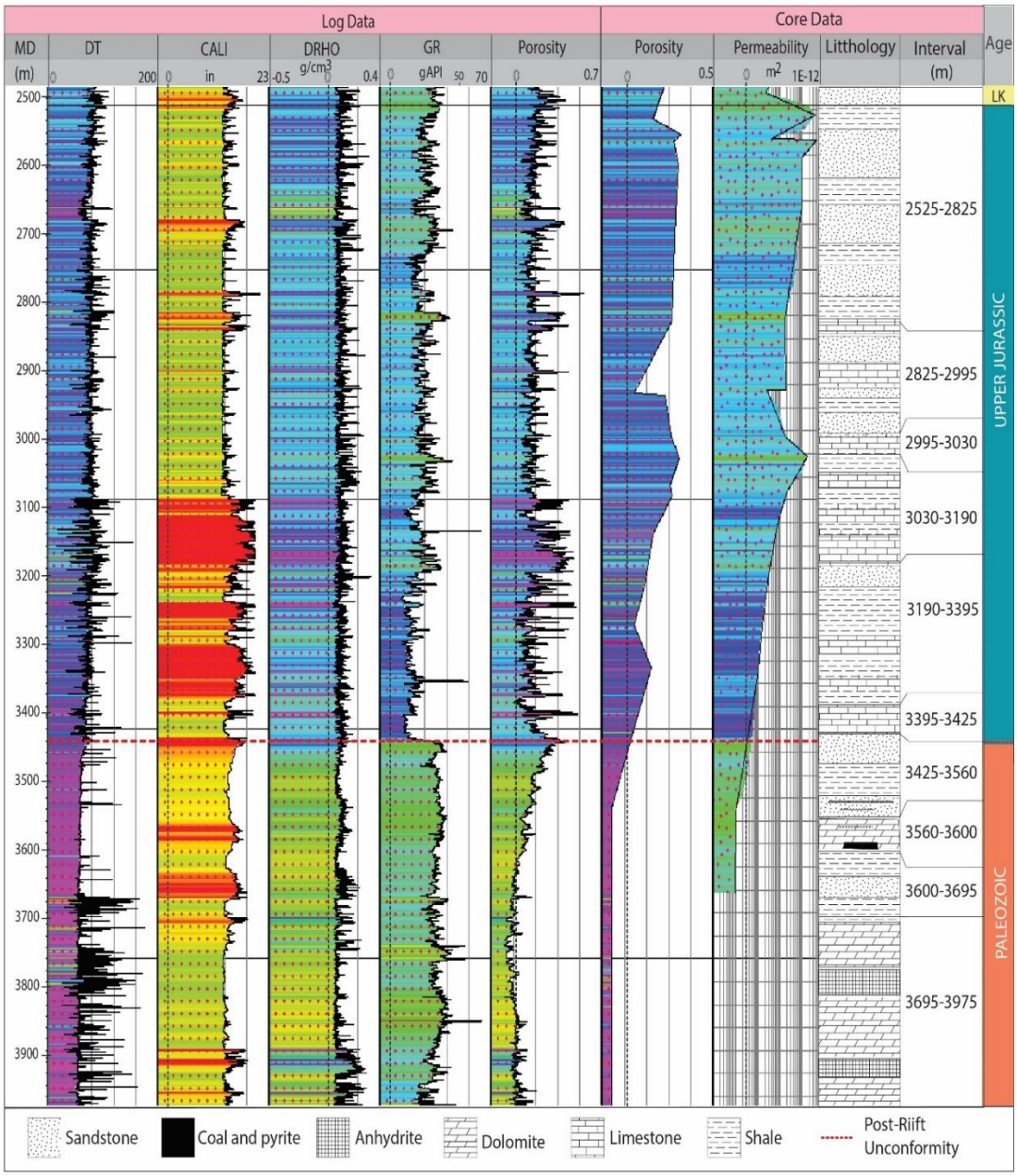

Figure 3-8: COST GE-1 well data logs correlated with core samples for stratigraphy and rock physical properties.

3.6.1 CO_2 Screening and calculations

The comparable volume of CO_2 occupying the pore space in a specified storage reservoir is calculated using estimations of subsurface pore volumes and site fluid volumes in static CO_2 storage calculations. The Carbon Sequestration Leadership Forum has developed static and volumetric-based methodologies to estimate static CO_2 storage potential (Bachu, 2007; Bradshaw et al., 2007; Bachu, 2008b; Gorecki et al., 2009a; Gorecki et al., 2009b; Goodman et al., 2011; Zhou et al., 2011; Blondes et al., 2013; Sanguinito et al., 2017). The potential CO_2 storage resource of the offshore saline aquifer in this study was quantified and mapped using the US DOE-NETL methodology (Laboratory and Energy, 2008; Goodman et al., 2011; Goodman et al., 2016). Equation 3-1 summarizes this methodology:

$$GCO_2 = A \times h \times \varphi \times \rho CO_2 \times Esaline \quad \text{Equation 3-1}$$

Where, the total area (A), net-to-gross thickness (h), and average effective porosity (φ) of the reservoir are utilized to evaluate offshore resources, with gamma-ray 40 gAPI and permeability (k) 9.87×10^{-14} m^2 encompassing the total pore volume.

The storage efficiency factor (Esaline) is used to minimize total pore volume to indicate the fraction of the pore space occupied by CO_2 (Goodman et al., 2011, 2016). The density of CO_2 (ρCO_2) at reservoir conditions is employed (GCO_2) to convert the CO_2 occupied pore volume to a mass of stored CO_2. According to DOE-NETL, the Esaline variable combines five principal efficiency factors (US DOE-NETL, 2008, 2010, 2012; Goodman et al., 2011). Equation 3-2 explains the specific efficiency variables:

$$E_{saline} = E_{An} \times E_{hn} \times E_{\rho e} \times E_V \times E_d \quad \text{Equation 3-2}$$

Geologically, the net effective pore volume is the net-to-total area (E_{An}), net-to-gross thickness (E_{hn}), and effective-to-total porosity ($E_{\rho e}$). The ratio of the net pore volume with a permeability

greater than or equal to 9.87×10^{-14} m^2 to the net reservoir pore volume with a permeability greater than or equal to 1.97×10^{-13} m^2 provides the net effective pore volume. The remaining efficiency factors are fluid displacement terms, volumetric displacement efficiency (E_V) accounts for water saturation, and microscopic displacement efficiency (E_d) accounts for the volume of rock involving an injection well contacted by CO_2 related to fluid conditions and displacement.

Equations 3-1 and 3-2 are used to estimate the storage capacity of the open system saline aquifer probabilistically. The satisfactory convergence for probabilistic resource estimations are used for this study corresponding to the DOE method (Goodman et al., 2016; Sanguinito et al., 2017; Sanguinito et al., 2018). The storage was supplied with grid data generated from the depth, net thickness, and effective porosity. Reservoir pressure and temperature were calculated based on the pressure and temperature gradients from the COST GE-1 well.

The CO_2 density is calculated using the CO_2 solubility model corresponding to Duan et al. and Bahadori et al. (Duan et al., 2006; Bahadori et al., 2009). Statistical distributions from regional net-to-total pore volume grid data and direct consequence injection simulations were used to assess storage efficiency in terms of geology and displacement efficiency. A cutoff permeability of greater than or equal to 1.97×10^{-13} m^2 was applied to the greater than or equal to 9.87×10^{-14} m^2 reservoir interval to account for uncertainty in the predicted net pore volume available for CO_2 storage. The three geologic efficiency parameters, EAn, Ehn, and Eρe, were combined into one parameter to describe the net-to-total reservoir pore volume efficiency and use available data to determine storage efficiency as in equations 3-2 and 3-3 were developed as in equation 3-4 (Goodman et al., 2016; Fukai et al., 2020):

$$E_{PVn}^{s} = E_{An} \times E_{hn} \times E_{\rho e} \quad \text{Equation 3-3}$$

$$E_{saline} = E_{PVn}^{s} \times E_{V}^{s} \times E_{d}^{s} \quad \text{Equation 3-4}$$

The superscript is introduced to the E_{PVn} parameter to indicate a stochastic calculation parameter determined by specific data(Goodman et al., 2016). The geologic efficiency factor is provided probability (P) values for the 0.10 percentage (P10) and 0.90 percentage (P90) values based on statistical distributions of the pore volume fractions obtained from the grid cells in the storage. Goodman et al. (2011) utilized Monte Carlo simulations to estimate the estimates (P10, P50, and P90) of efficiency factors for different lithologies based on data from the US and Canadian carbon sequestration atlases (Gorecki et al., 2009a). The clastics, dolomites, and limestone are three lithological media with projected efficiencies ranging from 0.4 to 5.5 percent. The results align with previous investigations on how open-system saline formations work in various global regions (Bickle, 2009; Gorecki et al., 2009b; Kopp et al., 2009; Szulczewski and Juanes, 2009).

CO_2 storage perspective resource estimation excel analysis (CO_2-SCREEN) is an Excel-based method and tool developed by the US-DOE-NETL to screen geologic formations using an enhanced US-DOE-NETL approach (Gorecki et al., 2009a; Goodman et al., 2011; Bachu, 2015; Goodman et al., 2016; Levine et al., 2016; Sanguinito et al., 2018). CO_2 Storage prospeCtive Resource Estimation Excel aNalysis (CO_2-SCREEN) is a tool that estimates potential CO_2 storage resources for geologic formations, ranging from large regional assessments to specific sites that could be developed for commercial storage. This tool is an interactive version of the US-DOE methodology for improving potential CO_2 storage resources in saline aquifers based on increased available data and improved geologic interpretation (Goodman et al., 2016). CO_2-SCREEN is a publicly available tool obtained on the NETL Energy Data eXchange (EDX) (Sanguinito et al., 2017; Sanguinito et al., 2018). CO_2-SCREEN comprises an Excel spreadsheet for inputs and outputs and a GoldSim Player file for Monte Carlo simulations (Goodman et al., 2016; Sanguinito et al., 2018). The Excel file provides the key values for subsurface geological and physical characteristics, specifies storage efficiency factor ranges, and sets other formation-related parameters matching lithologies and fundamental formation characteristics. The GoldSim

Player file analyzes the Excel saved file input data, calculations CO_2 storage probability estimates using Monte Carlo methods and exports the response directly to the Excel file (Goodman et al., 2016; Sanguinito et al., 2018).

3.6.2 CO_2-SCREEN applying

Established on well log data from the Upper Jurassic sandstone layers in the mid-south Atlantic Ocean, this study employs CO_2-SCREEN. From the COST GE-1 well, depth, thickness, porosity, temperature, and pressure data are the first parameters input into the Excel file for the saline formation of the CO_2-SCREEN (Table 3-3). I applied the value from Sanguinito et al. (2018) for the storage efficiency factor ranges, which have already calculated in the application, represented by a P10 and P90 range for the dolomite lithology.

Grid cells for storage efficiency factors are controlled through CO_2-SCREEN. The grid cells determine the storage efficiency ranges according to the dolomite lithology. The initial geology and reservoir data are the second set of input physical variables for CO_2-SCREEN. The geophysical interpretation included thickness readings from the COST GE-1 well, a porosity log (Figure 3-8), bottom-hole temperature, and pressure (Figure 3-9). The gridding approach in CO_2-SCREEN is used to accommodate geographic and geologic heterogeneity. This approach allows the simultaneous input of several rows of physical parameter data to obtain CO_2 storage resources on a grid cell by grid cell scale. The Upper Jurassic sandstone was arranged into 25 grid cells of about 83 km × 83 km (7,025 Km^2) for each grid. Grid cells with data on at least one physical parameter, including thickness or porosity, are identified for use in CO_2-SCREEN (Table 3-3). A normal distribution with temperature and pressure inputs is used to reflect density, and a log-odds distribution is used to define storage efficiency (Sanguinito et al., 2017). The CO_2 storage results are calculated in million metric tons (Mt) for the saline aquifer.

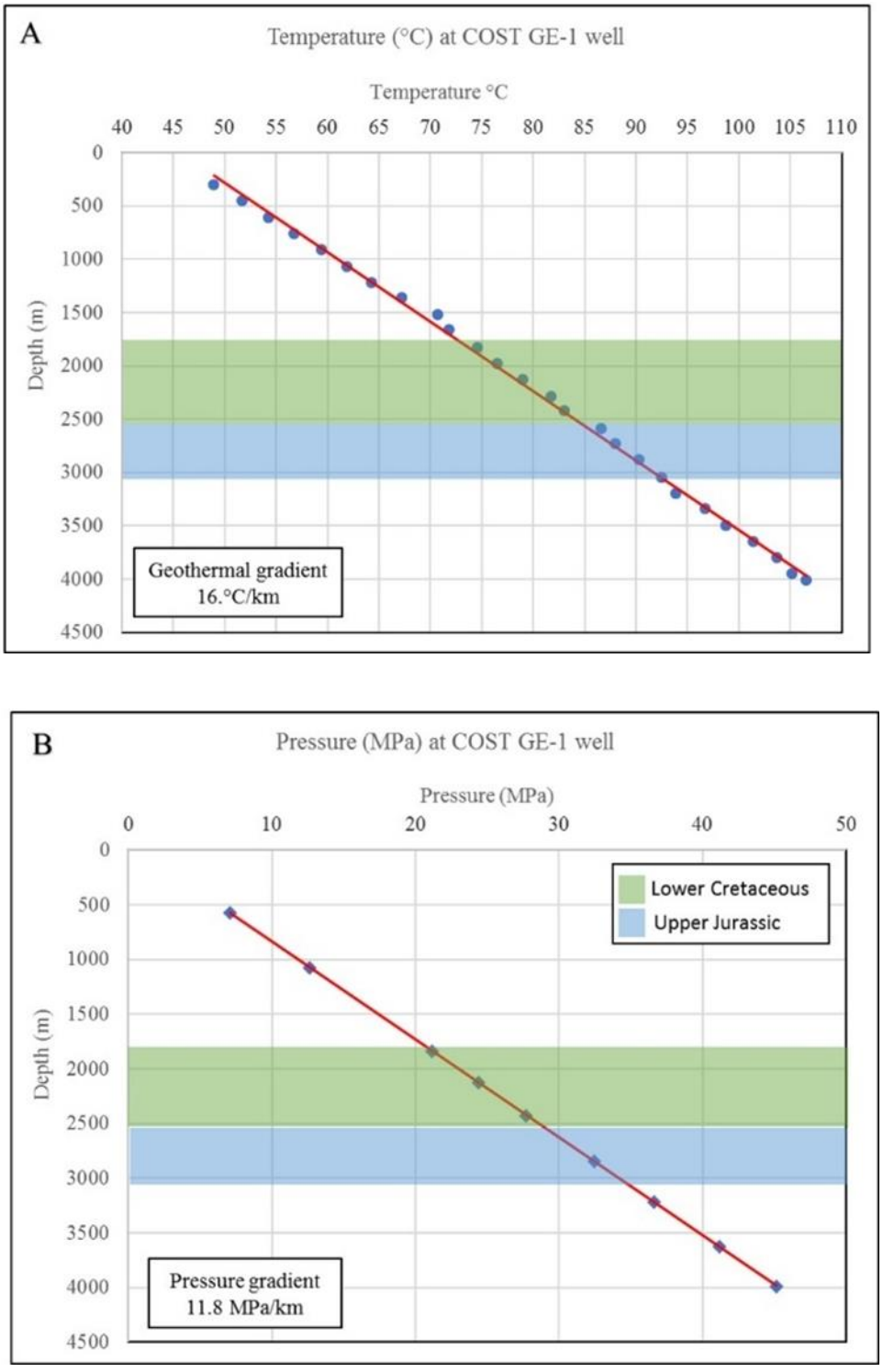

Figure 3-9: Demonstrates temperature (ºC) and Pressure (MPa) plotted against depth (m) for the COST GE-1 well. Panel A Temperatures were recorded from three temperature logs. The geothermal gradient of around 16 ºC/km is shown as the least-squares fit to the data from the two deepest temperature logs. Panel B Pressure measured from conventional drill-stem test data. The hydrostatic pressure gradient of around 11.8 MPa/km. This figure is summarized and modified after (Scholle, 1979; Amato and Bebout, 1980).

Table 3-3: CO_2-SCREEN Saline aquifer (Inputs excel sheet) shows the mean and standard deviation of the physical parameters for 25 grid cells of the Upper Jurassic sandstone reservoir.

Grid	Area (km²)	Gross Thickness (m)		Total Porosity (%)		Pressure (MPa)		Temperature (°C)	
		Mean	Std Dev	Mean	Std Dev	Mean	Std Dev	Mean	Std Dev
1	7024.675	40.62927	19.58812	0.33615	0.001063	46.92229	0.11545	89.79167	0.088388
2	7024.675	67.86936	18.93518	0.331639	0.002127	47.31262	0.16055	90.04167	0.088388
3	7024.675	94.64774	18.93518	0.327128	0.001063	47.62794	0.062417	89.84167	0.22981
4	7024.675	121.4261	18.93518	0.319609	0.004253	47.80448	0.062417	89.56667	0.035355
5	7024.675	148.2045	18.93518	0.309083	0.00319	47.98102	0.062417	89.66667	0.035355
6	7024.675	175.4446	19.58812	0.306075	0.001063	48.15756	0.062417	89.76667	0.035355
7	7024.675	202.6847	18.93518	0.295549	0.008507	48.3341	0.062417	89.86667	0.035355
8	7024.675	229.4631	18.93518	0.268481	0.010633	48.51064	0.062417	89.96667	0.035355
9	7024.675	256.7031	19.58812	0.248932	0.00319	50.2913	1.196697	90.06667	0.035355
10	7024.675	283.9432	18.93518	0.228877	0.010991	52.14695	0.11545	90.01667	0.070711
11	7024.675	310.7216	18.93518	0.218333	0.003536	52.4735	0.11545	89.99167	0.053033
12	7024.675	337.9617	19.58812	0.220833	0.001768	52.80004	0.11545	90.14167	0.053033
13	7024.675	364.7401	18.28224	0.213333	0.003536	53.12658	0.11545	90.29167	0.053033
14	7024.675	391.5185	19.58812	0.233896	0.018076	51.47401	1.283995	90.34167	0.017678
15	7024.675	418.7585	18.93518	0.269985	0.007443	49.74643	0.062417	90.36667	0.035355
16	7024.675	445.5369	18.93518	0.260962	0.013823	49.92297	0.062417	90.46667	0.035355
17	7024.675	472.777	19.58812	0.289534	0.034026	50.09952	0.062417	90.56667	0.035355
18	7024.675	500.0171	18.93518	0.339158	0.001063	50.27606	0.062417	90.66667	0.035355
19	7024.675	526.7955	18.93518	0.303068	0.026583	50.4526	0.062417	90.76667	0.035355
20	7024.675	553.5739	18.93518	0.254947	0.007443	50.62914	0.062417	90.86667	0.035355
21	7024.675	580.814	19.58812	0.242917	0.001063	50.80568	0.062417	90.86667	0.035355
22	7024.675	608.054	18.93518	0.23991	0.001063	51.76536	0.616178	89.99167	0.583363
23	7024.675	634.8324	18.93518	0.236902	0.001063	52.80004	0.11545	89.09167	0.053033
24	7024.675	661.6108	18.93518	0.233895	0.001063	53.12658	0.11545	89.76667	0.53033
25	7024.675	677.5	18.93518	0.231302	0.00077	53.13008	0.112975	90.48067	0.025456

3.7 Results and discussion

The capacity for CO_2 storage potential of the Upper Jurassic sandstone layers is calculated based on the rock compositions and petrophysical properties from correlation of the COST GE-1 well to the Transco 1005-1 in the northern region and the Exxon 564-1 wells in the southeastern region. The potential reservoirs are associated with potential seals characterized and assessed in the Upper Jurassic section. The reservoirs are sealed by thick cap rocks mainly of shale, siltstone, anhydrite, and limestone. The Upper Jurassic reservoir consists of seven sandstone layers sealed by impermeable caprocks. The trapping mechanism characterized as an overlying seal, involves stratigraphic trapping through lateral facies extension. The Upper Jurassic sandstone reservoir comprises calcareous shale, anhydrite, limestone, fossil fragments, and gypsum. The average porosity of the reservoir ranges from 0.15 to 0.31. I used equation 3-1, which was developed earlier by Goodman et al. (2011), to apply the dolomite storage efficiency factors (E) at the regional formation scale, which are ranged from 0.64 and 5.36 percent for the probabilities of P10 and P90 (Table 3-4).

Table 3-4: The CO_2 storage resource results (CO_2-SCREEN output excel-sheet) for the Upper Jurassic sandstone reservoir in the study area. This table demonstrates the three probabilities of the dolomite storage resource (Mt) and storage efficiency (%) for the 25 grid cells.

Grid	Storage Resource (Mt)			Lithology	Storage Efficiency (%)		
	P_{10}	P_{50}	P_{90}		P_{10}	P_{50}	P_{90}
1	0.08	1.31	20.04	Dolomite	0.64	2.2	5.36
2	1.44	15.45	155.36	Dolomite	0.65	2.17	5.23
3	2.59	21.14	143.36	Dolomite	0.67	2.2	5.33
4	5.52	36.08	207.21	Dolomite	0.66	2.18	5.35
5	11.33	60.22	280.35	Dolomite	0.65	2.2	5.31
6	14.17	68.77	283.74	Dolomite	0.67	2.18	5.26
7	20.35	85.06	314.3	Dolomite	0.68	2.18	5.28
8	24.94	103.54	356.5	Dolomite	0.66	2.19	5.33
9	29.77	113.3	351.91	Dolomite	0.67	2.2	5.31
10	28.46	102.07	307.27	Dolomite	0.67	2.19	5.27
11	14.07	50.59	144.15	Dolomite	0.68	2.17	5.21
12	14.2	52.38	146.63	Dolomite	0.66	2.22	5.33
13	13.67	47.74	131.24	Dolomite	0.65	2.2	5.3
14	9.52	33.72	88.73	Dolomite	0.66	2.19	5.28
15	44.38	156.44	407.46	Dolomite	0.65	2.18	5.3
16	27.16	90.42	229.61	Dolomite	0.67	2.18	5.29
17	20.44	72.37	180.78	Dolomite	0.66	2.21	5.24
18	31.13	107.78	268.49	Dolomite	0.65	2.22	5.28
19	28.96	94.07	233.88	Dolomite	0.68	2.17	5.28
20	19.83	63.5	155.95	Dolomite	0.68	2.19	5.33
21	27.86	93.04	228	Dolomite	0.66	2.21	5.33
22	19.52	65.01	155.03	Dolomite	0.67	2.23	5.27
23	25	83.84	204.9	Dolomite	0.66	2.21	5.35
24	37.07	122.34	293.95	Dolomite	0.67	2.21	5.3
25	54.23	180.33	425.49	Dolomite	0.67	2.23	5.26
Total	525.71	1920.48	5714.31	-	-	-	-
Average	21.03	76.82	228.57	-	0.66	2.20	5.31

The uncertainty of CO_2 density incorporated with the variety of depths and thicknesses in the Upper Jurassic section can be reduced by CO_2-SCREEN application to calculate the CO_2 storage capacity based on the grid area, depth, and physical rock properties. Temperature and pressure for each grid area of the reservoirs are based on the geothermal gradient and hydro-static pressure gradient from the COST GE-1 well (Figure 3-9). I assumed that the geothermal gradient at the COST GE-1 well (16 ^{o} C) and hydro-static pressure gradient (0.011 MPa/m) are constant across the study area. The density values of supercritical CO_2 are already considered in the CO_2-SCREEN approach based on the depth (Goodman et al., 2016; Sanguinito et al., 2018).

For high accuracy and comparison, I estimate the potential storage resources of the Upper Jurassic reservoir calculated for the regional area. The area is detected where seismic profiles and well data are densely concentrated in the mid-south Atlantic planning area, covering approximately 176,000 Km^2. The storage resource was detected based on the abundance and density of the data. I considered three probability values (P10, P50, and P90) for each grid area to determine each grid cell's geologic storage efficiency factor. For the integrity and safety of CO_2 storage, I interpreted and evaluated impermeable rock units that are signed as seals. Although the seismic interpretation indicated no significant fault has detected in the Upper Jurassic section, the uniform lateral stratigraphy is a considerable concern due to the lack of well data in the study area. The potential storage resources were calculated for the Upper Jurassic reservoir. The total capacity of the Upper Jurassic storage resources with a geologic storage efficiency of dolomite (0.64–5.36 percent) ranged between 526 and 5,714 Mt of CO_2 at P10 and P90 for the study area (Table 3-4). At P50, the average storage resource per unit area of the Upper Jurassic in the study area is approximately 0.011 Mt CO_2/Km^2 with uncertainty incorporated thickness changes is approximately ±0.00046 Mt/ Km^2.

CHAPTER IV

LITHOFACIES CLASSIFICATION OF WELL LOG DATA IN THE OFFSHORE ATLANTIC, SOUTHEASTERN UNITED STATES, USING MACHINE LEARNING APPROACH

4.1 Introduction

The main reservoir characteristics include lithology, clay volume, grain size, water saturation, porosity, and permeability are obtained through rock properties evaluation by well log interpretation and core sample analysis. The petrophysical analysis is fundamental since that supplies a key source of data for reservoir characterization. Well log data is required in characterizing subsurface resources and understanding the reservoir. Wire-line logs provide continuous records of geological formations and provide geophysicists with important data on the properties of the rocks. These characteristics are essential for evaluating individual well formations and field-wide subsurface resource estimates. Well logging techniques identify hydrocarbon zones, calculate hydrocarbon volumes, and perform multiple other operations (Ellis and Singer, 2007; Choubey and Karmakar, 2021). However, in reservoir characterization, some

procedures are required to determine shale volume (Vsh), water saturation (Sw), porosity (p), permeability (k), elasticity (AI, SI), reflectivity coefficient (R), and others. The physical characterization of subsurface samples is the traditional method for detecting lithofacies (Gao, 2011; Tewari and Dwivedi, 2019). Thus, an analytical procedure is more accurate to determine lithology directly from core samples, and it is extremely expensive and time-consuming (Payenberg et al., 2000; Zhong et al., 2021). Wire-line logging has increased significantly since the first electrical log was recorded in a well in a local oil field in France in the mid-1920s (Selley, 1998; Govett, 2007).

The rock facies is a geologic term that refers to classifying rock layers into assignable units due to physical features, composition, formation, or other characteristics (Moore and Liou, 1979; Niu et al., 2002). Various facies are referred to as the lithofacies discussed in this chapter. Facies identification is a critical feature of geologic exploration, and it comprises identifying a category for geological formations based on characteristics. This chapter utilized a classifier to predict facies classification of the given five wells datasets (i.e. regardless of which a well has being described or not described) in Southeast Georgia Embayment offshore Southeast United States (Figure 4-1).

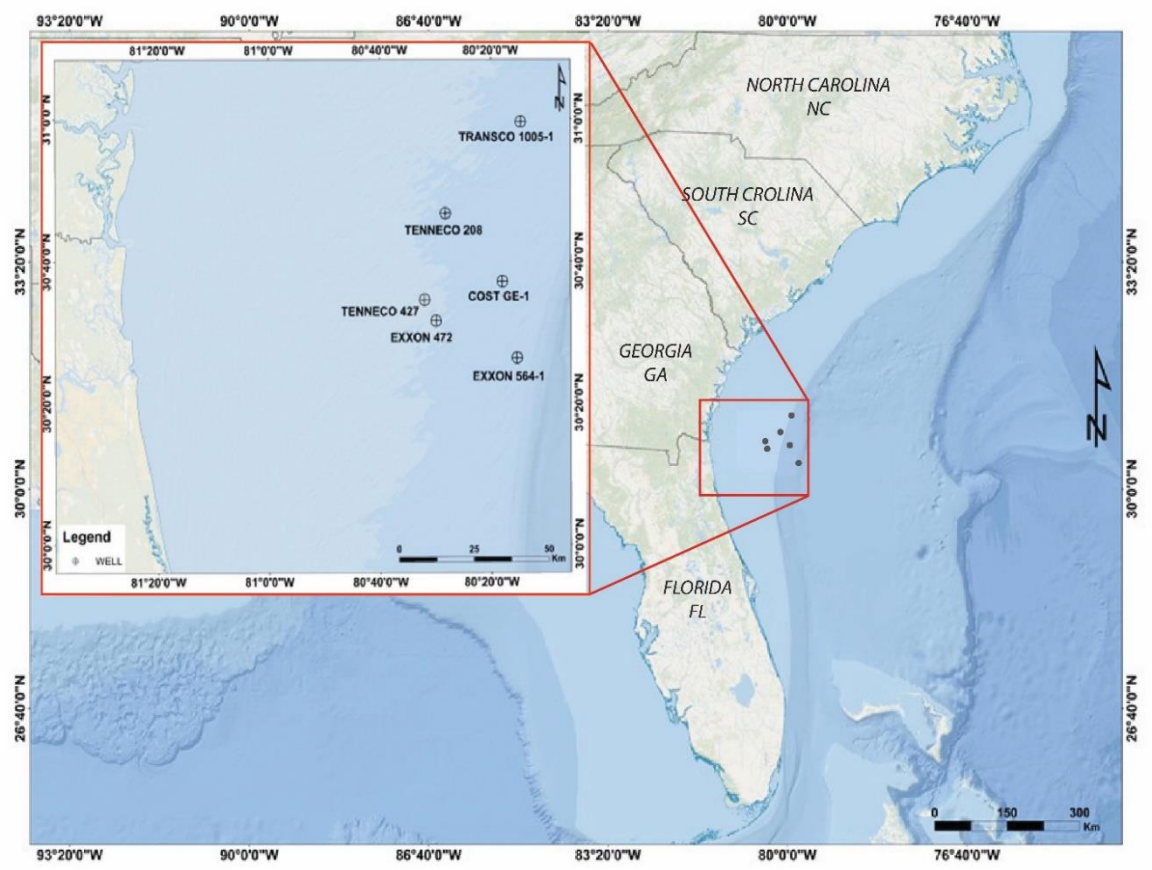

Figure 4-1: Well locations in southeast Georgia Embayment, offshore southeastern United States.

4.2 Machine learning approach

Machine learning has enticed numerous scientific aspects and progressively conquered the oil-gas industry. Multivariate statistical techniques have been utilized to reduce the difficulty of facies classification from well log measurements (Wolf and Pelissier-Combescure, 1982; Kapur et al., 1998). Grouping and clustering of similar features were used for rock facies classification (Wolf and Pelissier-Combescure, 1982). Multivariate clustering is the first successful attempt applied to recognize and correlate the facies between the wells (Gill et al., 1993). The Machine Learning (ML) algorithms developed and applied the C parameter in the computer vision industry to

determine and identify the facies (Lawrence et al., 1997).

The algorithms used in this study are: Support Vector Classifier (SVM) and Random Forest Classifier (RFC). Where, the Support Vector Machine (SVM) assembles a hyperplane, that is, margin/street is the distance between the vectors, and the support vectors are data points near the hyperplane on all sides (Joachims, 2002). If the hyperplane has a narrow margin/street, it needs a further parameter adjustment, but if the hyperplane has a wide margin/street, it is a reliable classification. The C optimizer factor describes the support vector machines (SVM) optimization and misclassifying essential to be avoided in each training example (Joachims, 2002; Guo et al., 2010).

That is, compared the accuracy of the predicted facies classification values to the actual facies classification values per each algorithm. In the machine learning approach, the wells datasets must be split into training and testing datasets. However, the five given wells are divided into three wells for training set: TRANSCO 1005-1 well, TENNECO 427-1 well, and EXXON 472-1 well, as well as two wells for testing set: 387 COST GE-1 well, and EXXON 564-1 well. Thus, I identified the facies classification features used for the three training and the two testing wells as shown in the table 4-1. However, three wells are trained for the well log curves' which resulted the count, mean, standard deviation, minimum, 25%, 50%, 75%, and maximum are shown in the table 4-2.

Table 4-1: Training data preparing shown a count 45598 rows and 12 columns including facies class number, lithology, well name, depth (ft), and eight features (well logs) of dataset.

	Facies	Formation	Well	DEPT	GR	CALI	DT	ILD	RHOB	SP	PHIND	DeltaPHI
0	5	Anh	TENNECO 427-1	371.5	0	0	56.3498	15.417	0	2.5	NaN	NaN
1	5	Anh	TENNECO 427-2	372	0	0	56.3498	15.417	0	2.5	NaN	NaN
2	5	Anh	TENNECO 427-3	372.5	0	0	56.3498	15.417	0	2.5	NaN	NaN
3	5	Anh	TENNECO 427-4	373	0	0	56.3498	15.417	0	2.5	NaN	NaN
4	5	Anh	TENNECO 427-5	373.5	0	0	56.1597	15.5597	0	2.25	NaN	NaN
...	...	...	...	...	...	...	...	...	...	...	...	...
45593	6	LS	TRANSCO 1005-1	11698	25.7	0	59.8095	1599.5576	0	-59.75	NaN	NaN
45594	6	LS	TRANSCO 1005-2	11698.5	25.7	0	59.8095	1599.5576	0	-59.75	NaN	NaN
45595	6	LS	TRANSCO 1005-3	11699	25.7	0	59.8095	1599.5576	0	-59.75	NaN	NaN
45596	6	LS	TRANSCO 1005-4	11699.5	25.7	0	59.8095	1599.5576	0	-59.75	NaN	NaN
45597	6	LS	TRANSCO 1005-5	11700	25.7	0	59.8095	1599.5576	0	-59.75	NaN	NaN

Table 4-2: Demonstrates the data set and shows that the total count row reached 45,598 vectors and eleven columns of features in the data set. The feature vectors consist of the eight variables; Gamma-ray (GR), Calibration (CALI), Sonic (DT), Resistivity (ILD), Density (RHOB), Spontaneous (SP), Neutron-density porosity (PHIND), and absolute Neutron-density porosity difference (DeltaPHI).

	Facies	DEPT	GR	CALI	DT	ILD	RHOB	SP	PHIND	Delta PHI
Count	45598	45598	45598	45598	45598	45598	45598	45598	37726	37942
Mean	3.44	5249.7	39.19	9.027	93.88	257.18	-75.9	-1.84	166.5	0.183
Std	2.05	2820.1	28.29	6.003	28.31	3525.3	267.9	46.73	155.3	0.195
Min	1	200.5	-0.1	0	-999	-1	-999	-101.8	0	0
25%	2	3135.6	20.8	0	78.29	0.920	0	-39.5	49.9	0.03
50%	3	5150.5	34.05	10.95	92.38	1.368	2.2	0	136.5	0.12
75%	6	7050.3	58.3	13.25	106.1	36.644	2.4	34.75	249.8	0.24
Max	6	11700	409.5	21	207.3	162754	3.5	537	966.6	0.74

4.3 Methodology

This study demonstrates a classification algorithm subjected as a support vector machine to identify lithofacies based on well logs data. A support vector machine (SVM) is a supervised ML algorithm that is required to supply training data to learn the relationships between the features and the classes to be assigned. Measuring error, reducing error, and evaluating results are the most common components of ML algorithms (Dreiseitl and Ohno-Machado, 2002). The measuring error is the equation used to represent the machine learning problems and is called the objective function or loss function. Supervised learning is a part of Machine Learning processing of training data placed into the algorithm that retains expected solutions as labels. A typical supervised learning assignment is classification. In this chapter, the datasets have labeled facies classes as a number at a 0.5 ft interval. The workflow of the method in this study was created to evaluate the facies classification model (Figure 4-2). I provided eight features into the algorithms and output a facies class. Support Vector Machines and Random Forests are the most influential and prevalent supervised learning algorithms that were utilized in this study.

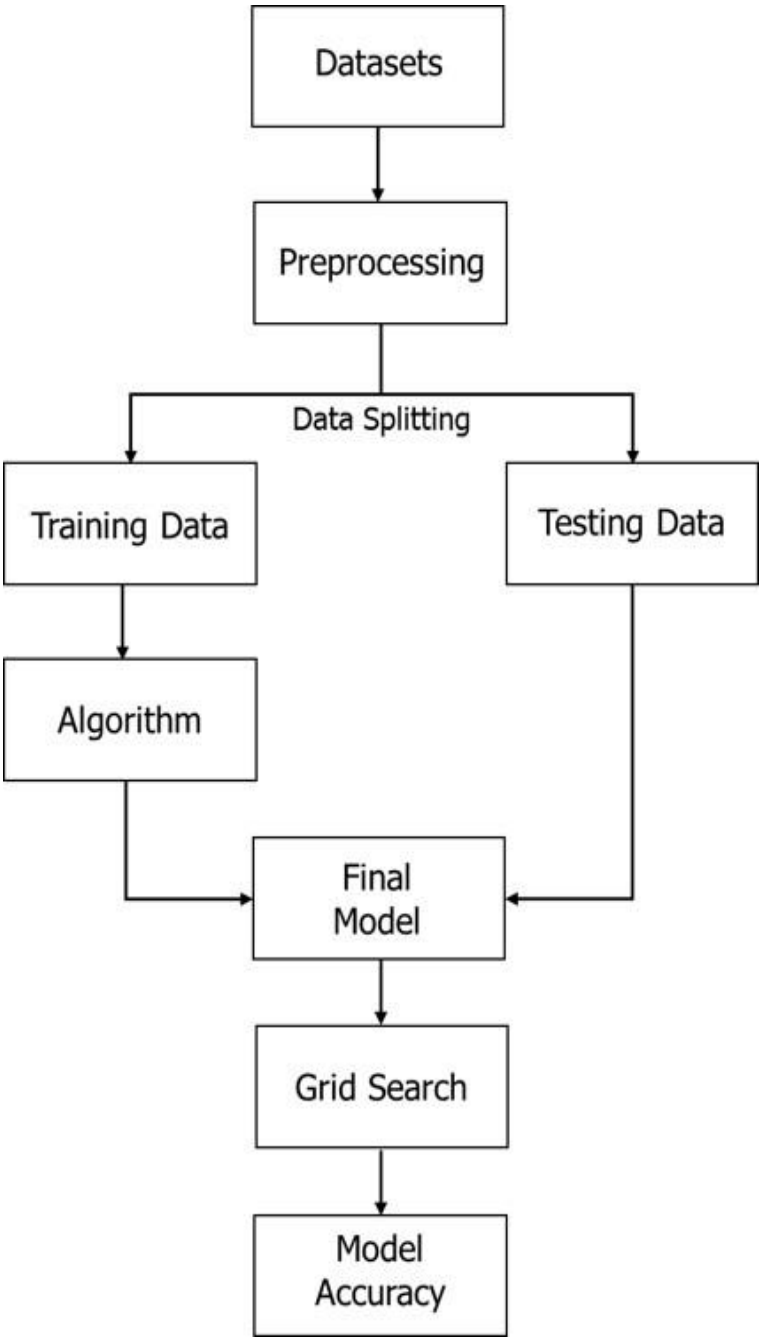

Figure 4-2: Workflow chart of the method.

4.3.1 Datasets

The features of datasets are the geophysical logs data from five offshore exploration wells (TRANSCO 1005, COST GE-1, TENNECO 427, EXXON 472, and EXXON 564) (Figure 4-1). Only COST GE-1 well has core lithofacies classes that have been identified based on the well core description (Poag, 1978; Dillon et al., 1979; Scholle, 1979). Applying cutoff rules to inefficient well log curves by facies and cross-plots of log curves can speed up the classification process (Figure 4-3). This study modified and combined the SEG approach (Hall, 2016) and the approach of (Chen and Zeng, 2018) to classify the rock facies of the dataset.

4.3.2 Data preprocessing

Six lithofacies classes labeled from 1 to 6 were labeled to characterize rock facies for the five wells (three training sets and two testing sets of wells). I settled on six classes of lithofacies by offsetting two factors:

1. The maximum number of facies distinguishable based on petrophysics properties that are subtracted by well log curves.

2. The minimum number of facies is required for accurate characterization of the physical variability of the formation.

Gamma Ray (GR) logs are usually used for shale content calculations, correlation, and mineral analysis. GR estimates γ-ray emissions from radioactive formations. Different formations may have different γ-ray signatures. Gamma Ray logs Resistivity (ILD) calculates the subsurface materials' ability to either inhibit or resist electrical conditions. By examining neutron energy losses in porous formations, a formation’s porosity could be calculated through the average neutron-density porosity (PHIND). The highest hydrogen concentration area in the formation is where Neutron energy loss may occur. Based on neutron logs, the porosity difference in

formation is measured through finding the Neutron-density porosity difference (DeltaPHI). These six facies are sandstone (SS), Shaley sandstone (ShSS), Sandy shale (SSSh), Shale (Sh), Anhydrite (Anh), and Limestone (LS) (Figure 4-3), which are consistently labeled and statistically classified into facies classes from number 1 to number 6. Facieses classes of the training data have been classified based on AAPG (2004) (Asquith et al., 2004; WIKI, 2017). However, the accuracy of the classifier is evaluated by comparing the facies labels for the training wells set with the predicted wells set, and misclassification of the neighboring facies can occur.

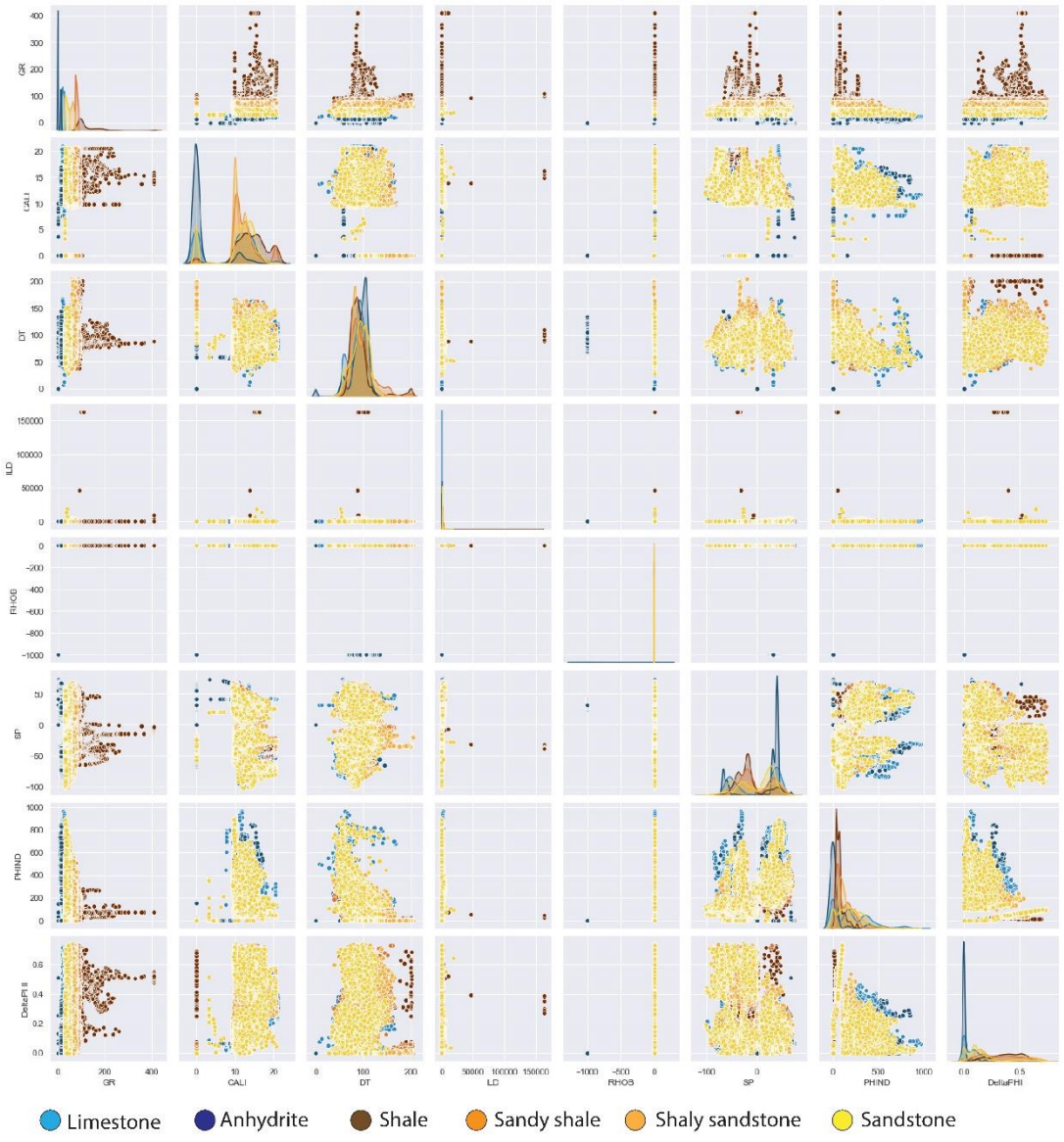

Figure 4-3: Cross-plots of eight wireline logs: Gamma ray (GR), calibration (CALI), sonic (DT), lateral (ILD), density (RHOB), spontaneous potential (SP), neutron-density porosity (PHI), and neutron-density porosity difference (DeltaPHI) of the train wells with six color keys for each specific rock facies category.

4.3.1 Dataset-splitting:

The data of five well logs in the study area have been split into training and testing data. The training data included TENNECO427-1, EXXON 472-1, and TRANSCO 1005-1 well log curves. The training data have been processed, and facies labels have been marked and plotted. The data set is associated with various facies types in machine learning terminology. The "pandas" library is used to stack the data into a data frame, which provides a suitable data structure for operating with well-log data. The data set includes eight features and a facies label (Figures 4-4, 4-5, and 4-6). These figures show the curves for the training data plotted for TENNECO 427-1, EXXON 472-1, and TRANSCO 1005-1 wells along with six signed facies classes. The dataset features (eight log curves) are GR, CALI, DT, ILD, RHOB, SP, PHIND, and Delta PHI. The color scale in the facies column indicates six classes signed at a depth interval of 0.5 ft. Statistical distribution of the six facies classes for the training data were plotted on a bar graph (Figure 4-7), which shows that Shaley Sandstone is widely distributed in the dataset, and Shale is the lowest distributed.

4.3.2 ML Outcomes

Based on the datasets and preprocessed, figures 4-4, 4-5, and 4-6 are constructed to show the facies classification of the training wells dataset. Facies are labeled at 0.5 ft depth intervals with six log measurements in the eight facies classification features dataset (figure 4-4, 4-5, and 4-6). Then the six well log measurements were assembled in a bar graph to represent the facies distribution in training wells (Figure 4-7). A cross plot is then constructed to aid with visualizing the log measurements and facies classes present in the well log curves (Figure 4-3). The exact process occurs for the testing wells facies classification. The testing well log curve data is then compared to the training well log curve data, and the information is presented on a heatmap that represents the accuracy of the predicted compared to the accurate values of the six log

measurements. In the Random Forest Classifier (RFC), a sample of primary datasets has been pulled and built for the classification pattern. The output has highlighted and assigned most of the forest using the voting techniques. The stacking method was applied to increase the resulted accuracy and statistically decrease any statistical modeling error that may arise when a function is closely aligned to a small sample size. Because of this, the model is only effective regarding the original data set and not in connection to any new datasets. This process obtains the prediction average from multiple decision trees (Breiman, 2001). Due to the law of large numbers, random forest is an ensemble-based algorithm that does not overfit and is a good tool for making predictions (Breiman, 1999; 2001). Therefore, selecting suitable hyperparameters makes all the ML models good predictors. Reducing error is the same as optimizing the objective function (Müller et al., 1997). There are multiple optimization various techniques, such as gradient descent (Wan et al., 2007; Chapelle and Wu, 2010)

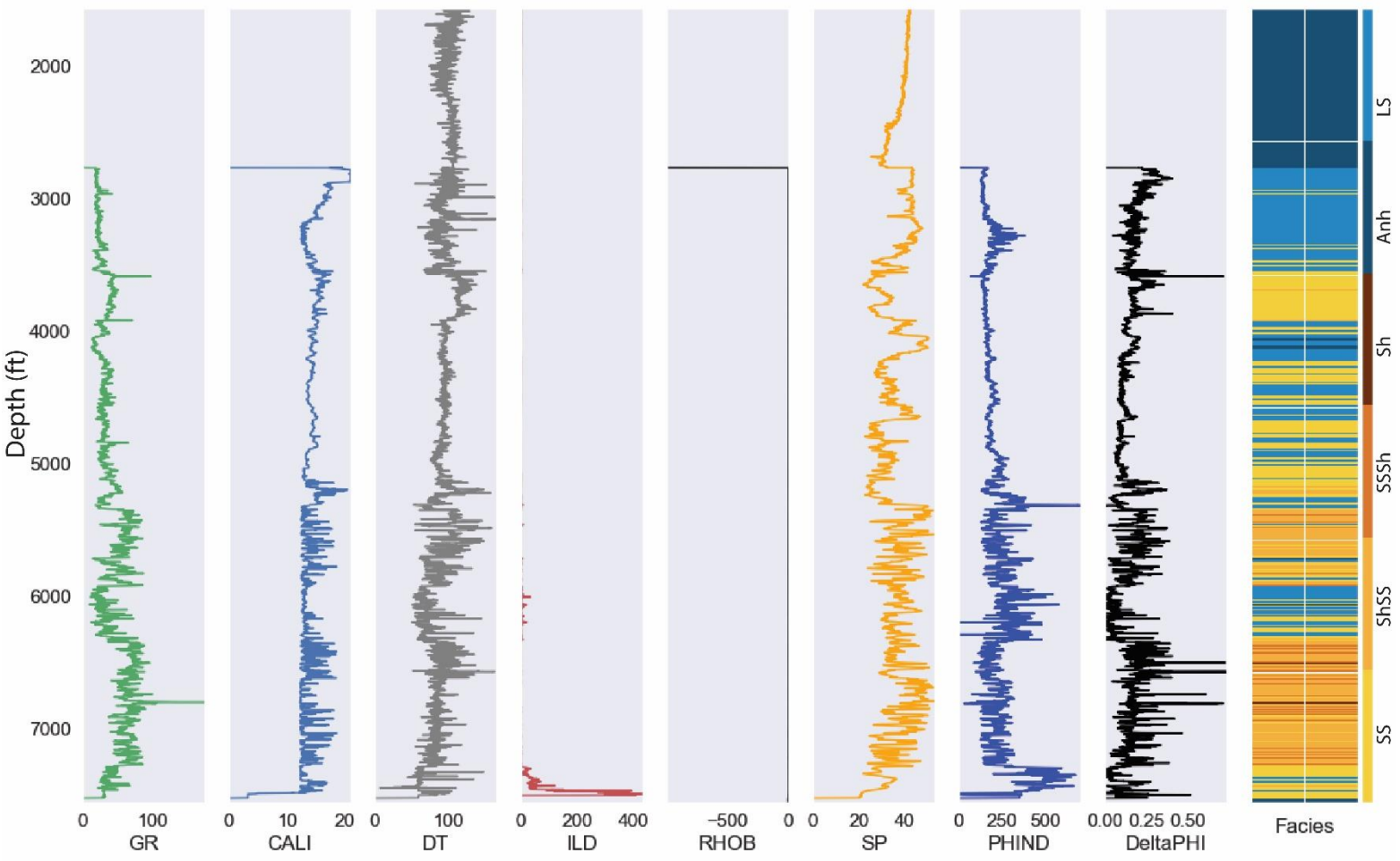

Figure 4-4: Well log curves plot for TENNECO 427-1 well along with six facies classes signed at 0.5 ft. Eight log curves are GR, CALI, DT, ILD, RHOB, SP, PHIND, and DeltaPHI. The color scale in the facies column indicates six facies classes that are signed at 0.5 ft intervals.

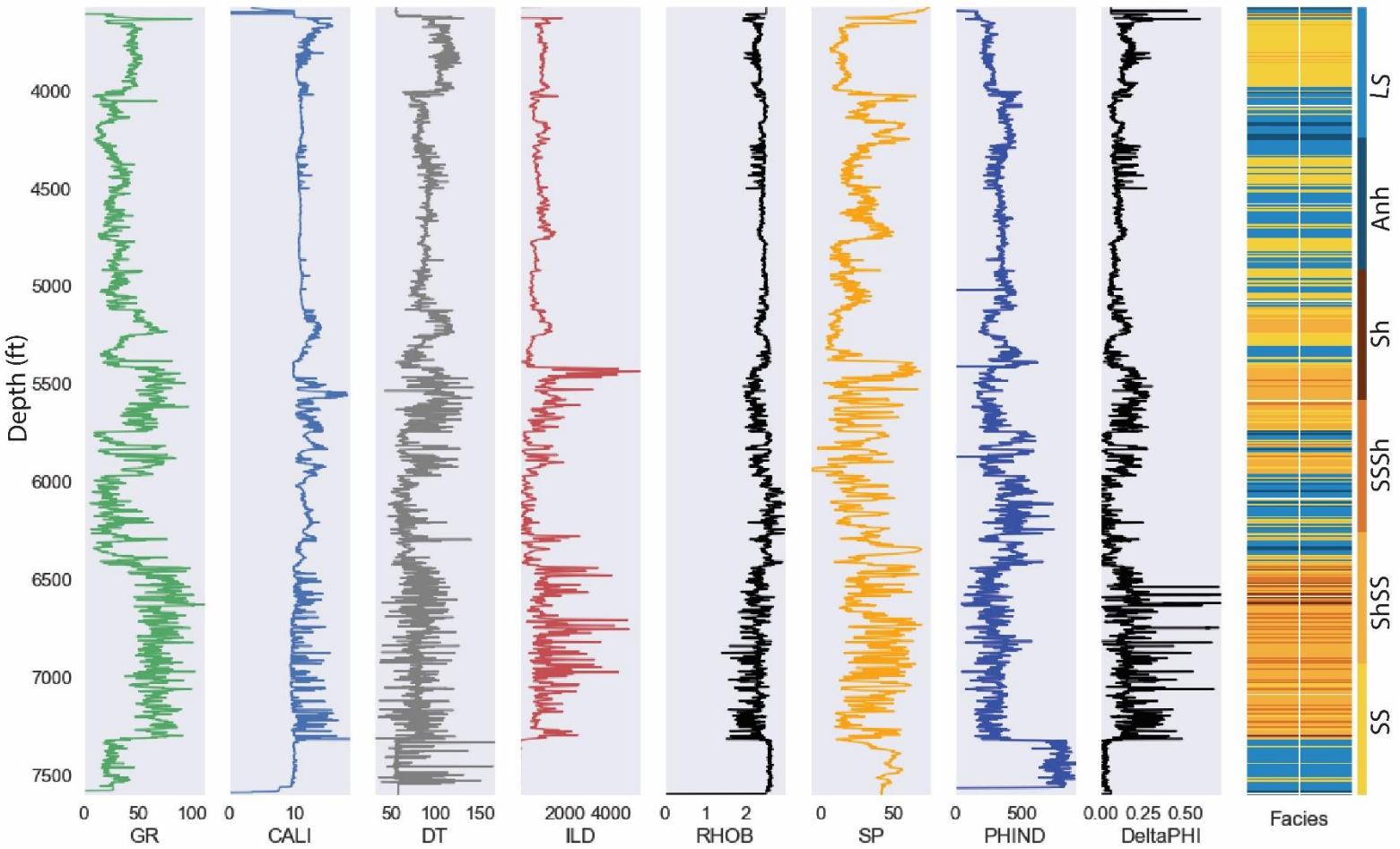

Figure 4-5: Well log curves plot for EXXON 472-1 well along with six facies classes signed at 0.5 ft. Eight log curves are GR, CALI, DT, ILD, RHOB, SP, PHIND, and DeltaPHI. The color scale in the facies column indicates six facies classes that are signed at 0.5 ft intervals.

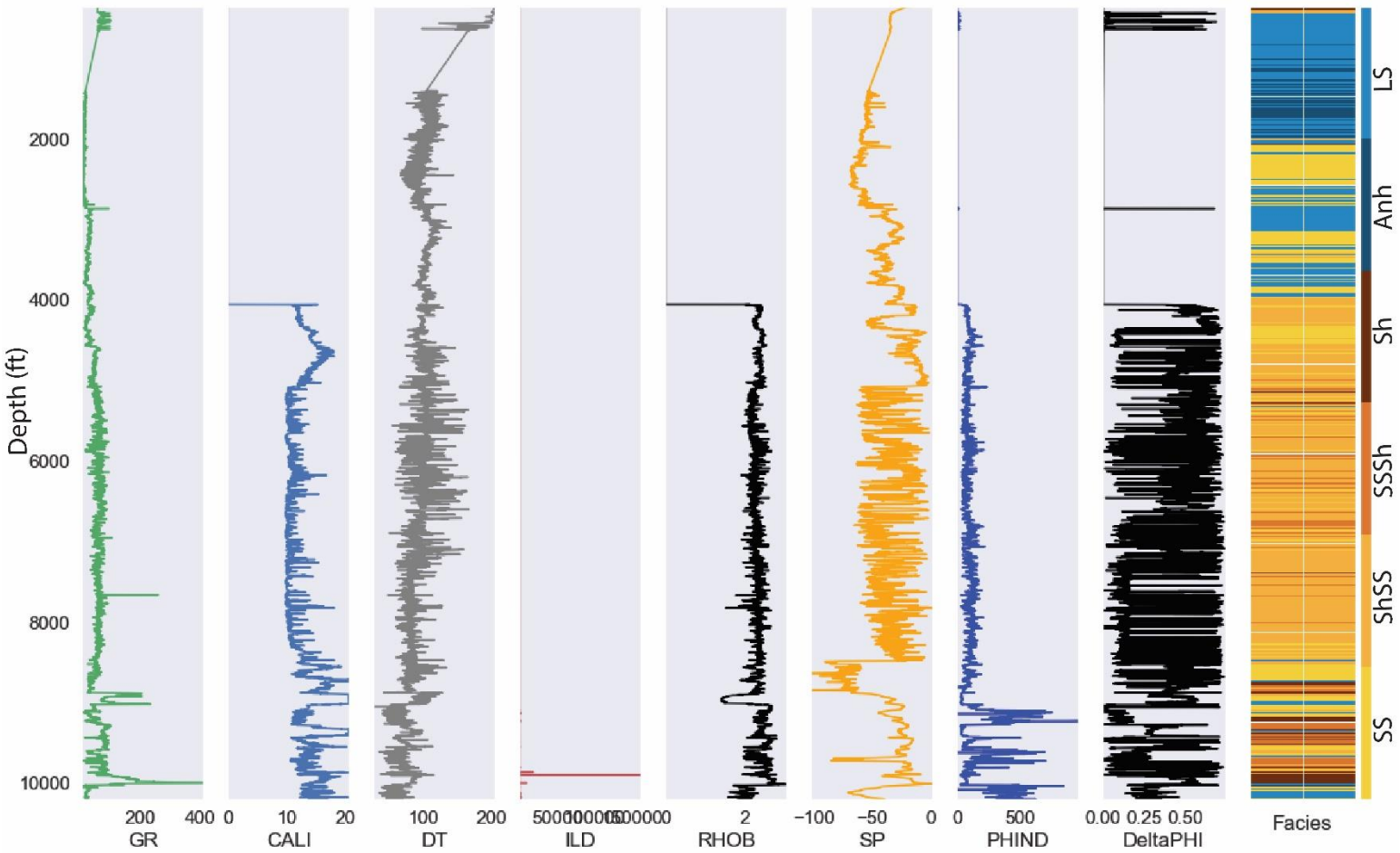

Figure 4-6: Well log curves plot for TRANSCO 1005-1 well along with six facies classes signed at 0.5 ft. Eight log curves are GR, CALI, DT, ILD, RHOB, SP, PHIND, and DeltaPHI. The color scale in the facies column indicates six facies classes that are signed at 0.5 ft intervals.

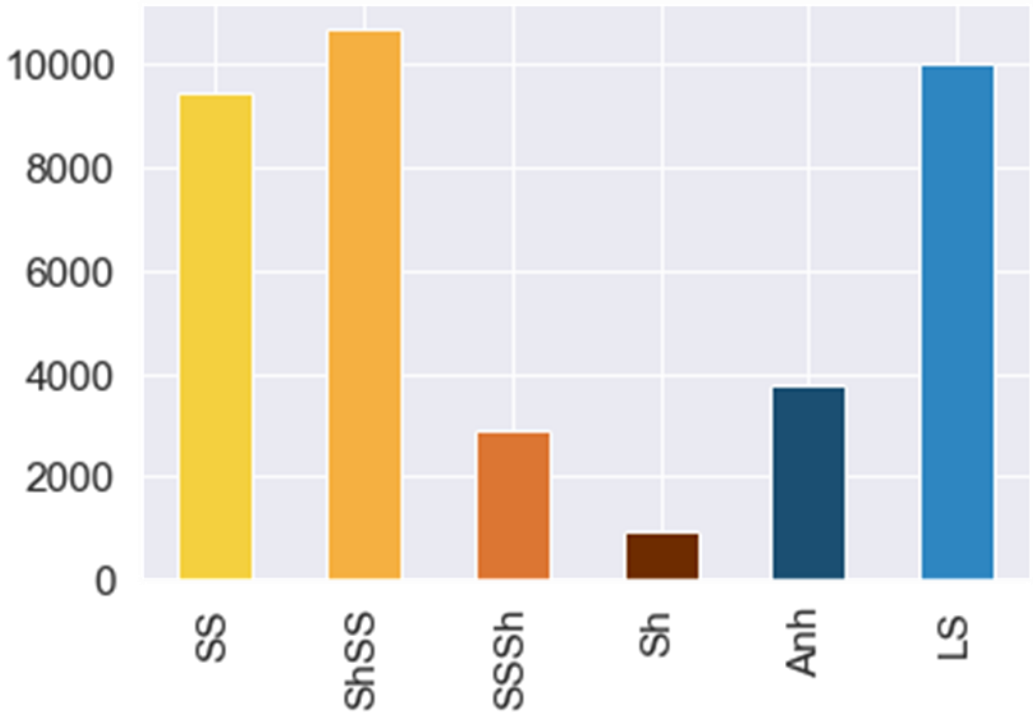

Figure 4-7: Represents the distribution of facies in the three training well dataset.

The confusion matrix is used to assess the performance of a classifier in the evaluation result. The general idea is to count how often instances of class A are classified as instances of class B, and the F-1 score is commonly used to assess classification algorithm results (Baluja et al., 2000; Baesens et al., 2003). In this chapter, I applied F-1 score of the ML industry standard equations (Equation 4.1, 4.2, and 4.3) that provided by Baluja et al. (2000) to measure the results of the testing wells. Precision and Recall in equation (4.1) can be calculated from equations (4.2) and (4.3), where true positive is the correct number of the predicted facies, false positive is the predicted number of facies which is in x-class, and false negative is the predicted number of facies which is not in x-class (Table 4-3). In table 4-4, the precision, recall, and F-1 score were calculated for all the facies classes and the macro average and weight were collected based on the values from table 4-3. The accuracy of the F-1 score was calculated based on the F-1 values for the six lithofacies classes (Table 4-4).

$$\frac{1}{F1} = \frac{1}{2}\left(\frac{1}{Precision} + \frac{1}{Recall}\right) \quad 4.1$$

$$Precision = \frac{True\ positive}{True\ positive + False\ negative} \quad 4.2$$

$$Recall = \frac{True\ positive}{True\ positive + Falsenegative} \quad 4.3$$

Table 4-3: Illustrates the negative and positive for the actual and predicted number of facies relationship, used to identify precision and recall (in equations 4.2 and 4.3).

Predict / Actual	Negative	Positive
Positive	False negative	True positive
Negative	True negative	False positive

Table 4-4: Demonstrates the precision, recall, and F-1 score calculated using equations (4.1, 4.2, and 4.3).

Number	Facies class	Precision	Recall	F1-score	Support
1	SS	0.98	0.96	0.97	1894
2	ShSS	0.98	0.99	0.99	2197
3	SSSh	0.94	0.98	0.96	529
4	Sh	1	0.87	0.93	187
5	Anh	0.97	0.89	0.93	766
6	LS	0.94	0.98	0.96	1973
Accuracy				0.97	7546
Macro avg		0.97	0.96	0.96	7546
Weighted avg		0.97	0.97	0.97	7546

4.3.3 Grid Search

Grid search describes a technique for finding an ideal hyperparameters model. Hyperparameters cannot be found in training data, unlike parameters. As a result, I built a model for each set of hyperparameters in order to determine the appropriate ones. Since I am essentially brute-forcing all potential combinations, grid search is regarded as a pretty conventional hyperparameter optimization technique. The models are then tested against one another. Naturally, the model with the highest accuracy is considered the greatest. Hyperparameters are established before training a machine learning model, unlike parameters. Optimizing these hyperparameters is essential to satisfy a model to a dataset. However, it is unusual that hyperparameter values on one dataset are superior to another. Therefore, optimizing the hyperparameters evolves more complex. In this method, I used two hyperparameters that aid quick learning environment: gamma and C-value. Both gamma and C values are set before the training models, however, the C-value is associated with controlling the Support Vector Classifier (SVC) training dataset error, and the gamma is associated with giving curvature weight to the Random Forest Classifier (RFC) training dataset error. Gamma and C-value provide six graphs that represent the accuracy classification of the training data with C and gamma vales ranging from 10^{-4} to 10 (Figure 4-8). The six graphs indicate that the accuracy of the training well facies classification. High accuracy value can be identified with low C-value, and high curvature is identified with high gamma value.

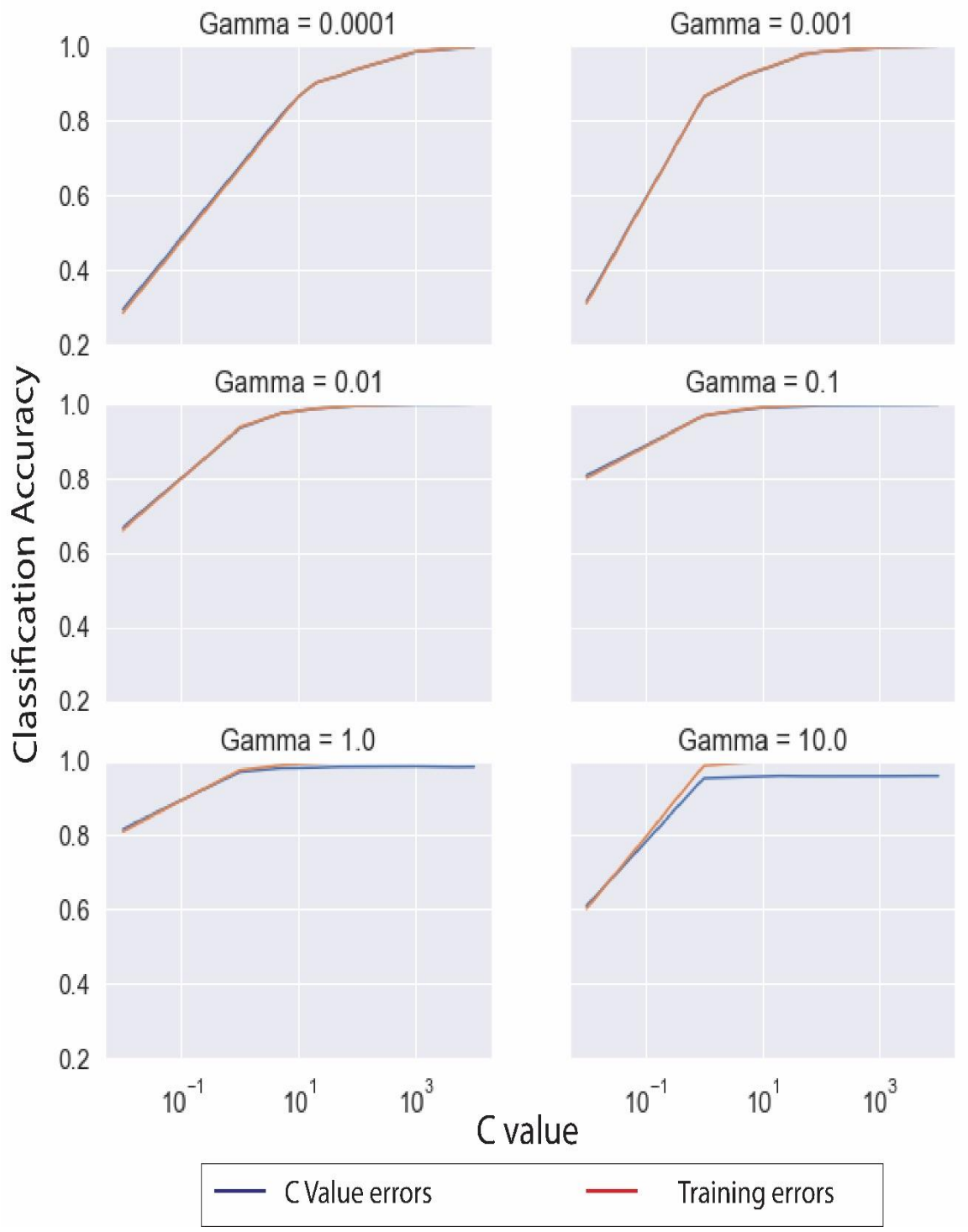

Figure 4-8: Gamma and C-value graph to determine the accuracy classification of the training data.

4.4 Results and discussion

The algorithms are trained on three wells of the dataset to predict lithofacies, including Sandstone, Shaley Sandstone, Sandy Shale, Shale, Anhydrite, and Limestone. Then, these algorithms are tested on two other wells. In order to measure the model performance for both algorithms, the evaluation matrix (confusion matrix) is calculated the precision, recall, and F1-score values (Table 4-4). The high performance of precision, recall, and F1-score values greater than 95% indicate that the ML techniques successfully categorized the Sandstone, Shaley Sandstone, Sandy shale, and Limestone. Shale and Anhydrite lithofacies classes demonstrated high precision, acceptable recall, and F1-score values of 93%, indicating acceptable accuracy for classification in Machine Learning. From the confusion matrix of the lithofacies classes, the ML methods present high accuracy of the predicted facies classification: Sandstone, Shaley Sandstone, Sandy shale, and Limestone. However, Shale and Anhydrite obtained the lowest accuracy based on the predicted to actual; the ML techniques have reasonably obtained accuracy. The RFC and SVC both resulted in very accurate predicted values, SVC has a 98.05% accuracy, and RFC has a 100% accuracy. The classification accuracy was chosen based on the C and gamma values. Figure 4-8 demonstrates that the lowest error occurrence in the training data is at a gamma value of 0.1 and a C value of 10.

The predicted results are presented as the best solution decision of the model on a heatmap that represents the predicted to actual values (Figure 4-9). The predicted to actual comparison supports the high confidence of the predictive model that has been completed regarding hyperparameter optimization. All the results above have been considered to apply a predictive model for facies classification on COST GE-1 and EXXON 564-1 wells (Figures 4-10 and 4-11). The supervised Machine Learning (ML) Model has successfully classified the predicted lithofacies. Although misclassification can occur due to the challenge of classifying thin rock

beds and the similarity of petrophysics rock properties in some rock beds, however, training the ML model increases the confidence in the facies classification accuracy succession (Figures 4-9 and 4-12).

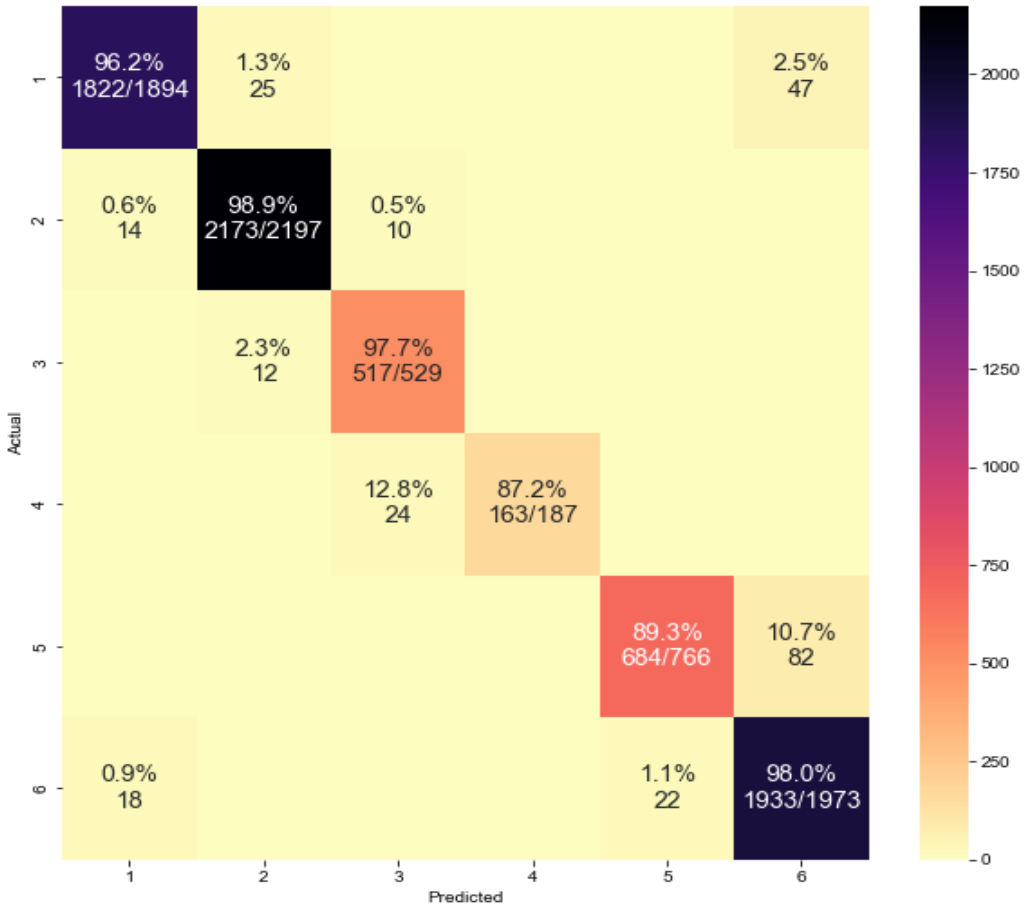

Figure 4-9: A heatmap representation of the comparison between the predicted to actual values for the training data.

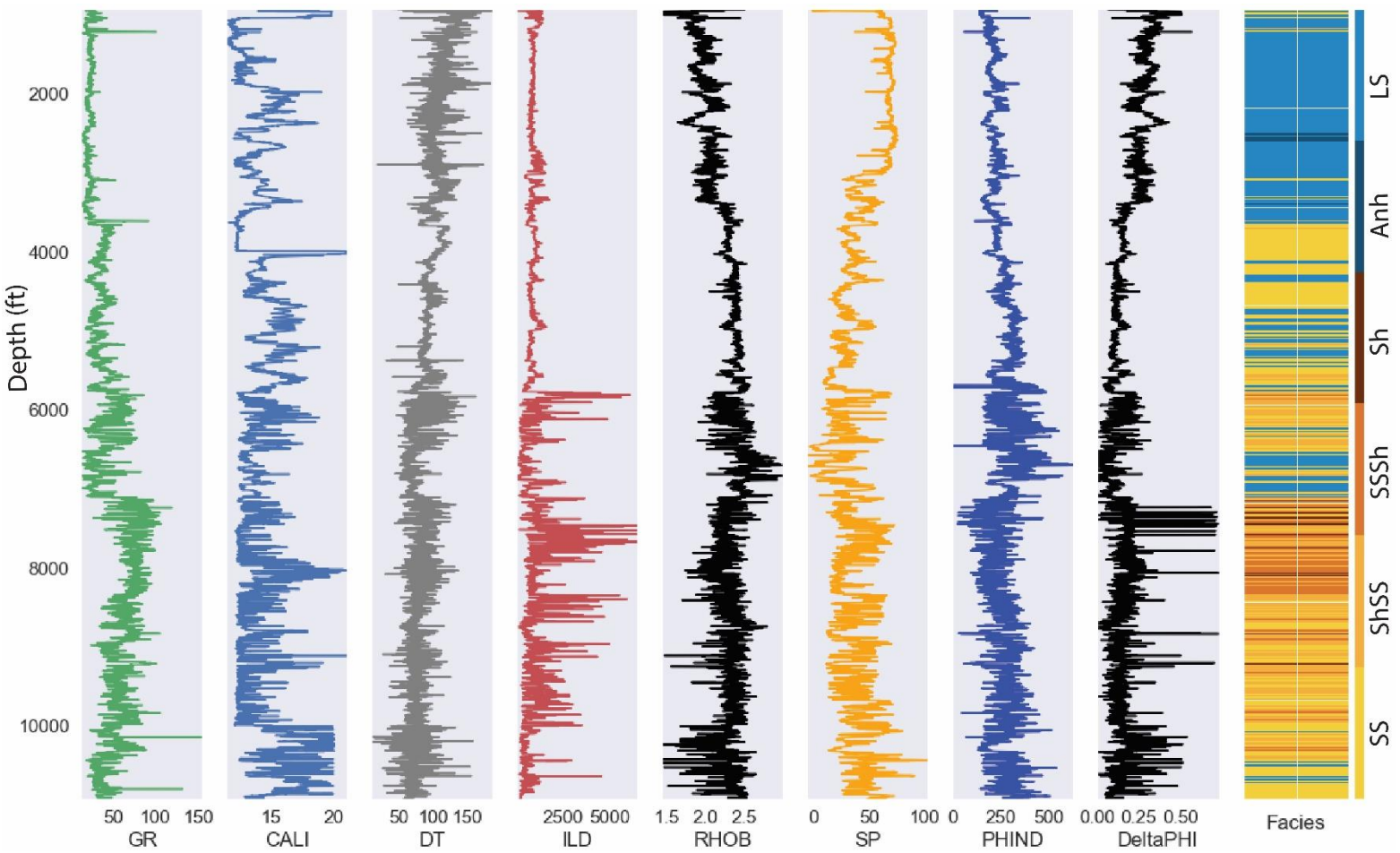

Figure 4-10: Well log curves plot for COST GE-1 well along with six facies classes signed at 0.5 ft. Eight log curves are GR, CALI, DT, ILD, RHOB, SP, PHIND, and DeltaPHI. The color scale in the facies column indicates six facies classes that are signed at 0.5 ft intervals.

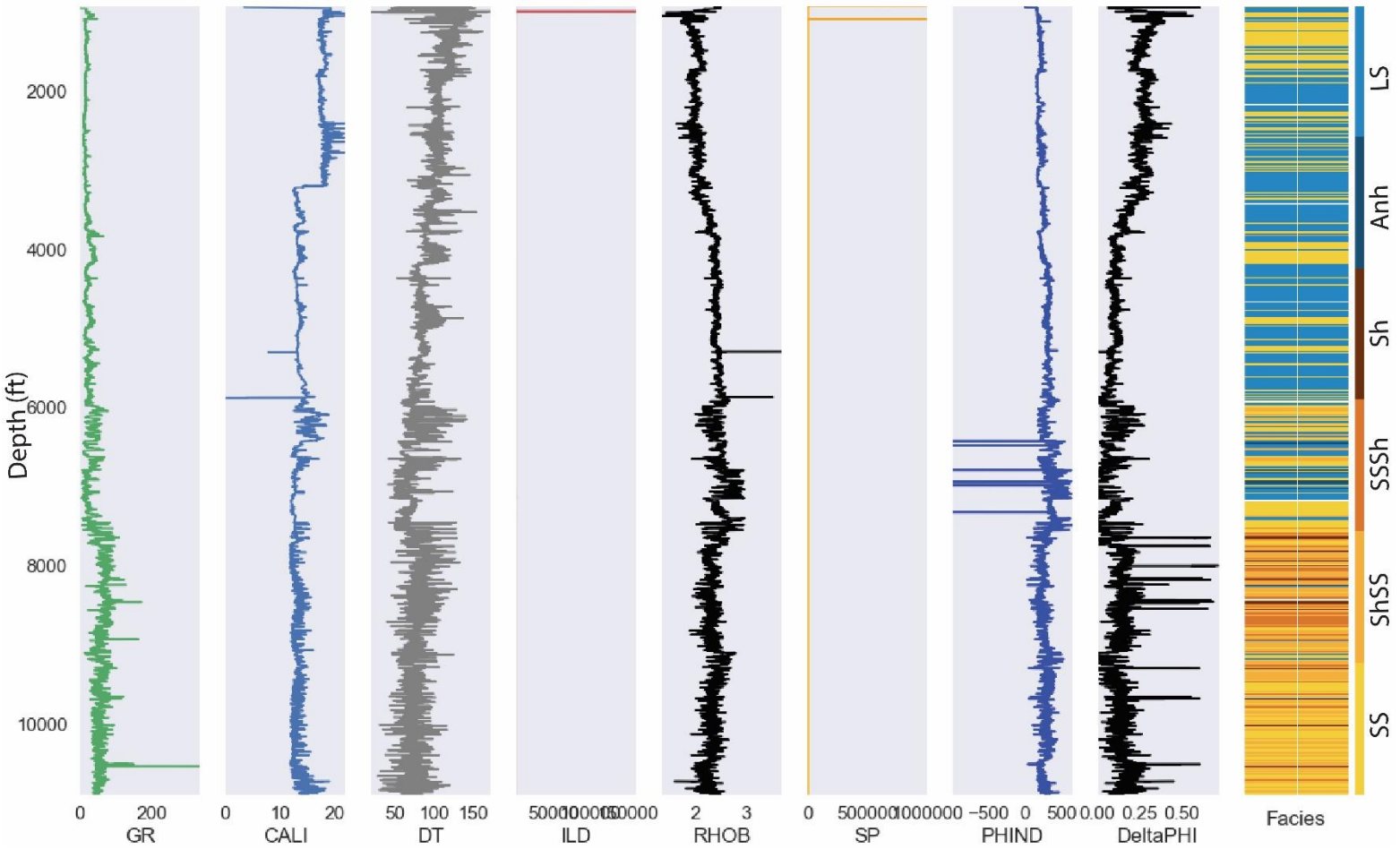

Figure 4-11: Well log curves plot for EXXON 564-1 well along with six facies classes signed at 0.5 ft. Eight log curves are GR, CALI, DT, ILD, RHOB, SP, PHIND, and DeltaPHI. The color scale in the facies column indicates six facies classes that are signed at 0.5 ft intervals.

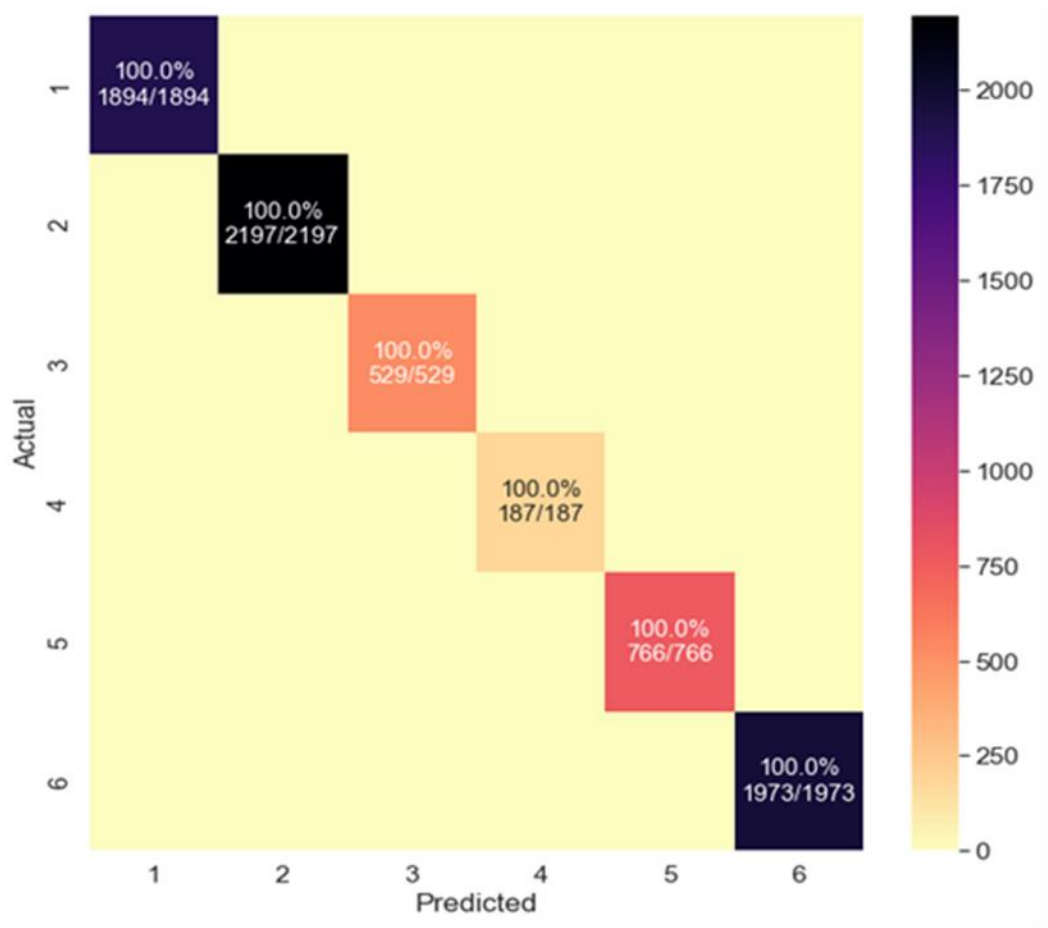

Figure 4-12: A heatmap representation of the comparison between the predicted to actual values for the testing data.

CHAPTER V

SUMMARY AND CONCLUSIONS

This dissertation presents the first comprehensive study to identify and evaluate the CO_2 storage potential in the Lower Cretaceous and the Upper Jurassic sections of the mid-south Atlantic offshore Southeastern United States.

Based on the analysis of three wells in the Southeast Georgia Embayment, the CO_2 geological storage resource estimate has provided evidence of three significant permeable storage strata isolated by impermeable seals in the depth interval of 1,767.84 - 2,529.84 m. In addition, the analysis of the COST GE-1 well, I identified widely and unsystematically porosity ranges from 0.17 to 0.32 as well as, the permeabilities are between 2.1×10-13 and 5.43×10-13 m2 (i.e. low percent of sandstone and high percent of dolomite). These layers are suitable reservoir rocks qualified to be permanent CO_2 storage.

The US DOE methodology is calculated pore volume spaces to estimate the geologic CO_2 storage

potential capacity in Million tons (Mt). The capacity for CO_2 storage potential of the Lower Cretaceous section was calculated based on the rock compositions and petrophysical properties at the COST GE-1 well. Three potential reservoirs are associated with four potential seals characterized and assessed. According to Scholle (1979), the trapping mechanism indicated by an overlying seal involves stratigraphic variations. The prospective storage resources of the three reservoirs were calculated locally, where seismic profiles and well data were densely concentrated in the Southeast Georgia Embayment (10,000 Km^2), and regionally, where I suggested a regional storage resource of 200,000 Km^2. I considered three probability values (P90, P50, and P10) of each reservoir for determining the geologic storage efficiency factor in both areas. This study suggests that the CO_2 storage capacity ranges approximately from 48.98 to 376.70 Mt locally and from 450.85 to 4705.46 Mt regionally in three Lower Cretaceous reservoirs with geologic storage efficiency from 0.65% to 5.4%.

The average storage resource potential is approximately 82 tons of CO_2 that could be safely stored per 1 Km^2 offshore of the Lower Cretaceous section at a probability of 0.5. The most considerable CO_2 storage resource value for reservoir R1 was > 3.2 tone/Km^2. The intermediate and lowest values at P50 in reservoirs R3 and R2 are less than or equal to 2.7 tone/Km^2.

The uncertainty associated with the subsurface data gap is incorporated into the storage resource evaluation due to the legacy of seismic data and the relatively limited well data available over the study area.

The Upper Jurassic Offshore CO_2 storage resource assessments were calculated to create an initial, screening-level limitation on the CO_2 storage potential of the deep saline aquifer in the mid-south Atlantic region, assisting in delineating and identifying storage resources and their respective categories at regional levels scales. Assessments of offshore storage resources were

based on efficient information integration approaches that included data availability analysis and formation-specific storage efficiency calculations relevant to offshore regions.

In this study, offshore-specific storage efficiency values were calculated using available data in the study area as inputs in probabilistic volumetric calculations for the regional grids. The targeted site was selected based on the regional storage potential and well data coverage observed within a 176,000 Km^2 area. The P10 and P90 probability values ranged from 0.2 to 0.8 for net-to-gross area, 0.17 to 0.68 for net-to-gross thickness, 0.53 to 0.71 for effective-to-total porosity, 0.26 to 0.43 for volumetric displacement, and 0.57 to 0.64 for microscopic displacement. The offshore storage zone is a combined net-to-total pore volume data set derived from geologic storage efficiency terms. With a storage efficiency factor of 3.2 at P10 and 5.36 at P90, the distribution of dynamic simulation results produced displacement efficiencies. Regional prospective storage resources for CO_2 storage have been estimated to range from 0.5 to 5.7 Gt. This study has proven that the Upper Jurassic sandstone reservoir can store at least 0.01 Mt of CO_2 per square kilometer at P50. Due to the legacy of seismic data and the relatively limited well data available across the research area, the uncertainty associated with subsurface data gaps is incorporated into the storage resource evaluation.

The detailed characterization of key petrophysical properties such as pore volume and permeability for the potential storage zone suggests that targeted net reservoir intervals contain average porosities ranging from 0.15 to 0.32 and mean permeabilities ranging from 9.87x10-14 to 9.97x10-13 m2, according to other key outcomes and findings. These porosities and permeabilities are within the range reported for the COST GE-1 well in the Southeast Georgia Embayment. These geologic and displacement efficiency probabilities were based on core, log, seismic, and biostratigraphic data. The Upper Jurassic interval of interest used to have a total storage efficiency of 0.64 to 5.36 percent at P10 to P90. The regional static storage resource

calculations show that the storage resources under consideration are suitable for safe and permanent storage for industrial emissions and power plants.

Based on the well core description, only one well has core lithofacies classes that have been identified. I have prepared data by labeling six lithofacies classes to characterize rock facies for the five wells (three training and two testing wells). Then, I used Gamma Ray logs Resistivity (ILD) to calculate the subsurface materials' ability to either inhibit or resist electrical conditions. I used the average neutron-density porosity (PHIND) to calculate the formation's porosity by examining neutron energy losses in porous formations. The area of the formation with the highest hydrogen concentration is where neutron energy loss will happen. The neutron-density porosity difference has been used to calculate the porosity difference in the formation based on neutron logs (DeltaPHI).

However, the facies classification is used the Support Vector Classifier (SVC) and Random Forest classifier (RFC) machine learning algorithms, where are trained and tested for the five given offshore wells in Southeast Georgia Embayment. The SVC and RFC algorithms are applied to develop the F-1 score classification. The evaluation matrix calculated the precision, recall, and F1-score values to measure the model performance in each algorithm to assess the accuracy of the classifiers (SVC and RFC) for the evaluation result. The lowest F-1 score value was 93% which is considered an acceptable accuracy for classification in the used machine learning approach. The SVC has a 98.05% accuracy, and the RFC has a 100% accuracy. This means that both of these algorithms are resulted in reliable and accurately predicted values. Despite the possibility of misclassification due to the difficulty of distinguishing thin rock beds and the similarity of some rock beds' petrophysical properties, training the ML model increases confidence in the accuracy of the facies classification. The selected code lines used in ML approach are shown in appendix.

REFERENCES

Almayahi, D.S., Knapp, J.H., and Knapp, C. (2022). Quantitative Evaluation of CO_2 Storage Potential in the Offshore Atlantic Lower Cretaceous Strata, Southeastern United States. *Energies* 15**,** 4890.

Almutairi, K.F. (2018). Assessment of upper cretaceous strata for Offshore CO_2 storage: Southeastern United States.

Amato, R., and Bebout, J. (1980). Geologic and operational summary, COST No. G-1 well, Georges Bank area. *North Atlantic OCS. US Geol Surv Open-File Rep***,** 80-268.

Amato, R.V., and Bebout, J.W. (1978). "Geological and operational summary: cost No. GE-1 well, Southeast Georgia Embayment Area, South Atlantic OCS". Geological Survey, Washington, DC (USA)).

Asquith, G.B., Krygowski, D., and Gibson, C.R. (2004). *Basic well log analysis.* American Association of Petroleum Geologists Tulsa.

Bachu, S. (2003). Screening and ranking of sedimentary basins for sequestration of CO 2 in geological media in response to climate change. *Environmental Geology* 44**,** 277-289.

Bachu, S. (Year). "Estimation of CO_2 Storage Capacity in Geological Media - Phase 2 - Prepared by the Task Force on CO_2 Storage Capacity Estimation for the Technical Group (TG) of the Carbon Sequestration Leadership Forum (CSLF)").

Bachu, S. (2008a). CO_2 storage in geological media: Role, means, status and barriers to deployment. *Prog. Energy Combust. Sci.* 34**,** 254-273.

Bachu, S. (Year). "Comparison between methodologies recommended for estimation of CO_2 storage capacity in geological media", in: *Carbon Sequestration Leadership Forum, Phase III Report*).

Bachu, S. (2015). Review of CO_2 storage efficiency in deep saline aquifers. *Int. J. Greenhouse Gas Control* 40**,** 188-202.

Badley, M., Price, J., Dahl, C.R., and Agdestein, T. (1988). The structural evolution of the northern Viking Graben and its bearing upon extensional modes of basin formation. Journal of the Geological Society 145, 455-472.

Baesens, B., Van Gestel, T., Viaene, S., Stepanova, M., Suykens, J., and Vanthienen, J. (2003). Benchmarking state-of-the-art classification algorithms for credit scoring. *Journal of the operational research society* 54**,** 627-635.

Bahadori, A., Vuthaluru, H.B., and Mokhatab, S. (2009). New correlations predict aqueous solubility and density of carbon dioxide. *International Journal of Greenhouse Gas Control* 3**,** 474-480.

Baluja, S., Mittal, V.O., and Sukthankar, R. (2000). Applying machine learning for high-performance named-entity extraction. *Computational Intelligence* 16**,** 586-595.

Bickle, M.J. (2009). Geological carbon storage. *Nature Geoscience* 2**,** 815-818.

Blondes, M.S., Brennan, S.T., Merrill, M.D., Buursink, M.L., Warwick, P.D., Cahan, S.M., Cook, T.A., Corum, M.D., Craddock, W.H., and Devera, C.A. (2013). *National assessment of geologic carbon dioxide storage resources: methodology implementation.* US Department of the Interior, US Geological Survey.

Boote, S.K., and Knapp, J.H. (2016). Offshore extent of Gondwanan Paleozoic strata in the southeastern United States: The Suwannee suture zone revisited. *Gondwana Res.* 40**,** 199-210.

Bradshaw, J., Bachu, S., Bonijoly, D., Burruss, R., Holloway, S., Christensen, N.P., and Mathiassen, O.M. (2007). CO_2 storage capacity estimation: issues and development of standards. *Int. J. Greenhouse Gas Control* 1**,** 62-68.

Breiman, L. (1999). 1 RANDOM FORESTS--RANDOM FEATURES.

Breiman, L. (2001). Random forests. *Machine learning* 45**,** 5-32.

Brennan, S.T., Burruss, R.C., Merrill, M.D., Freeman, P.A., and Ruppert, L.F. (2010). A probabilistic assessment methodology for the evaluation of geologic carbon dioxide storage. *US Geological Survey Open-File Report* 1127**,** 31.

Chadwick, A., Arts, R., Bernstone, C., May, F., Thibeau, S., and Zweigel, P. (2008). *Best Practice for the Storage of CO_2 in Saline Aquifers-Observations and Guidelines from the SACS and CO_2STORE projects.* British Geological Survey.

Chapelle, O., and Wu, M. (2010). Gradient descent optimization of smoothed information retrieval metrics. *Information retrieval* 13**,** 216-235.

Chen, J., and Zeng, Y. (2018). Application of machine learning in rock facies classification with physics-motivated feature augmentation. *arXiv preprint arXiv:1808.09856*.

Choubey, S., and Karmakar, G. (2021). Artificial intelligence techniques and their application in oil and gas industry. *Artificial Intelligence Review* 54**,** 3665-3683.

Cumming, L., Gupta, N., Miller, K., Lombardi, C., Goldberg, D., Ten Brink, U., Schrag, D., Andreasen, D., and Carter, K. (2017). Mid-Atlantic US Offshore Carbon Storage Resource Assessment. *Energy Procedia* 114**,** 4629-4636.

Dalziel, I.W., Dalla Salda, L.H., and Gahagan, L.M. (1994). Paleozoic Laurentia-Gondwana interaction and the origin of the Appalachian-Andean mountain system. *Geological Society of America Bulletin* 106**,** 243-252.

Dellagiarino, G. (2001). *Geological & Geophysical Data Acquisition: Outer Continental Shelf Through 2000.* US Department of the Interior, Minerals Management Service, Resource.

Dillon, W.P., Klitgord, K.D., and Paull, C.K. (1983). *Mesozoic development and structure of the continental margin off South Carolina.* US Department of the Interior, Geological Survey.

Dillon, W.P., Paull, C.K., Buffler, R.T., and Fail, J.-P. (1979). Structure and Development of the Southeast Georgia Embayment and Northern Blake Plateau: Preliminary Analysis: Rifted Margins.

Dillon, W.P., and Popenoe, P. (1988). The Blake Plateau Basin and Carolina Trough. *The Geology of North America* 2**,** 291-328.

Dillon, W.P., Popenoe, P., Grow, J.A., Klitgord, K.D., Swift, B.A., Paull, C.K., and Cashman, K.V. (1982). Growth Faulting and Salt Diapirism: Their Relationship and Control in the Carolina Trough, Eastern North America: Rifted Margins: Field Investigations of Margin Structure and Stratigraphy.

Dooley, J., Dahowski, R., Davidson, C., Bachu, S., Gupta, N., and Gale, J. (2005). "A CO_2-storage supply curve for North America and its implications for the deployment of carbon dioxide capture and storage systems," in *Greenhouse Gas Control Technologies 7*. Elsevier), 593-601.

Dreiseitl, S., and Ohno-Machado, L. (2002). Logistic regression and artificial neural network classification models: a methodology review. *Journal of biomedical informatics* 35**,** 352-359.

Duan, Z., Sun, R., Zhu, C., and Chou, I.-M. (2006). An improved model for the calculation of CO_2 solubility in aqueous solutions containing Na+, K+, Ca2+, Mg2+, Cl−, and SO42−. *Marine chemistry* 98**,** 131-139.

Ehlig-Economides, C., and Economides, M.J. (2010). Sequestering carbon dioxide in a closed underground volume. *Journal of Petroleum Science and Engineering* 70**,** 123-130.

Ellis, D.V., and Singer, J.M. (2007). *Well logging for earth scientists.* Springer.

Ennis-King, J., and Paterson, L. (Year). "Reservoir engineering issues in the geological disposal of carbon dioxide", in: *Fifth International Conference on Greenhouse Gas Control Technologies, Cairns*), 290-295.

Esposito, R.A., Pashin, J.C., Hills, D.J., and Walsh, P.M. (2010). Geologic assessment and injection design for a pilot CO_2-enhanced oil recovery and sequestration demonstration in a heterogeneous oil reservoir: Citronelle Field, Alabama, USA. *Environmental Earth Sciences* 60**,** 431-444.

Fukai, I., Keister, L., Ganesh, P.R., Cumming, L., Fortin, W., and Gupta, N. (2020). Carbon dioxide storage resource assessment of Cretaceous-and Jurassic-age sandstones in the Atlantic offshore region of the northeastern United States. *Environmental Geosciences* 27**,** 25-47.

Gao, D. (2011). Latest developments in seismic texture analysis for subsurface structure, facies, and reservoir characterization: A review. *Geophysics* 76**,** W1-W13.

Gill, D., Shomrony, A., and Fligelman, H. (1993). Numerical zonation of log suites and logfacies recognition by multivariate clustering. *AAPG bulletin* 77**,** 1781-1791.

Global, C. (2012). Institute (GCCSI), 2014. *The global status of CCS*.

Goodman, A., Hakala, A., Bromhal, G., Deel, D., Rodosta, T., Frailey, S., Small, M., Allen, D., Romanov, V., and Fazio, J. (2011). US DOE methodology for the development of geologic storage potential for carbon dioxide at the national and regional scale. *Int. J. Greenhouse Gas Control* 5**,** 952-965.

Goodman, A., Sanguinito, S., and Levine, J.S. (2016). Prospective CO_2 saline resource estimation methodology: Refinement of existing US-DOE-NETL methods based on data availability. *International Journal of Greenhouse Gas Control* 54**,** 242-249.

Gorecki, C., Sorensen, J., Bremer, J., Ayash, S., Knudsen, D., Holubnyak, Y., Smith, S., Steadman, E., and Harju, J. (2009a). Development of storage coefficients for carbon dioxide storage in deep saline formations. *Energy & Environmental Research Center (EERC), University of North Dakota. Report No*.

Gorecki, C.D., Sorensen, J.A., Bremer, J.M., Knudsen, D., Smith, S.A., Steadman, E.N., and Harju, J.A. (Year). "Development of storage coefficients for determining the effective CO_2 storage resource in deep saline formations", in: *SPE International Conference on CO_2 Capture, Storage, and Utilization*: OnePetro).

Gorecki, C.D., Sorensen, J.A., Bremer, J.M., Knudsen, D., Smith, S.A., Steadman, E.N., and Harju, J.A. (Year). "Development of Storage Coefficients for Determining the Effective CO_2 Storage Resource in Deep Saline Formations", in: *SPE International Conference on CO_2 Capture, Storage, and Utilization*, (SPE-126444-MS).

Govett, R. (2007). History of the Oil and Gas Industry on the Gulf Coast.

Gray, K. (2010). "Carbon Sequestration Atlas of the United States and Canada". Southern States Energy Board, Peachtree Corners, GA (United States)).

Guo, L., Wu, Y., Zhao, L., Cao, T., Yan, W., and Shen, X. (2010). Classification of mental task from EEG signals using immune feature weighted support vector machines. *IEEE Transactions on Magnetics* 47**,** 866-869.

Gupta, N. (2019). "Mid-Atlantic US Offshore Carbon Storage Resource Assessment Project (Final Technical Report)". Battelle Memorial Institute, Columbus, OH (United States)).

Hall, B. (2016). Facies classification using machine learning. *The Leading Edge* 35**,** 906-909.

Hart, P.E. (Year). "NAMSS-A NATIONAL ARCHIVE OF MARINE SEISMIC SURVEYS", in: *2007 GSA Denver Annual Meeting*).

Hendriks, C., Graus, W., and Van Bergen, F. (2004). Global carbon dioxide storage potential and costs. *Ecofys, Utrecht* 64.

Hertel, T.W., Golub, A.A., Jones, A.D., O'hare, M., Plevin, R.J., and Kammen, D.M. (2010). Effects of US maize ethanol on global land use and greenhouse gas emissions: estimating market-mediated responses. *BioScience* 60**,** 223-231.

Holloway, S. (2007). Carbon dioxide capture and geological storage. *Philosophical Transactions of the Royal Society A: Mathematical, Physical and Engineering Sciences* 365**,** 1095-1107.

Hortle, A., Michael, K., and Azizi, E. (2014). Assessment of CO_2 storage capacity and injectivity in saline aquifers–comparison of results from numerical flow simulations, analytical and generic models. *Energy Procedia* 63**,** 3553-3562.

Joachims, T. (2002). *Learning to classify text using support vector machines.* Springer Science & Business Media.

Kapur, L., Lake, L.W., Sepehrnoori, K., Herrick, D.C., and Kalkomey, C.T. (Year). "Facies prediction from core and log data using artificial neural network technology", in: *SPWLA 39th annual logging symposium*: OnePetro).

Kopp, A., Class, H., and Helmig, R. (2009). Investigations on CO_2 storage capacity in saline aquifers: Part 1. Dimensional analysis of flow processes and reservoir characteristics. *International Journal of Greenhouse Gas Control* 3**,** 263-276.

Laboratory, N.E.T., and Energy, U.S.O.O.F. (2008). *Carbon sequestration atlas of the United States and Canada.* National Energy Technology Laboratory.

Lawrence, S., Giles, C.L., Tsoi, A.C., and Back, A.D. (1997). Face recognition: A convolutional neural-network approach. *IEEE transactions on neural networks* 8**,** 98-113.

Levine, J.S., Fukai, I., Soeder, D.J., Bromhal, G., Dilmore, R.M., Guthrie, G.D., Rodosta, T., Sanguinito, S., Frailey, S., and Gorecki, C. (2016). US DOE NETL methodology for estimating the prospective CO_2 storage resource of shales at the national and regional scale. *International Journal of Greenhouse Gas Control* 51**,** 81-94.

Lizarralde, D., Holbrook, W.S., and Oh, J. (1994). Crustal structure across the Brunswick magnetic anomaly, offshore Georgia, from coincident ocean bottom and multi-channel seismic data. *J. Geophys. Res. B: Solid Earth* 99**,** 21741-21757.

Lokhorst, A., and Wildenborg, T. (2005). Introduction on CO_2 Geological storage-classification of storage options. *Oil & gas science and technology* 60**,** 513-515.

Maher, J.C., and Applin, E.R. (1971). "Geologic framework and petroleum potential of the Atlantic Coastal Plain and Continental Shelf", in: Professional Paper. US Govt. Print. Off.).

Manancourt, A., and Gale, J. (2005). A review of capacity estimates for the geological storage of carbon dioxide. *Greenhouse Gas Control Technologies 7***,** 2051-2054.

Metz, B., Davidson, O., De Coninck, H., Loos, M., and Meyer, L. (2005). "IPCC special report on carbon dioxide capture and storage". Intergovernmental Panel on Climate Change, Geneva (Switzerland). Working Group III).

Moore, D.E., and Liou, J. (1979). Mineral chemistry of some Franciscan blueschist facies metasedimentary rocks from the Diablo Range, California. *Geological Society of America Bulletin* 90**,** 1737-1781.

Müller, K.-R., Smola, A.J., Rätsch, G., Schölkopf, B., Kohlmorgen, J., and Vapnik, V. (Year). "Predicting time series with support vector machines", in: *International conference on artificial neural networks*: Springer), 999-1004.

Niu, Y., Gilmore, T., Mackie, S., Greig, A., and Bach, W. (Year). "Mineral chemistry, whole-rock compositions, and petrogenesis of Leg 176 gabbros: data and discussion", in: *Proceedings of the Ocean Drilling Program, scientific results*: Ocean Drilling Program College Station, TX), 1-60.

Okwen, R., Yang, F., and Frailey, S. (2014). Effect of geologic depositional environment on CO_2 storage efficiency. *Energy Procedia* 63**,** 5247-5257.

Payenberg, T.H., Lang, S.C., and Koch, R. (2000). A simple method for orienting conventional core using microresistivity (FMS) images and a mechanical goniometer to measure directional structures on cores. *Journal of Sedimentary Research* 70**,** 419-422.

Pinet, P.R., and Popenoe, P. (1985). A scenario of Mesozoic-Cenozoic ocean circulation over the Blake Plateau and its environs. *Geol. Soc. Am. Bull* 96**,** 618-626.

Poag, C.W. (1978). Stratigraphy of the Atlantic continental shelf and slope of the United States. *Annual Review of Earth and Planetary Sciences* 6**,** 251-280.

Poppe, L.J., Popenoe, P., Poag, C.W., and Swift, B.A. (1995). Stratigraphic and palaeoenvironmental summary of the south-east Georgia Embayment: a correlation of exploratory wells. *Marine and petroleum geology* 12**,** 677-690.

Rodosta, T., Bromhal, G., and Damiani, D. (2017). US DOE/NETL carbon storage program: advancing science and technology to support commercial deployment. *Energy Procedia* 114**,** 5933-5947.

Sanguinito, S., Goodman, A.L., and Sams Iii, J.I. (2018). CO_2-SCREEN tool: Application to the oriskany sandstone to estimate prospective CO_2 storage resource. *International Journal of Greenhouse Gas Control* 75**,** 180-188.

Sanguinito, S.M., Goodman, A., and Levine, J. (2017). "NETL CO_2 Storage prospeCtive Resource Estimation Excel aNalysis (CO_2-SCREEN) User's Manual". National Energy Technology Lab.(NETL), Pittsburgh, PA,(United States)).

Schlumberger (2016). Schlumberger petrel manual 2014. (2016, June 20). *http://isegunque.ddns.net/236.html*.

Scholle, P.A. (1979). *Geological studies of the COST GE-1 well, United States South Atlantic outer continental shelf area.* US Department of the Interior, Geological Survey.

Schrag, D.P. (2009). Storage of carbon dioxide in offshore sediments. *Science* 325**,** 1658-1659.

Selley, R.C. (1998). *Elements of petroleum geology.* Gulf Professional Publishing.

Smyth, R.C.a.H., Susan D and Meckel, Timothy and Breton, Caroline and Paine, Jeffrey G and Hill, Gerald R and Andrews, John R and Lakshminarasimhan, Srivatsan and Herzog, Howard and Zhang, Hongliang Henry and Others (2007). Potential sinks for geologic storage of carbon dioxide generated in the Carolinas. *US Bureau of Econ Geol, summary report*.

Solomon, S., Carpenter, M., and Flach, T.A. (2008). Intermediate storage of carbon dioxide in geological formations: a technical perspective. *International journal of greenhouse gas control* 2**,** 502-510.

Szulczewski, M., and Juanes, R. (2009). A simple but rigorous model for calculating CO_2 storage capacity in deep saline aquifers at the basin scale. *Energy Procedia* 1**,** 3307-3314.

Tewari, S., and Dwivedi, U. (2019). Ensemble-based big data analytics of lithofacies for automatic development of petroleum reservoirs. *Computers & Industrial Engineering* 128**,** 937-947.

Thomas, D.C., and Benson, S.M. (2005). *Carbon Dioxide Capture for Storage in Deep Geologic Formations-Results from the CO_2 Capture Project: Vol 1-Capture and Separation of Carbon Dioxide from Combustion, Vol 2-Geologic Storage of Carbon Dioxide with Monitoring and Verification.* Elsevier.

Tissot, B.P., and Welte, D.H. (1978). "An Introduction to Migration and Accumulation of Oil and Gas," in *Petroleum Formation and Occurrence*. Springer), 257-259.

U.S. (2015). *Department of Energy, Office of Fossil Energy, Office of Fossil Energy* [Online]. CRC press. Available: https://www.netl.doe.gov/File%20Library/Research/Coal/carbon-storage/atlasv/ATLAS-V-2015.pdf [Accessed August 20, 2015].

Van Der Meer, L.B., and Yavuz, F. (2009). CO_2 storage capacity calculations for the Dutch subsurface. *Energy Procedia* 1**,** 2615-2622.

Wan, L., Ng, W.K., Han, S., and Lee, V.C. (Year). "Privacy-preservation for gradient descent methods", in: *Proceedings of the 13th ACM SIGKDD international conference on Knowledge discovery and data mining*), 775-783.

Warwick, P.D., Blondes, M.S., Brennan, S.T., Corum, M.D., and Merrill, M.D. (2013). US Geological survey geologic carbon dioxide storage resource assessment of the United States. *Energy Procedia* 37**,** 5275-5279.

Wiki, A. (2017). "Well log analysis for reservoir characterization".).

Wolf, M., and Pelissier-Combescure, J. (Year). "FACIOLOG-automatic electrofacies determination", in: *SPWLA 23rd Annual Logging Symposium*: OnePetro).

Zhong, R., Tsang, M., Makusha, G., Yang, B., and Chen, Z. (2021). Improving estimation of rock mechanical properties using machine learning.

Zhongming, Z., Linong, L., Xiaona, Y., Wangqiang, Z., and Wei, L. (2020). EIA expects US energy-related carbon dioxide emissions to fall 11% in 2020.

Zhou, D., Zhao, Z., Liao, J., and Sun, Z. (2011). A preliminary assessment on CO_2 storage capacity in the Pearl River Mouth Basin offshore Guangdong, China. *International Journal of Greenhouse Gas Control* 5**,** 308-317.

Zhou, Q., Birkholzer, J.T., Tsang, C.-F., and Rutqvist, J. (2008). A method for quick assessment of CO_2 storage capacity in closed and semi-closed saline formations. *Int. J. Greenhouse Gas Control* 2**,** 626-639.

APPENDICES

Facies Classification Coding

```
%matplotlib inline
import pandas as pd
import numpy as np
import matplotlib as mpl
import matplotlib.pyplot as plt
import matplotlib.colors as colors
from mpl_toolkits.axes_grid1 import make_axes_locatable
from pandas import set_option
set_option("display.max_rows", 10)
filename = 'well_logs_inputs_trainset.csv'
training_data = pd.read_csv(filename)
training_data
training_data['Well_Name'] = training_data['Well_Name'].astype('category')
training_data['Formation'] = training_data['Formation'].astype('category')
training_data['Well_Name'].unique()
# 1=SS  2=ShSS   3=SSSh 4=Sh 5=Anh 6=LS
facies_colors = ['#F4D03F', '#F5B041','#DC7633','#6E2C00','#1B4F72','#2E86C1']
facies_labels = ['SS', 'ShSS', 'SSSh', 'Sh', 'Anh','LS']
#facies_color_map is a dictionary that maps facies labels to their respective colors
```

```
for ind, label in enumerate(facies_labels):

facies_color_map[label] = facies_colors[ind]

def label_facies(row, labels):

return labels[ row['Facies'] -1]

training_data.loc[:,'FaciesLabels'] = training_data.apply(lambda row: label_facies(row,
facies_labels), axis=1)

training_data.describe()

def make_facies_log_plot(logs, facies_colors):

#make sure logs are sorted by depth

logs = logs.sort_values(by='DEPT')

cmap_facies = colors.ListedColormap(

facies_colors[0:len(facies_colors)], 'indexed')

ztop=logs.DEPT.min(); zbot=logs.DEPT.max()

cluster=np.repeat(np.expand_dims(logs['Facies'].values,1), 100, 1)

f, ax = plt.subplots(nrows=1, ncols=9, figsize=(19, 12))

ax[0].plot(logs.GR, logs.DEPT, '-g')

ax[1].plot(logs.CALI, logs.DEPT, '-')

ax[2].plot(logs.DT, logs.DEPT, '-', color='0.5')

ax[3].plot(logs.ILD, logs.DEPT, '-', color='r')

ax[4].plot(logs.RHOB, logs.DEPT, '-', color='black')

ax[5].plot(logs.SP, logs.DEPT, '-', color='orange')

ax[6].plot(logs.PHIND, logs.DEPT, '-', color='blue')

ax[7].plot(logs.DeltaPHI, logs.DEPT, '-', color='yellow')

im=ax[8].imshow(cluster, interpolation='none', aspect='auto', cmap=
cmap_facies,vmin=1,vmax=6)

divider = make_axes_locatable(ax[8])
cax = divider.append_axes("right", size="10%", pad=0.05)

cbar=plt.colorbar(im, cax=cax)

cbar.set_label((15*' ').join(['SS', 'ShSS', 'SSSh', 'Sh', 'Anh','LS']))
```

```
cbar.set_ticks(range(0,1)); cbar.set_ticklabels('')
for i in range(len(ax)-1):
ax[i].set_ylim(ztop,zbot)
ax[i].invert_yaxis()
ax[i].grid()
ax[i].locator_params(axis='x', nbins=3)
ax[0].set_xlabel("GR")
ax[0].set_xlim(logs.GR.min(),logs.GR.max())
ax[1].set_xlabel("CALI")
ax[1].set_xlim(logs.CALI.min(),logs.CALI.max())
ax[2].set_xlabel("DT")
ax[2].set_xlim(logs.DT.min(),logs.DT.max())
ax[3].set_xlabel("ILD")
ax[3].set_xlim(logs.ILD.min(),logs.ILD.max())
ax[4].set_xlabel("RHOB")
ax[4].set_xlim(logs.RHOB.min(),logs.RHOB.max())
ax[5].set_xlabel("SP")
ax[5].set_xlim(logs.SP.min(),logs.SP.max())
ax[6].set_xlabel("PHIND")
ax[6].set_xlim(logs.PHIND.min(),logs.PHIND.max())
ax[7].set_xlabel("DeltaPHI")
ax[7].set_xlim(logs.DeltaPHI.min(),logs.DeltaPHI.max())
ax[8].set_xlabel('Facies')
ax[1].set_yticklabels([]); ax[2].set_yticklabels([]); ax[3].set_yticklabels([])
ax[4].set_yticklabels([]);
ax[5].set_yticklabels([]);ax[6].set_yticklabels([]);ax[7].set_yticklabels([]);ax[8].set_yticklabels([)
ax[8].set_xticklabels([])
f.suptitle('Well: %s'%logs.iloc[0]['Well_Name'], fontsize=15,y=0.95)
```

VITA

Dawod Salman Banay Almayahi

Candidate for the Degree of

Doctor of Philosophy

Dissertation: EVALUATION OF CO_2 STORAGE POTENTIAL IN OFFSHORE STRATA, MID-SOUTH ATLANTIC: SOUTHEAST OFFSHORE STORAGE RESOURCE ASSESSMENT (SOSRA)

Major Field: Geology

Biographical:

Education:

Completed the requirements for the Doctor of Philosophy in Geology at Oklahoma State University, Stillwater, Oklahoma in July, 2022.

Completed the requirements for the Master of Science in Geology at University of Basrah, Basrah, Iraq in 2005.

Completed the requirements for the Bachelor of Science in Geology at University of Basrah, Basrah, Iraq in 2001.